

Nucleon-Nucleon Correlations and the Quarks Within - Relating the EMC Effect and Short-Range Correlations

Or Hen

*Massachusetts Institute of Technology, Cambridge,
MA 02139*

Gerald A. Miller

*Department of Physics,
University of Washington, Seattle,
WA 98195*

Eli Piasetzky

*School of Physics and Astronomy,
Tel Aviv University, Tel Aviv 69978,
Israel*

Lawrence B. Weinstein

*Department of Physics,
Old Dominion University, Norfolk,
VA 23529*

(Dated: April 22, 2022)

This article reviews our current understanding of how the internal quark structure of a nucleon bound in nuclei differs from that of a free nucleon. We focus on the interpretation of measurements of the EMC effect for valence quarks, a reduction in the Deep Inelastic Scattering (DIS) cross-section ratios for nuclei relative to deuterium, and its possible connection to nucleon-nucleon Short-Range Correlations (SRC) in nuclei. Our review of the available experimental and theoretical evidence shows that there is a phenomenological relation between the EMC effect and the effects of SRC that is not an accident. There is an underlying cause of both effects: the influence of strongly correlated neutron-proton pairs is largely responsible. This conclusion needs to be solidified by the future experiments and improved theoretical analyses that are discussed herein.

Contents

I. Introduction - Short Range Correlations (SRC) and Nuclear Dynamics	2	D. Beyond Conventional Nuclear Physics: Nucleon Modification	24
A. The challenge of describing nuclei	3	1. Mean field	25
B. The need for short range correlations/Beyond the nuclear shell model	4	2. Suppression of point-like configurations	26
1. Spectroscopic factors	4	3. Six-quark bags and the EMC Effect	28
2. From the NN Interaction to the Shell Model and Beyond	6		
3. Short-ranged two-nucleon clusters	8		
II. Hard scattering and Short-Range Correlations	10	IV. The EMC - SRC Correlation	28
A. Hard Reactions	10	A. Experimental Overview	28
B. Inclusive Scattering	11	B. Theory Overview	30
C. Exclusive Scattering	14	1. High momentum nucleons and PLC suppression	30
D. Universal Properties of Short Range Correlations in Nuclei	17	2. Effective Field Theory	31
III. Deep Inelastic Scattering (DIS) and the EMC effect	18	3. The Isovector EMC Effect	32
A. DIS and nucleon structure functions	19	4. Summary	33
B. The EMC effect	20	C. Are the nucleons in the correlated pair really nucleons?	33
C. Why Conventional nuclear physics cannot explain the EMC effect	22	D. Determining the structure function of a free neutron	33
1. Nucleons only	22	1. The Deuteron IMC Effect	33
2. Nucleons plus pions	23	2. The Free Neutron Structure Function	34
		3. The d/u ratio at large x_B	35
		V. Existing electromagnetic form factor searches	35
		A. Polarization transfer in the $(\vec{e}, e' \vec{p})$ reaction	36
		B. Polarization transfer in the $(\vec{e}, e' \vec{n})$ reaction	37
		C. The (e, e') reaction and the Coulomb Sum Rule (CSR)	37
		VI. Future directions in nuclear deep inelastic scattering and detecting short-ranged correlations	38

A. Experiment	38
1. Inclusive EMC and SRC Measurements	38
2. Polarized EMC Measurements	39
3. Semi-Inclusive and Exclusive SRC Measurements	40
4. Tagged Structure function Measurements	40
5. Parity Violating Deep Inelastic Scattering	42
B. Theory	42
VII. The way we think it is and the ways to check	43
VIII. Acknowledgments	43
IX. Appendix	43
A. Understanding the np relative wave function	43
B. Basic terminology	45
C. Why center-of-mass and relative coordinates factorize	46

I. Introduction - Short Range Correlations (SRC) and Nuclear Dynamics

Nuclear physics is one of the oldest fields in modern physics. Its history (Wong, 1998) separate from atomic physics, can be said to start with the discovery of radioactivity in 1896 by Henri Becquerel. Less than ten years later Rutherford used hard scattering (see Section II.A) of alpha particles to discover that the nucleus is a tiny object at the heart of the atom. In 1932 Chadwick discovered a neutral particle of about the same mass as the proton that he called the neutron. This discovery allowed scientists to understand that the binding energy accounted for less than one percent of the nuclear mass. Thus it is natural to say that the nucleus is made of neutrons and protons. In 1935 Yukawa suggested a theory of the strong force to explain how the nucleus holds together. In the Yukawa interaction a virtual particle, later called a meson, mediated a force between nucleons. This force explained why nuclei did not fall apart due to proton repulsion, and it also explained why the attractive strong force had a shorter range than the electromagnetic proton repulsion. Thus we may think of the stable nucleus as a tight ball of neutrons and protons (collectively called nucleons), held together by the strong nuclear force.

This basic picture has been studied for many years. Early models treated heavy nuclei, which could contain hundreds of nucleons, as classical liquid drops. The liquid-drop model can reproduce many features of nuclei, including the general trend of binding energy with respect to mass number, as well as nuclear fission.

The liquid drop idea cannot explain more detailed properties of nuclei. Quantum-mechanical effects (which can be described using the nuclear shell model developed initially by Mayer (Mayer, 1950) and Jensen (Haxel *et al.*, 1949)) explained that nuclei with certain numbers of neutrons and protons (the magic numbers 2, 8, 20, 28, 50, 82, 126, ...) are particularly stable because their shells are filled. Many studies were devoted to understanding

how the liquid drop model, with its collective features, could be consistent with the shell model.

Detailed studies of nucleon-nucleon scattering indicated that their interaction contains something like a hard core, making the origin of the shell model even more mysterious than its coexistence with the liquid drop model. Brueckner and other early workers (see the references in (Gomes *et al.*, 1958)) showed that in the nuclear medium, the large, short-ranged effects of the strong nucleon-nucleon potential could be summed and treated in terms of a smoother object, defined as a G matrix. This idea allowed much of nuclear phenomena to be understood (at least qualitatively) in terms of the fundamental nucleon-nucleon interaction. The nucleus was made of nucleons, with the occasional evanescent meson existing as it propagated from nucleon to nucleon including the effects of nucleon-nucleon correlations.

After the single-particle shell model, the natural next step in describing nuclei is including the effects of two-nucleon correlations. The strong short-ranged nucleon-nucleon force that is averaged to make the mean-field G -matrix also causes a significant nucleon-nucleon correlation function (see the Appendix for definitions). However, definitive experimental evidence for correlations had to await high-energy (“hard-scattering”) reactions (Frankfurt and Strikman, 1981a) that could isolate the effects of ground-state correlations from the various two-body currents and final state interactions that occur in nuclear reactions (Hen *et al.*, 2014b; Korover *et al.*, 2014; Piasetzky *et al.*, 2006; Shneor *et al.*, 2007; Subedi *et al.*, 2008; Tang *et al.*, 2003).

Meanwhile, deep inelastic scattering on nucleons led to the discovery that the nucleons are made of quarks. However due to the small ($\leq 1\%$) nuclear binding energy and the idea of quark-gluon confinement, it was thought that quarks had no explicit role in the nucleus and that therefore nuclei could still be described in terms of nucleons and mesons. The simple and compelling nucleon/meson picture of the nucleus was shaken to its core by the 1982 discovery of the EMC effect (Aubert *et al.*, 1983), the non-trivial dependence of the per-nucleon lepton deep inelastic scattering cross section on the specific nuclear target. The EMC effect showed that the quarks have a small but definite role in the nucleus, and that we need to understand this.

There are a number of fundamental unanswered questions about nuclear physics.

1. Is the nucleus really made of nucleons and mesons only?
2. How does the nucleus emerge from QCD, a theory of quarks and gluons?
3. How does the partonic content of the nucleus differ from that of N free neutrons plus Z free protons?

No one asked such questions before the EMC effect.

At first glance there appears to be little relation between nucleon-nucleon correlations and the EMC effect. However, there is a strong phenomenological connection between them (Weinstein *et al.*, 2011) that occurs for the valence quarks that carry large momentum and that connection is the subject of this review.

We now summarize our most important conclusions for the benefit of the reader:

- there is much indirect and direct evidence for the existence of nucleon-nucleon short-ranged correlations (SRC),
 - high energy (e, e') reactions at large values of x_B (the Bjorken scaling variable) show that all nuclei have similar momentum distributions at large momentum, implying that strongly-correlated two-nucleon clusters exist in the nuclear ground state,
 - high energy ($p, 2pN$) and ($e, e'pN$) reactions show that two-nucleon correlations exist and are dominated, at certain nucleon momenta, by np pairs, and
 - a consequence of this np dominance is the possible inversion of the kinetic energy sharing in nuclei with $N > Z$ (i.e., that protons might have more kinetic energy than neutrons in neutron-rich nuclei).
- conventional (non-quark) nuclear physics cannot account for the EMC effect,
- models need to include nucleon modification to account for the EMC effect. These models can modify the structure of either:
 - mean field nucleons, or
 - nucleons belonging to SRC pairs.
- there is a phenomenological connection between the strength of the EMC effect and the probability that a nucleon belongs to a two-nucleon SRC pair ($a_2(A)$).
- the influence of SRC pairs can account for the EMC-SRC correlation because both effects are driven by high virtuality nucleons with squared four-momentum not equal to the square of the mass $p^2 \neq M^2$,
- the connection between the EMC effect and the coefficients $a_2(A)$ has been derived using two completely different theories, so that this connection is no accident
- nuclei must contain a small percentage of baryons that are not nucleons. Such baryons exist in the short-ranged correlations and are the source of the EMC effect.

We aim to critically discuss the reasons for these conclusions and provide enough details for the reader to appreciate the progress that has been made in recent years. The remainder of this article describes the experimental and theoretical evidence for the existence of two-nucleon short range correlations and the properties thereof; the theoretical and experimental facts regarding deep inelastic scattering, nucleon structure functions and the EMC effect; and, the need for nucleon modification to explain the EMC effect. It will then present the unexpected correlation between the strength of the EMC effect in a given nucleus and the probability that a nucleon in that nucleus belongs to an SRC pair. The ensuing discussion presents theoretical ideas connecting SRC and EMC physics, and explores the idea that the SRC-EMC correlation can be used to determine the structure function of a free neutron. The final sections are concerned with other evidence that the nuclear medium modifies the structure of bound nucleons, and future directions for experimental and theoretical research. The Appendix presents formal definitions of the terms we use, and also explains some equations used in the main text. Specific locations of the various subjects are listed in the Table of Contents.

A. The challenge of describing nuclei

Nucleons bound in nuclei move under the influence of the strong interaction as effected by short-ranged two and three body potentials. Solving the Schroedinger equation of the A -body system was initially an impossibly daunting challenge, so that understanding the vast array of relevant experimental data required the use of models.

The nuclear shell model was one of the earliest and perhaps most powerful models. In this model, each nucleon moves independently in the average field produced by the other nucleons. This shell model provides a reasonable description of many nuclear properties and is the fundamental starting point for all efforts to provide a theory of nuclei. Its explanation of the nuclear magic numbers is a major accomplishment in the history of physics. Despite this, early research involving collective degrees of freedom established that the single particle picture of nuclei could not be complete. More generally, corrections to the shell model can be classified broadly in terms of the relevant distances needed to describe the various phenomena. There are both long-ranged (\sim the size of the nucleus) and short-ranged (\sim the size of the nucleon) phenomena.

The strong nucleon-nucleon force is known to bind medium and heavy nuclei, all with about the same average central density of $\rho_A = 0.16$ nucleons/fm 3 . Thus, the average distance between nucleons is about $1/\rho_A^{1/3} = 1.8$ fm. The radius of a nucleon is about $r = 0.86$ fm, so that most (but not all) of the time it does not overlap in space with other nucleons. The nucleon has a volume of $V = \frac{4}{3}\pi r^3 = 2.5$ fm 3 and a density of $\rho_N = 0.4$ fm $^{-3}$.

Thus $\rho_N/\rho_A = 2.5$ and the *maximum* nuclear density, even without nucleons overlapping, is 2.5 times the *average* nuclear density.

The fact that a nucleon has about 2.5 times larger density than the nuclear central density and that nucleons move in the nucleus with about a quarter of the velocity of light opens up the possibility of large local density fluctuations. These also lead to large local momentum fluctuations via the uncertainty principle. The strong short range repulsive force between nucleons restrains the size of these fluctuations, but since its range is smaller than a fermi, the density and momentum fluctuations in nuclei can still be quite large.

Another important length scale that enters into lepton-nucleon or nucleus scattering must be examined. This is the coherence length, or Ioffe length (Gribov *et al.*, 1966; Ioffe, 1969): $l_I = \frac{2}{Mx_B} \approx \frac{0.4 \text{ fm}}{x_B}$, where $x_B = \frac{Q^2}{2M\nu}$. Here M is the nucleon mass, Q^2 is the negative of the square of the virtual exchanged photon four-momentum, and ν is its energy. This length is the typical distance between the absorption and re-emission of the virtual photon. This length must be short enough to resolve the relevant inter-nucleon distance scales of the order of a fermi. Thus, our attention here is drawn only to the region x_B greater than about 0.3. This is the region where valence quarks are dominant and the sea is almost invisible.

The diverse features described above indicate that understanding the broad diversity of nuclear phenomena requires the use of many experimental tools. Since electromagnetic interactions are well-understood and presumably simple, electron scattering has long been used as a tool to investigate different aspects of nuclear structure. We examine the use of electron scattering to probe the validity of the single-particle shell model in the next subsection.

B. The need for short range correlations/Beyond the nuclear shell model

1. Spectroscopic factors

The use of electro-induced proton knockout reactions on nuclei, $A(e, e'p)$, provided early evidence for the qualitative validity of the shell model (Frullani and Mougey, 1984). These studies complemented the use of many low-energy nuclear reactions, such as (d, p) and (p, pp) . Later on, more detailed studies using higher energy electron beams determined the limits of the validity of the shell model. We next explain how this happened.

In the $(e, e'p)$ reaction the electron knocks out a nucleon so that an initial nuclear state $|i\rangle$ of A nucleons is converted to a final nuclear state $|f\rangle$ of $A - 1$. The reaction can be analyzed in terms of spectroscopic factors (Macfarlane and French, 1960), which are probabilities that all but one of the nucleons will find them-

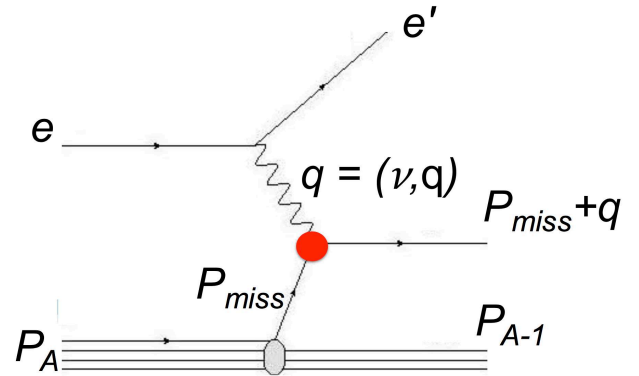


FIG. 1: The $A(e, e'p)$ reaction in the Plane Wave Impulse Approximation. A nucleus of four-momentum P emits a nucleon of four-momentum p that absorbs a virtual photon of four-momentum q to make a nucleon of four momentum $p + q$, with $(p + q)^2 = M^2$, where M is the nucleon mass. The blob represents the in-medium electromagnetic form factors.

selves in the final state. More formally, if one considers a single-particle state of quantum numbers α , the spectroscopic factor S_α is given by the square of the overlap: $S_\alpha = |\langle f | b_\alpha | i \rangle|^2$, where b_α destroys a nucleon. If the independent particle model were exact, then S_α would be unity for each occupied state α . Thus measuring S_α is a useful way to study the nuclear wave functions and the limitations of the independent particle model.

In the Plane Wave Impulse Approximation (PWIA), an electron transfers a single virtual photon with momentum \mathbf{q} and energy ν (sometimes written ω) to a single proton, which then leaves the nucleus without reinteracting (see Fig. 1).

In PWIA, neglecting relativistic corrections, the cross section factorizes in the form (Kelly, 1996)

$$\frac{d\sigma}{d\nu d\Omega_e dE_{\text{miss}} d\Omega_p} = K \sigma_{ep} S(E_{\text{miss}}, \mathbf{p}_{\text{miss}}) \quad (1)$$

where $K = E_p p_p / (2\pi)^3$ is a kinematical factor, E_p and p_p are the energy and momentum of the outgoing proton, σ_{ep} is the electron cross section (De Forest, 1983a) for scattering by a bound proton, and S is the spectral function, the probability of finding a nucleon in the nucleus with momentum \mathbf{p}_{miss} and separation energy E_{miss} . The missing momentum and missing energy are given by:

$$\begin{aligned} \mathbf{p}_{\text{miss}} &= \mathbf{q} - \mathbf{p}_p \\ E_{\text{miss}} &= \nu - T_p - T_{A-1} \end{aligned} \quad (2)$$

where T_p and T_{A-1} are the kinetic energies of the detected proton and residual (undetected) $A - 1$ nucleus.

The knocked-out proton then interacts with other nucleons as it leaves the nucleus; these final state interaction (FSI) effects have been typically calculated using either an optical model at low momenta (Kelly, 1996) or using the eikonal or Glauber approximations at higher momenta (Ryckebusch *et al.*, 2003; Sargsian *et al.*, 2005b). Calculations where the wave function of the knocked-out proton are distorted by FSI are referred to as distorted wave impulse approximation calculation (DWIA). In DWIA, the $(e, e'p)$ cross section does not exactly factorize as in the PWIA. However, factorization is a good approximation at $Q^2 \gg p_{\text{miss}}^2$ and the cross section is approximately proportional to a distorted spectral function S^D (Kelly, 1996). Neither PWIA nor DWIA calculations conserve current because the initial and final wave functions of the model calculations are not orthogonal and because the effective NN interactions used in the initial and final states are different. Furthermore, Eq. (1) assumes that the bound nucleon moves non-relativistically.

Thus, $(e, e'p)$ measurements should be sensitive to the spectral function, i.e., to the momentum and energy distributions of nucleons in the nucleus. Fig. 2 shows the $^{16}\text{O}(e, e'p)$ cross section at $Q^2 = 0.8 \text{ GeV}^2$ and $\nu = 0.439 \text{ GeV}$ plotted versus missing energy at several different missing momenta and plotted versus missing momentum for the two p -shell states. There are sharp peaks at $E_{\text{miss}} = 12$ and 18 MeV , corresponding to proton knockout from the $1p_{1/2}$ and $1p_{3/2}$ shells, a broad peak at $E_{\text{miss}} \approx 40 \text{ MeV}$ corresponding to proton knockout from the $1s$ shell (and other processes), and a long tail extending to large E_{miss} , especially at the largest missing momenta. The momentum distribution calculations shown in Fig. 2(lower) use an optical potential, a modern bound state wave function, and an off-shell cross section σ_{ep} and fit only the magnitude (see Ref. (Gao *et al.*, 2000) for details). The calculations describe the data well, except for the fact that the ratio of data to theory (the spectroscopic factor) is approximately 0.7. This means that the experiment only measured 70% of the expected number of p -shell protons.

This depletion of the spectroscopic factor was observed over a wide range of the periodic table (see Fig. 3) for both valence nucleon knockout using the $(e, e'p)$ reaction (Lapikas, 1993) and stripping using the $(d, {}^3\text{He})$ reaction (Kramer *et al.*, 2001). Only about 60–70% of the expected valence nucleon strength was observed. The missing strength implies the existence of long range correlations and short range correlations in nuclei. Our focus will be on the short range correlations.

In the DWIA independent particle shell model we would expect that the spectroscopic factors are unity and that there is little cross section at large E_{miss} . The fact that spectroscopic factors are significantly less than unity for all nuclei, and that there is significant cross section at large missing energy indicates that this simple model picture omits important physics. This is not surprising,

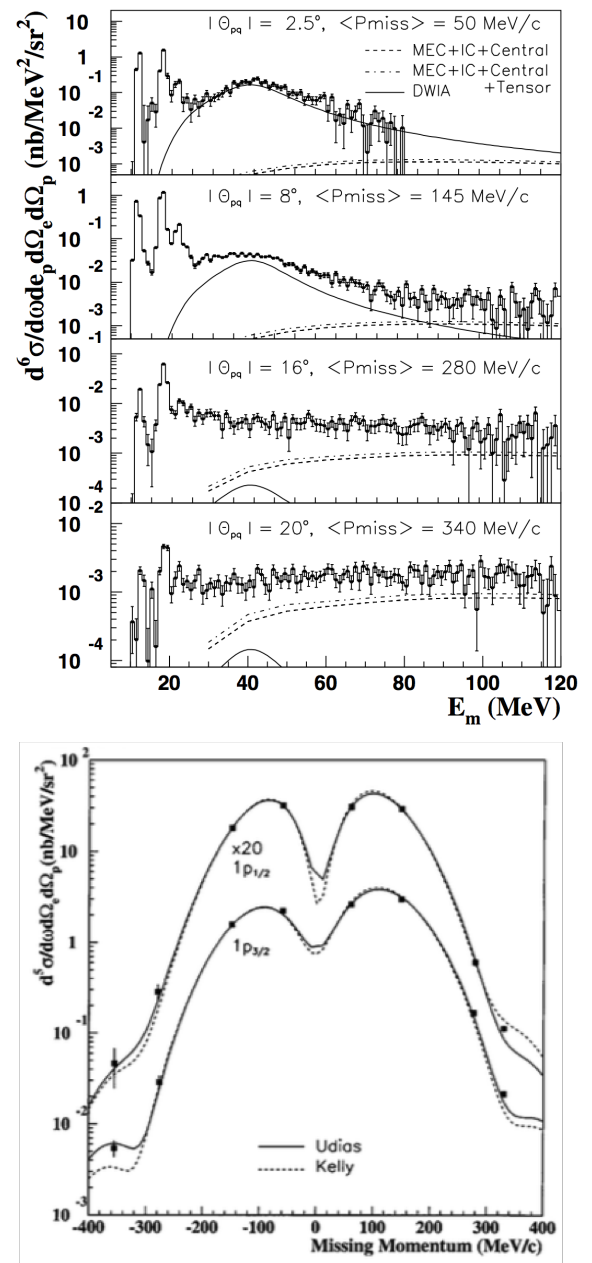


FIG. 2: (upper) The $\text{O}(e, e'p)$ cross section plotted versus missing energy at $Q^2 = 0.8 \text{ GeV}^2$ and $\nu = 0.439 \text{ GeV}$ for different angles, θ_{pq} , between the proton spectrometer and \mathbf{q} . The curve labelled DWIA is a distorted wave impulse approximation calculation of s -shell knockout; the other curves are calculations of two-nucleon knockout including meson exchange currents (MEC), delta production (IC), and central and/or tensor correlations. Figure adapted from (Liyanage *et al.*, 2001). (lower) The cross section plotted versus missing momentum for the $1p_{1/2}$ and $1p_{3/2}$ states. Figure adapted from (Gao *et al.*, 2000). The curves show DWIA calculations. See (Fissum *et al.*, 2004; Gao *et al.*, 2000; Liyanage *et al.*, 2001) for details.

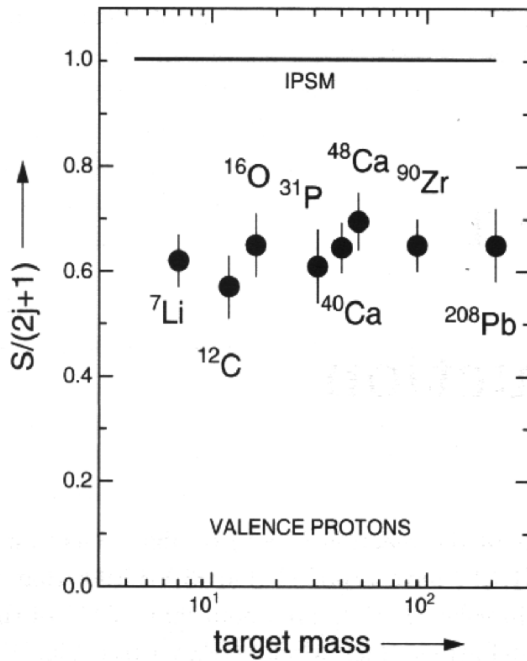


FIG. 3: The percentage spectroscopic factors (the ratio of measured cross sections to those calculated with the Independent Particle Shell Model) for valence nucleon knockout ($e, e'p$). Adapted from (Lapikas, 1993).

since the short-ranged nature of the strong nuclear forces implies that nucleons must be influenced by nearby nucleons. There is no fundamental one-body potential in the nucleus, unlike the central one-body Coulomb potential that binds electrons to form the structure of the atom.

Indeed, since the NN forces are short ranged, the fact that the shell model approximation has any relevance is somewhat surprising. In the early days of nuclear physics, the fundamental question of nuclear physics was: how does the very successful shell model of the nucleus emerge in spite of the strong short-ranged interactions between nucleons?

We next answer this fundamental question, then examine the consequences of the answer.

2. From the NN Interaction to the Shell Model and Beyond

How can the mean-field shell model arise from a system made of nucleons interacting by strong short-ranged forces? An answer to this question was provided early on by Brueckner & Goldstone, see the review by Bethe (Bethe, 1971). The strong two-nucleon interactions encoded by the potential V , constructed to reproduce experimentally measured scattering observables and believed to include strong repulsion at short distance and attraction at longer ranges, are summed to form the T

matrix of scattering theory and the G -matrix for bound states. The operator G is obtained from T by modifying the propagator of the Lippmann-Schwinger equation to include the effects of the Pauli principle and to use the appropriate self-consistent (single) nucleon energies. The G matrix is considerably weaker than V . For example, even if the potential is infinitely strong, the product $V\Psi$ of the potential with the wave function obtained from the chosen Hamiltonian would be finite and well behaved. Schematically, one has $G\Phi = V\Psi$, where Φ is the shell-model two-nucleon wave function. Calculations show that G is reasonably smooth and can be used as input in higher-order calculations.

The theory proceeds by forming the nuclear mean field U through the Hartree-Fock method employing the G -matrix, and the first approximation to the wave function is the anti-symmetrized product of single particle wave functions engendered by U . However, the complete nuclear wave function is obtained in a perturbative hole-line expansion that includes two-particle – two-hole excitations and other excitations which incorporate correlations. The presence of such correlations is demanded by the theory.

Later work formulated a relativistic version of Brueckner theory in which the Dirac equation replaces the Schrödinger equation (Anastasio *et al.*, 1983; Brockmann and Machleidt, 1984). There is also a light front version (Miller and Machleidt, 1999a; Miller, 2000).

The Brueckner theory approach described above presumes that the two-nucleon potential contains strong short-distance repulsion. Early attempts to construct soft potentials (i.e., lacking the strong repulsion) that also reproduce scattering data did not succeed in obtaining interactions that could be used perturbatively to calculate nuclear bound states (Bethe, 1971). The lack of success of soft-interaction is now known to be caused in large measure by the omission of three-body forces. Relativistic G -matrix calculations include important three-body forces (Anastasio *et al.*, 1983; Brockmann and Machleidt, 1984; Miller and Machleidt, 1999a; Miller, 2000). There are also fundamental three-nucleon forces, such as those involving an intermediate Δ resonance. in addition to true three-body forces, induced multi-nucleon forces occur as a result of some simplifications of the Hamiltonian (Bogner *et al.*, 2010).

Much more has been learned since Bethe's 1971 review. (1) Our understanding of the connection between the NN interaction and the underlying theory of QCD is much improved. (2) Our ability to make fundamental first-principles calculations of nuclear energies is also much improved. (3) However, it is possible that improved treatments of nuclear energy levels decrease our ability to understand the nuclear high-momentum transfer interactions of interest in this review. (4) We now know that 2nd order interactions of the NN potential have a major effect on the density distribution and the correlation

function in all existing approaches.

(1) Chiral effective field theory provides a low-energy version of QCD, guided by chiral symmetry, in which one obtains the potential as an expansion in powers of (Q/Λ_χ) where Q is a generic external momentum or the pion mass, and Λ_χ is the chiral symmetry breaking scale of about 1 GeV. Such approaches have the advantage of being systematically improvable for low-energy observables. See for example the review (Bedaque and van Kolck, 2002). In such theories the short distance interaction can be treated as a contact interaction, modified by the inclusion of a cut-off, and the longer ranged interactions are accounted for by one and two pion (or more) exchange interactions (Machleidt and Entem, 2011). The advantage gained is that different parts of the potential are divided to more easily understood long ranged contributions and presumably unknown short-ranged contributions.

(2) Modern first-principles calculations of nuclear spectra have been applied to an ever increasing mass range. One of the main tools is the use of soft potentials, which do not connect low-relative momentum states to those of high relative momentum. This greatly simplifies the calculations by increasing the validity of perturbation theory and other approximation techniques.

The softness (involving low momentum) or hardness (involving higher momentum) of the potential is determined by the value of the cutoff see *e.g.* (Epelbaum *et al.*, 2009; Machleidt and Entem, 2011). Such potentials introduce a cutoff in momentum space at fairly low values of momenta. Typically, the momentum-space potential obtained from Feynman diagrams, $V(\mathbf{p}, \mathbf{p}')$, is replaced:

$$V(\mathbf{p}, \mathbf{p}') \rightarrow V(\mathbf{p}, \mathbf{p}') e^{-(\frac{p'}{\Lambda})^n} e^{-(\frac{p}{\Lambda})^n} \quad (3)$$

with $p = |\mathbf{p}|$, $p' = |\mathbf{p}'|$, Λ ranges between 400 and 500 MeV and n ranges from 2 to 4. These are very strong cut-offs in momentum that introduce significant non-locality to the nucleon-nucleon interaction. This causes difficulties in maintaining conservation of the electromagnetic currents (Gross and Riska, 1987).

Another approach uses renormalization group methods to generate a soft NN potential from a hard interaction either by integrating out high momentum components (in the case of V_{low-K}), or by using the similarity renormalization group (Bogner *et al.*, 2010). This potential is perturbative in the sense that the Born series for scattering converges. Furthermore, many-body perturbation theory starting from a Hartree-Fock bound state can be applied to the nuclear bound state problem.

(3) But there is another more general issue that arises in trying to understand high momentum transfer nuclear reactions. The ability to originate and predict the results of experiments that probe short-ranged correlations (as was done in (Frankfurt and Strikman, 1981a, 1988b)) depends on the idea that the simple impulse approximation

is the best way to think about the relevant kinematics and reaction physics. This simplicity may be lost if one uses dynamics generated by the different intent of simplifying nuclear spectroscopy. We explain. Let us suppose that the renormalization group successfully eliminates matrix elements of the nucleon-nucleon (or inter-nucleon) potential connecting low and high relative momentum states, leading to an accurate reproduction of nuclear binding energies and spectra. This procedure would also lead to wave functions without high-momentum components and truly short ranged-correlations. However, it would be necessary to consistently transform all other operators (Anderson *et al.*, 2010; Neff *et al.*, 2015) in order to calculate observables. For high momentum transfer reactions, the renormalization group changes a known simple probe, described by a single-nucleon operator, into a more complicated probe describable by unknown (in practice) A -nucleon operators. This could prevent the efficient analysis of any high momentum transfer experiment. The same remark holds for chiral potentials. The use of cutoff, as in Eq. (3) leads to the violation of current conservation in electromagnetic interactions unless the currents are modified substantially. For example, one could use minimal substitution, which would introduce terms involving several powers of the electromagnetic potential A^μ . This means that the simplicity of using electromagnetic probes would be lost because of the need to use very complicated operators to analyze experiments. Again we reach the same conclusion: the use of potentials with strong momentum-dependence is not optimum for the purpose of using high momentum transfer electromagnetic processes to understand the short-range structure of nuclei.

(4) Second order effects of the tensor term of the one-pion exchange potential are common to all of these approaches, since the beginning (Bethe, 1971; Bogner *et al.*, 2005; Brown, 1967; Holt *et al.*, 2013; Machleidt, 1989) and through to the current days of effective field theory. These effects are large enough to cause convergence difficulties in the application of Brueckner theory (Vary *et al.*, 1973), and also cause challenges in defining the power counting which defines any effective field theory (Bedaque and van Kolck, 2002).

The effect of this on the relative s -wave function of two nucleons in nuclei can be characterized by the effective potential

$$V_{00} = V_T \frac{1}{E - H_0} Q V_T, \quad (4)$$

where V_T is the tensor potential, the subscript 00 indicates an s -wave to s -wave matrix element, H_0 is the Hamiltonian in the absence of V_T , and Q is a projection operator taking the Pauli principle into account. The operator V_{00} has a major effect on the density distribution and correlation function (as discussed in the Appendix). These effects occur in *all* existing approaches. A major

purpose of this review is to show that the influence of the correlations induced by the tensor force is manifest in high momentum transfer reactions.

To summarize, nuclear theorists have made tremendous progress in understanding the connections between NN potentials and QCD, as well as in calculating nuclear energies and states. High momentum transfer experiments are easier to analyze using well-defined current operators, rather than using transformed A -nucleon operators with a renormalization-group-transformed potential. These well-defined current operators can be used if the effects of correlations are maintained in the nuclear wave function instead of being hidden in the current operators through the use of the renormalization group or very soft NN potentials. However, regardless of approach, the influence of the correlations induced by the tensor force is manifest in all theoretical approaches to date, and, as we shall see, is manifest in high momentum transfer reactions.

3. Short-ranged two-nucleon clusters

As discussed in previous Sections, in the nucleus, nucleons behave approximately as independent particles in a mean field created by their average interaction with the other nucleons. But occasionally (20 – 25% in medium/heavy nuclei) two nucleons get close enough to each other so that temporarily their singular short range interaction cannot be well described by a mean field approximation. **These are the two nucleon short-ranged correlations (2N-SRC), defined operationally in experiments as having small center of mass momentum and large relative momentum.** These pairs are predominantly neutron-proton pairs. Colle *et al.* (Colle *et al.*, 2015) show that it is predominantly nucleon-nucleon pairs in a nodeless relative- S state of the mean-field that create these 2N-SRC. The force between the nucleons in the pair is predominantly a tensor force which creates a pair with the quantum numbers of the deuteron ($S = 1, T = 0$), a neutron-proton system (Vanhalst *et al.*, 2011).

The two nucleons in 2N-SRC have a typical distance of about 1 fm which means that their local density is a few times higher than the average nuclear density. The relative momentum of the two nucleons in the pair can be a few times the Fermi momentum, k_F , which is large. SRC of more than two nucleons probably also exist in nuclei, and might have higher density than that of the 2N-SRC. However their probability is expected to be significantly smaller than the probability of 2N-SRC (Bethe, 1971).

The 2N-SRC are isospin-dependent fluctuations. For example, the deuteron is the only bound two-nucleon system. We know now that density fluctuations involving one neutron and one proton occur more often than those involving like-nucleons, see Sect. II C. Therefore we ex-

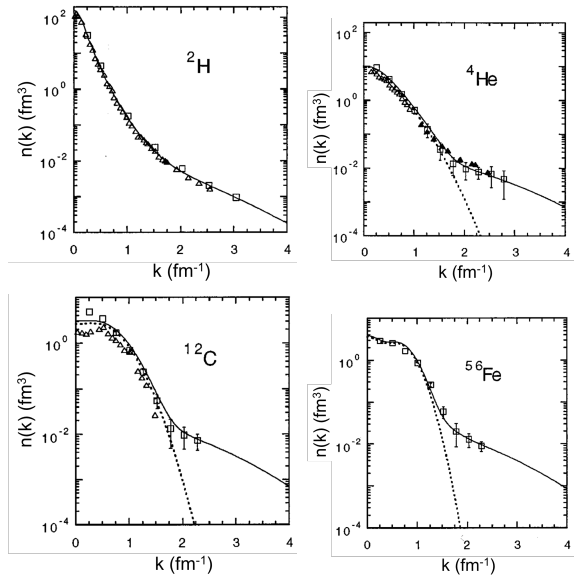


FIG. 4: The nucleon momentum distributions $n_0(k)$ (dashed line) and $n(k)$ (solid line) plotted versus momentum in fm^{-1} for the deuteron, ${}^4\text{He}$, ${}^{12}\text{C}$ and ${}^{56}\text{Fe}$. Figure adapted from (Ciofi degli Atti and Simula, 1996a).

amine the deuteron first.

The simplest nucleus, the deuteron has spin $S = 1$, isospin $T = 0$, and $J^\pi = 1^+$. The relevant quantity for electron scattering is $n(k)$ which is the probability of finding a nucleon of momentum between k and $k + dk$. This function is the sum of two terms, one arising from the $l = 0$ (s -wave), and the other from the $l = 2$ (d -wave). At momenta of interest for short range correlated pairs (i.e., p significantly greater than $p_F \approx 250 \text{ MeV}/c$, where p_F is the typical Fermi momentum for medium and heavy nuclei), the otherwise-small d -wave becomes very important. This is especially true at $p \approx 400 \text{ MeV}/c$ where there is a minimum in the s -wave. In the Argonne V18 potential (Wiringa *et al.*, 2014b) the d -wave component is due to the pion exchange tensor force. The combination of d - and s -waves leads to a “broad shoulder” in the deuteron momentum distribution, which extends from about 300 to 1400 MeV/c in the AV18 potential. See Sect. IX for an explanation. This broad shoulder is also a dominant feature in the tail of the single-nucleon momentum distributions computed with realistic internucleon interactions, see Fig. 4, in particular with the AV18 potential for $A \leq 12$ (Wiringa *et al.*, 2014b) and more effective approaches for heavier systems (Ciofi degli Atti and Simula, 1996b; Ryckebusch *et al.*, 2015).

”This broad shoulder is also a dominant feature in the tail of the single-nucleon momentum distribution calculated with realistic local NN interactions (see Fig.4), in particular with the AV18 potential in $A \leq$

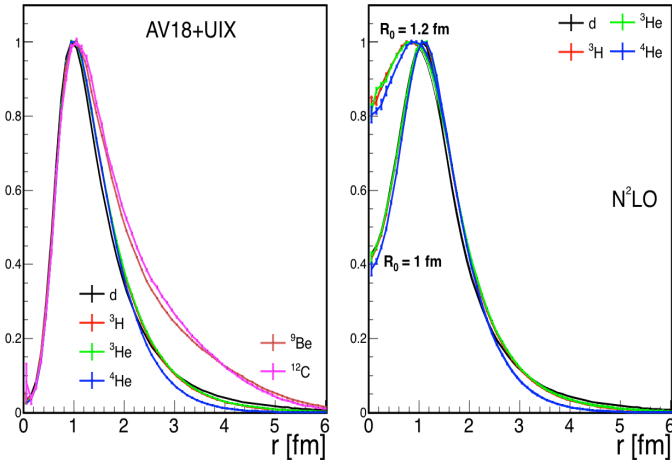


FIG. 5: Scaled two-body distribution function $\rho_{2,1}^A(r)/A$ (see Eq. (83)) for nuclei with $A = 2, 3, 4$. A correlation hole is seen for all of these nuclei. The two sets of curves are obtained with the AV18+UIX (left) and N^2LO (right) potentials. Figure adapted from (Chen *et al.*, 2016). The meaning of R_0 is discussed in the text.

12(Wiringa....)."

We can also consider the spatial wave function of the nucleus. The short range part of the NN interaction gives a correlation hole at small NN relative distances, see Fig. 5. Precise definitions are given in Sect. IX. Calculations with various bare realistic interactions show that, apart from a normalization factor depending upon the different number of pairs in different nuclei, the relative two-nucleon density $\rho_{rel}(r)$ and its spin-isospin components $\rho_{ST}^{N_1 N_2}(r)$ at $r \leq 1.5$ fm exhibit similar correlation holes, generated by the interplay of the short-range repulsion and the intermediate-range tensor attraction of the NN interaction, with the tensor force governing the overshooting at $r \simeq 1.0$ fm. The correlation hole is universal, in that it is almost independent of the mass A of the nucleus (C. Ciofi degli Atti, 2015). The depth of the correlation hole depends on the short-distance behavior of the potential. The value of R_0 shown in Fig. 5 refers to the cutoff on the short distance N^2LO nucleon-nucleon potential, as defined in (Gezerlis *et al.*, 2014). A correlation hole is seen to occur for $R_0 = 1$ fm, but is much less deep for $R_0 = 1.2$ fm. The use of such a soft potential may not be suitable in the present context because it predicts erroneous nucleon-nucleon phase shifts for the 3D_1 partial wave, and also for lab energies greater than 250 MeV.

In summary, we state that short-range correlations in light nuclei have been examined recently theoreti-

cally from several points of view (Ciofi degli Atti, 2015; Feldmeier *et al.*, 2011; Rios *et al.*, 2014; Ryckebusch *et al.*, 2015; Vanhalst *et al.*, 2011, 2012; Weiss *et al.*, 2015; Wiringa *et al.*, 2014a). One consistent finding of such work is the dominance of np deuteron-like pairs ($ST = 10$) over other pairs at high momentum.

In momentum space, the existence of this universal correlation hole translates into nucleon momentum distributions $n_A(p)$ that are significant at large momentum ($p \geq p_F$) and that are similar for all nuclei, $n_A(p) \propto n_d(p)$, at these large momenta (Alvioli *et al.*, 2013; Ciofi degli Atti and Simula, 1996a; Frankfurt and Strikman, 1981a, 1988b). Frankfurt and Strikman realized that these could be measured with hard probes (see Section II).

Ciofi degli Atti and Simula (Ciofi degli Atti and Simula, 1996a; Ciofi degli Atti *et al.*, 1991b) used this similarity to model the nucleon spectral function $P(\mathbf{p}, E)$ (the joint probability to find a nucleon in a nucleus with momentum \mathbf{p} and removal energy E) for all nuclei

$$P(\mathbf{p}, E) = \langle \Psi | b^\dagger(\mathbf{p}) \delta(E - H) b(\mathbf{p}) \Psi \rangle, \quad (5)$$

where $|\Psi\rangle$ represents the nuclear wave function and spin, isospin and nuclear (A) labels are suppressed for simplicity. The momentum density $n(\mathbf{p})$ is given by

$$n(\mathbf{p}) = \int dE P(\mathbf{p}, E). \quad (6)$$

These authors write

$$P(\mathbf{p}, E) = P_0(\mathbf{p}, E) + P_1(\mathbf{p}, E) \quad (7)$$

where the subscript zero refers to values of E corresponding to low-lying intermediate excited states and subscript one refers to high-lying continuum states that are caused by the short-ranged correlations. Therefore one also has $n(\mathbf{p}) = n_0(\mathbf{p}) + n_1(\mathbf{p})$, where $n_1(\mathbf{p})$ is associated with the high momentum caused by short-ranged correlations. $n_0(p)$ is typically dominant for $p < 250$ MeV/c or so and $n_1(p)$ becomes dominant for larger values. Furthermore, $n_1(p)$ is almost independent of A at $p > 400$ MeV/c and attribute this to NN correlations. See Fig. 4.

SRC pairs are conventionally defined in momentum space as a pair of nucleons with high relative momentum and low center of mass (c.m.) momentum, where high and low are relative to the Fermi momentum of medium and heavy nuclei. Thus the most prominent effect of SRC will be to populate high-momentum states in the nuclear momentum distribution. As conventional mean-field theories predict only a very small high-momentum tail, the effect of SRCs there should be substantial. Formally, one needs the two-nucleon momentum density, $n(\mathbf{p}_1, \mathbf{p}_2)$ (see Section IX), where $\mathbf{p}_{tot} = \mathbf{p}_1 + \mathbf{p}_2$ and $\mathbf{p}_{rel} = \frac{1}{2}(\mathbf{p}_1 - \mathbf{p}_2)$ are the center of mass and relative momenta of the two nucleons. Studies of spectral functions show that at large values of p_{rel} , the two-nucleon momentum density factorizes:

$$n(\mathbf{p}_{tot}, \mathbf{p}_{rel}) = n(p_{tot})n(p_{rel}). \quad (8)$$

A justification of this factorization is presented in Sect. IX.

The coordinate-space correlation holes (Fig. 5) give similar NN relative (p_{rel}) momentum distributions (at large p_{rel}) in all nuclei. Exact calculations with the AV18 potential for ${}^4\text{He}$, show that, at small p_{tot} there is a minimum in p_{rel} for pp pairs at $p_{rel} = 400 \text{ MeV}/c$. This is because, at small p_{tot} , the pp pair must be in a relative s -state which has a minimum at $p_{rel} = 400 \text{ MeV}/c$, just like in deuterium. For np pairs, this minimum is filled in by the d -wave caused by the short range pion-exchange tensor force (Wiringa *et al.*, 2014b).

Thus, the combination of the minimum in the s -wave momentum distribution at $p \approx 400 \text{ MeV}/c$ and the filling in of this minimum by the d -wave pion-exchange tensor force, leads to the expected dominance of np correlated pairs over nn and pp pairs at $300 \leq p \leq 500 \text{ MeV}/c$. This ratio of np to pp pairs should decrease at relative momentum significantly greater than $400 \text{ MeV}/c$, the s -wave minimum (as we will discuss Section II).

Results from electron and proton scattering experiments indicate that the high-momentum tail of the momentum distribution of nucleons in nuclei is universal: in all measured nuclei, ranging from Deuterium to Gold, the high momentum distributions are similar and differ only by a scale factor (i.e. $n_A(p \geq p_F) = a_2(A/d) \cdot n_d(k)$). In medium and heavy nuclei (i.e., $A \geq 12$) these high-momentum nucleons account for 20 – 25% of the nucleons in the nucleus and are observed to primarily belong to SRC pairs, with proton-neutron (pn) pairs dominating over proton-proton (pp) and neutron-neutron (nn) pairs by a factor of about 20, even in neutron rich heavy nuclei. See Section II for details.

These facts described in this sub-section lead to an effective description of nuclei in momentum space as having two important regions: (1) a mean-field region ($k \leq p_F$), which accounts for about 80% of the nucleons, where the many-body dynamics result in single nucleons moving under the influence of an effective potential created by the residual $A - 1$ system and (2) a high-momentum region ($p \geq p_F$), which accounts for about 20% of the nucleons (but 70% of the kinetic energy (Benhar *et al.*, 1989; Polls *et al.*, 1994)), where nucleons are predominantly in the form of pn -SRC pairs, having a very weak interaction with the residual $A - 2$ system.

To summarize, the high momentum nucleons in nuclei are mainly due to 2N-SRC and are therefore associated with high density fluctuations in the nucleus. In what follows (see Section III.D) we will examine the hypothesis that these temporary high density/large momentum ‘hot spots’ are the sites where the nucleon internal structure is modified and the EMC effect is created. First, we will present the experimental evidence for short range correlations.

II. Hard scattering and Short-Range Correlations

A. Hard Reactions

In optics the resolving power is the minimum resolvable distance at which an imaging device can separate two closely spaced objects. This is normally proportional to the wavelength of the light. The smaller the wavelength, the better the resolution.

We often scatter particles to try to resolve the internal structure of a complex target. The sizes of the target and its constituents define the required resolving power. For example, to observe the nucleus of an atom one needs a spacial resolution of about 10 fm, to observe nucleons in nuclei one needs a resolution of about 1 fm, and to observe the partonic structure of a nucleon one needs sub-fermi resolution.

The spacial resolution of a scattering experiment is determined by the de Broglie wave length (λ) of the probe (scattering particle) and the momentum transfer of the reaction (q). We define as ‘hard’ a process that fulfills the following conditions: $\lambda \ll R$ and $qR \gg 1$, where R is the size of the target or the structure to be studied. In practice, these kinematic conditions are not always rigorously met. Nevertheless, as we next explain, the empirical results seem valid.

In this paper we are dealing with two reactions and the connection between them. Deep inelastic scattering (DIS) attempts to resolve the partonic structure of nucleons and quasielastic scattering (QE) attempts to resolve the nucleonic structure of nuclei. These reactions have different required resolutions and hence different kinematical conditions to achieve them.

For (e, e') DIS reactions, which are typically measured as a function of $x_B = Q^2/2M\nu$ for $x_B < 1$, there are two important parameters, the 4-momentum transfer squared of the virtual photon, Q^2 , and the invariant mass of the virtual photon plus struck nucleon, $W = \sqrt{M^2 + 2M\nu - Q^2}$. Since x_B, Q^2 , and W are all functions of the same two variables, only two are independent.

Early studies at the high energy facilities (SLAC and CERN) measured DIS for $5 \leq Q^2 \leq 50 \text{ GeV}/c^2$ and found that the ratios of DIS cross sections for $0.3 \leq x_B \leq 0.7$ are largely independent of Q^2 (Norton, 2003). The newer JLab experiments used lower lepton energies (typically 4 – 5 GeV) therefore lower Q^2 , $4 \leq Q^2 \leq 6 \text{ GeV}^2$ (Seely *et al.*, 2009a).

To observe the internal structure of a proton or neutron with DIS, the value of W needs to be large enough to avoid the influence of individual nucleon resonances, which cause the cross section to fluctuate rapidly with W . Typically this means $W \geq 2 \text{ GeV}$. The higher-energy SLAC and CERN measurements required $W \geq 2 \text{ GeV}$. However the lower-energy JLab data required only $W \geq 1.4 \text{ GeV}$.

For inclusive (e, e') QE scattering, there are again only two independent kinematical variables, normally chosen to be Q^2 and x_B . However, in addition to making sure that the resolving power is sufficient, we also need to optimize the kinematics to select scattering from high-momentum nucleons in the nucleus and to reduce the effects of non-single-nucleon currents. In order to resolve nucleons in SRC pairs, measurements are typically made at $Q^2 > 1.5$ (GeV/c) 2 . Large ($p > p_F$) minimum initial momentum of the struck nucleon (assuming no final state interactions) can be selected at $Q^2 > 1.5$ (GeV/c) 2 by choosing either $x_B \geq 1.5$ or $x_B \leq 0.6$ (see Section II.B). $x_B \geq 1$ is preferred, so that the energy transfer is smaller, inelastic processes (resonance production, meson exchange currents [MEC] and isobar configurations [IC]) are suppressed, and the reaction is more sensitive to the nuclear momentum distribution. Increasing Q^2 further suppresses MEC contributions. The inclusive QE scattering data discussed in Section II.B were measured at $x_B \geq 1.5$.

In exclusive and semi-exclusive reactions, $(e, e'p)$ and $(e, e'pN)$, large initial nucleon momenta can be selected directly and the x_B restrictions can be relaxed (see Section II.C).

B. Inclusive Scattering

We can probe the momentum distribution of nucleons in the nucleus through inclusive quasi-elastic electron scattering. Elastic scattering from a nucleon at rest occurs at fixed kinematics, $\nu = \frac{Q^2}{2M}$ (where ν is the energy transfer, M is the nucleon mass, and $Q^2 = \mathbf{q}^2 - \nu^2$ is the four-momentum transfer). This corresponds to $x_B = 1$. If all of the struck nucleons in a nucleus were at rest, the cross section would show a pronounced narrow peak—the quasi-elastic peak.

This peak is broadened by nucleon motion for electron scattering from bound nucleons. In order to study nuclear momentum distributions, experiments typically focus on the low energy transfer side of the QE peak, or $x_B \geq 1$. In this case the initial momentum of the struck nucleon must be in the opposite direction from the momentum transfer so that the final momentum of the struck nucleon $\mathbf{p}_f = \mathbf{q} + \mathbf{p}_i$ (in the absence of final state interactions or FSI) is less than the momentum transfer. As the energy transfer decreases, the final momentum of the struck nucleon must decrease and therefore the minimum initial momentum of the struck nucleon must increase.

The quasielastic inclusive electron scattering (e, e') cross section can be written in terms of a function F that depends on (Q^2, y) rather than (Q^2, ν) (Day *et al.*,

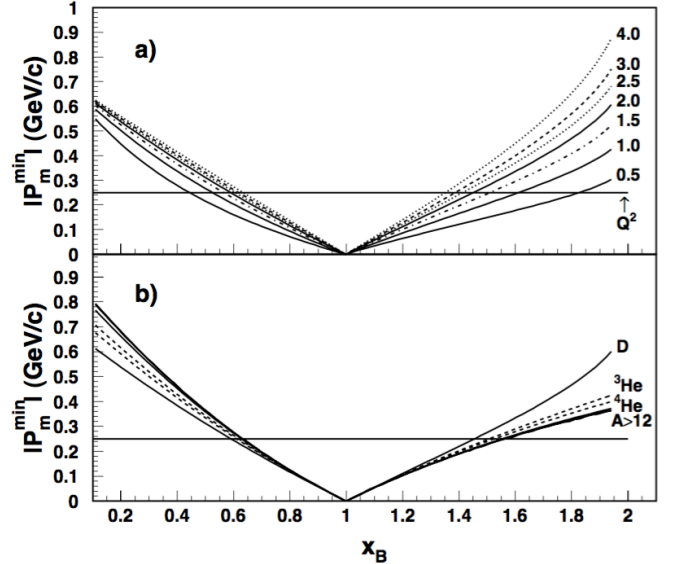


FIG. 6: The minimum momentum of the struck nucleon in inclusive (e, e') scattering as a function of x_B . The top panel shows the minimum momentum for deuterium for a variety of momentum transfers and the bottom panel shows the minimum momentum for a variety of nuclei at $Q^2 = 2$ GeV 2 . The residual $A - 1$ system is assumed to be in its ground state. Figure reproduced from (Egiyan *et al.*, 2003).

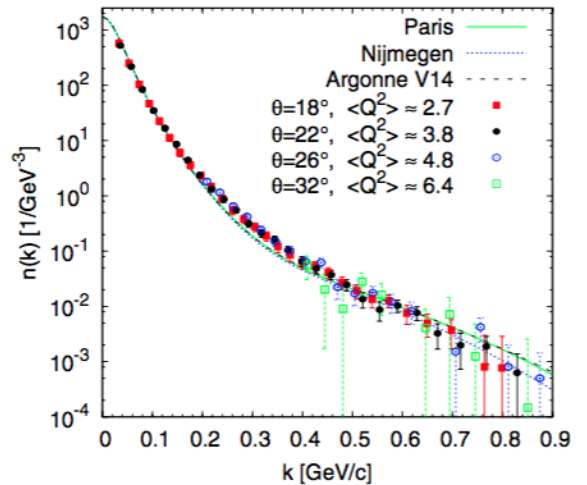


FIG. 7: Momentum distribution of the deuteron. Points show the results extracted from the experimental scaling function $F(y)$ at four different momentum transfers (Fomin *et al.*, 2012a). Curves show the calculated momentum distributions using three different NN potentials Paris (Lacombe *et al.*, 1981), Nijmegen (Stoks *et al.*, 1994b) and Argonne V14 (Wiringa *et al.*, 1995a). Figure reproduced from (Fomin *et al.*, 2012a), which uses k for momentum instead of p .

1987):

$$\frac{d^2\sigma(q, \nu)}{d\nu d\Omega} = F(y, Q^2)(Z\sigma_p + N\sigma_n) \frac{q}{\sqrt{M^2 + (y+q)^2}} \quad (9)$$

where $\sigma_{p,n}$ are the elastic scattering cross sections from a bound nucleon, the last term is the Jacobian $dy/d\nu$, and $y = y(Q^2, \nu)$ is the minimum momentum of the struck nucleon (assuming that the residual $A-1$ system is unexcited) (Arrington *et al.*, 2012; Day *et al.*, 1990).

Non-relativistically, y is the component of the struck nucleon's initial momentum (\mathbf{p}_i) in the direction of \mathbf{q} . The cross section at fixed y then includes an integral over the perpendicular components of \mathbf{p}_i . Relativistically, it is a little more complicated. y is determined from energy conservation, assuming no FSI and that the $A-1$ nucleus recoils with momentum y :

$$\nu + M_A = (M^2 + (q+y)^2)^{1/2} + (M_{A-1}^2 + y^2)^{1/2} \quad (10)$$

At the QE peak, $\nu = Q^2/(2M)$, $x_B = 1$, and $y = 0$. As ν decreases, x_B increases and y decreases. By selecting x_B or y (at fixed Q^2), we can select the minimum initial momentum of the struck nucleon (see Fig. 6). At large enough Q^2 the function $F(y, Q^2)$ scales and depends only on y (Ciofi degli Atti *et al.*, 1991a). The nucleon momentum distribution, $n(p=y)$, can be calculated from the derivative of the scaling function, $dF(y)/dy$, at large Q^2 :

$$n(p) = \frac{-1}{2\pi k} \frac{dF(p)}{dp}. \quad (11)$$

Fig. 7 shows the deuteron momentum distribution derived in this manner.

Although this method has very large uncertainties, we can compare the momentum distributions in different nuclei with reduced uncertainties by taking ratios of cross sections. We write the momentum density in terms of the light cone variable α_{tn} for the interacting nucleon belonging to the correlated pair,

$$\alpha_{tn} = 2 - \frac{\nu - q + 2M}{2M} (1 + \sqrt{1 - 4M^2/W^2}). \quad (12)$$

In this case we can write the cross section ratio in terms of the light-cone nucleon density at large Q^2 and $1.5 < x_B < 2$ as (Frankfurt *et al.*, 1993):

$$\frac{\sigma_{A_1}(x_B, Q^2)}{\sigma_{A_2}(x_B, Q^2)} = \frac{\int \rho_{A_1}(\alpha_{tn}, p_t) d^2 p_t}{\int \rho_{A_2}(\alpha_{tn}, p_t) d^2 p_t} \approx \frac{n_A(p)}{n_D(p)}. \quad (13)$$

Thus this ratio of cross sections should be a function of α_{tn} only, which, since it is a function of (Q^2, x_B) , is directly related to y , the minimum momentum of the struck nucleon. The approximate equality shown in Eq. (13) holds for $1.3 \leq \alpha_{tn} \leq 1.7$ and $p > p_F$. The second approximate equality appearing in Eq. (13) is obtained using the relation $k \approx M(1 - \alpha_{tn}/\sqrt{\alpha_{tn}})(2 - \alpha_{tn})$. Measured ratios should be less sensitive to the influence of

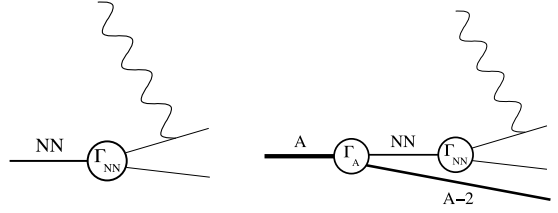


FIG. 8: A cartoon of electron quasielastic scattering from a nucleon in deuterium (left) and from a nucleon in a SRC pair in a heavier nucleus (right). The labels Γ_{NN} and Γ_A refer to the deuteron and nuclear vertex functions respectively.

final state interactions, as discussed below. Nevertheless, the accuracy of replacing cross section ratios by ratios of densities, as shown in Eq. (13), needs to be studied further. Furthermore, as yet there is no separate calculation of individual numerator and denominator terms of Eq. (13), *i.e.*, the basic cross section for the (e, e') reaction at large values of x_B .

Physics at large values of x_B . The next step is to use the inclusive (e, e') cross section to look for the effects of SRC pairs in nuclei by choosing kinematics where mean field nucleons cannot contribute to the reaction. This is done by using $x_B > 1$. Just as conservation of four-momentum ensures that $x_B = 1$ is the kinematic limit for scattering from a single nucleon, $x_B = 2$ is the kinematic limit for scattering from a cluster of two nucleons. Similarly $x_B = 3$ is the kinematic limit for scattering from a three-nucleon cluster.

As a result, we can expand the (e, e') cross section into pieces due to electrons scattering from nucleons in 2-, 3- and more-nucleon SRC (Frankfurt and Strikman, 1981a, 1988b; Frankfurt *et al.*, 1993)

$$\sigma(x_B, Q^2) = \sum_{j=2}^A a_j(A) \sigma_j(x_B, Q^2), \quad (14)$$

where $\sigma_j(x_B, Q^2) = 0$ for $x_B > j$ and the $\{a_j(A)\}$ are proportional to the probability of finding a nucleon in a j -nucleon cluster. This is analogous to treating nuclear structure in terms of independent nucleons, independent nucleon pairs, etc.

If we consider only the a_2 term, then we can write

$$a_2(A) = \frac{2}{A} \frac{\sigma_A(x_B, Q^2)}{\sigma_d(x_B, Q^2)}. \quad (15)$$

This approximation should be valid for $1.5 < x_B \leq 2$. The effect of neglecting clusters of three or more nucleons has never been studied. The accuracy this approximation depends on the lack of interference between amplitudes arising from scattering by clusters of different nucleon number.

If the momentum distribution for $|y| > p_{fermi}$ is dominated by nucleons in SRC pairs, then we expect that the momentum distributions for nucleus A and for deuterium should be almost identical. This similarity should show up as a plateau in the per-nucleon cross section ratio of the two nuclei. Fig. 8 shows a cartoon of this process.

The cross section ratio of nucleus A to deuterium or to ^3He has been measured at SLAC (Frankfurt *et al.*, 1993) and at Jefferson Lab (Egiyan *et al.*, 2003, 2006a; Fomin *et al.*, 2012a). They have all observed a plateau in the cross section ratio at $Q^2 > 1.4 \text{ GeV}^2$ and from $1.5 \leq x_B \leq 1.9$. See Fig. 9. This corresponds to $y \geq p_{thresh} = 275 \pm 25 \text{ MeV}/c$, which is larger than the Fermi momentum in medium and heavy nuclei.

However, in order to relate these observed plateaus to the ratio of momentum distributions in the different nuclei, we need to take into account the final state interactions (FSI) of the nucleon its correlated partner and with the residual system. For $Q^2 > 1 \text{ GeV}^2$ and $0.35 < \nu < 1 \text{ GeV}$, the space-time physics (Frankfurt *et al.*, 2008, 1993) of the inclusive process tells us that final state interaction effects occur predominantly within the two-nucleon correlation. Such effects are independent of the nuclear target, and should be small for large values of ν . The relevant values of ν are large enough so that final state interactions within the pair are not very important (Frankfurt and Strikman, 1981a, 1988b). Therefore, the effects of FSI will be approximately the same for high momentum nucleons in deuterium and in heavier nuclei and will predominantly cancel in the cross section ratios.

Some measurements, e.g., (Egiyan *et al.*, 2003, 2006a), applied isoscalar corrections to the ratios of Eq. 15 (i.e., they corrected for the unequal electron-proton and electron-neutron cross sections). Since the discovery of pn -dominance in SRC pairs (see Section II.C), these corrections are no longer applied (Fomin *et al.*, 2012a).

The flatness of the cross section ratio plateau at $Q^2 > 1.4 \text{ GeV}^2$ and from $1.5 \leq x_B \leq 1.9$ indicates the similarity of the momentum distributions in the two nuclei for $p > p_{thresh}$ and the validity of the expansion in Eq. 14. The onset of the plateau at $x_B = 1.5$ for $Q^2 > 1.4 \text{ GeV}^2$ indicates that the momentum distributions become similar at a threshold momentum of $p_i = p_{thresh} = 275 \pm 25 \text{ MeV}/c$ (Egiyan *et al.*, 2003). The height of the plateau, $a_2(A)$, indicates the relative probability that a nucleon in nucleus A has high momentum ($p > p_{thresh}$) relative to a nucleon in deuterium.

In a naive model, this relative probability for a nucleon to have high momentum equals the relative probability that it belongs to an NN SRC pair. However, even if all nucleons with $p > p_{thresh}$ belong to an NN SRC pair (see Section II.C), we still need to consider the effects of pair motion. The high momentum NN pair in the deuteron has center of mass momentum $p_{cm} = 0$. The non-zero center of mass momentum distribution of the pair in heavier nuclei will smear the high-momentum tail of the

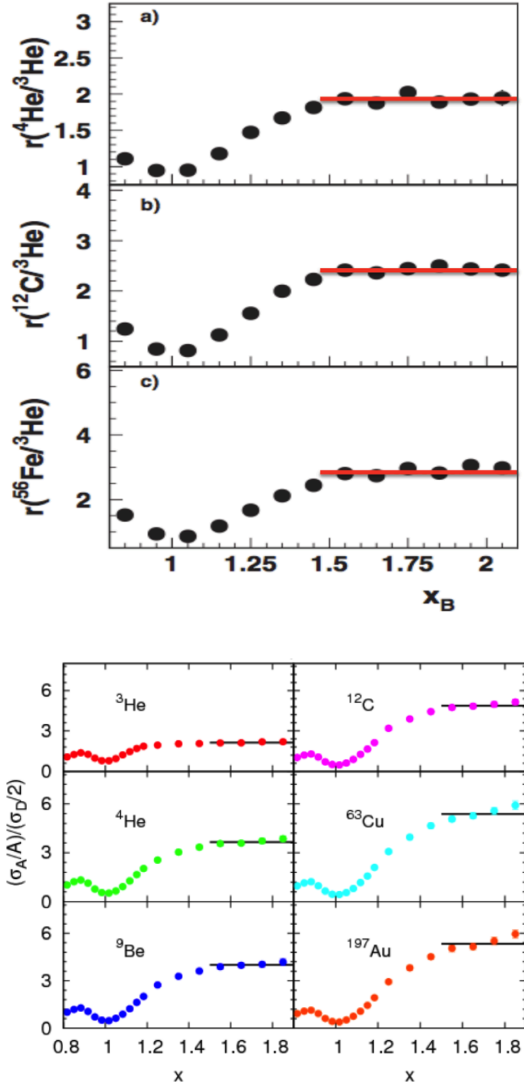


FIG. 9: Inclusive per-nucleon cross section ratios of (top) nuclei to ^3He from (Egiyan *et al.*, 2006a) at $1.4 < Q^2 < 2.6 \text{ GeV}^2$ and (bottom) nuclei to deuterium at $Q^2 = 2.7 \text{ GeV}^2$ (Fomin *et al.*, 2012a).

nucleon momentum distribution, increasing the cross section ratio in the plateau region (Ciofi degli Atti *et al.*, 1991b; Fomin *et al.*, 2012a; Vanhalst *et al.*, 2012). This was found to be about a 20% effect in Fe. Thus, while the ratio of the proportion of high-momentum nucleons in Cu to deuterium is $a_2(A) = 5.4 \pm 0.1$, the ratio of the number of SRC NN pairs in Cu to deuterium (using the Fe correction factor) is about 20% less, $R_{2N} = 4.3 \pm 0.3$ (Fomin *et al.*, 2012a).

Multiplying the 4% probability for a nucleon in deuterium to have momentum $p > p_{thresh}$ by the measured ratios in the plateau region ($a_2(A)$), as indicated by Eq. (13), gives us the probabilities for a nucleon to have

high momentum in ${}^4\text{He}$, C, Fe/Cu and Au to be 14%, 19%, 21% and 21% respectively (Fomin *et al.*, 2012a; Hen *et al.*, 2012).

Thus, the existence of a plateau in the measured per-nucleon cross section ratios of various nuclei to deuterium or ${}^3\text{He}$ at $Q^2 > 1.4 \text{ GeV}^2$ and $1.5 \leq x_B \leq 1.9$ shows that the momentum distributions of all nuclei at high momentum are similar and are thus dominated by 2N-SRC, that the threshold for “high momentum” is $p_{\text{thresh}} = 275 \pm 25 \text{ MeV/c}$, and that the probabilities for nucleons in nuclei to have high momentum range from 4% in deuterium to 21% in heavy nuclei.

While the inclusive scattering cross section ratios of carbon and iron to ${}^3\text{He}$ measured by Egiyan are flat for $1.5 < x_B < 2$, the ratios of carbon, copper and gold to deuterium measured by Fomin appear to slope upwards slightly. This is not due to the choice of nucleus in the denominator, since the ratio of ${}^3\text{He}$ to deuterium measured by Fomin is flat. This might be due to differences in kinematics. The Egiyan data covers $1.4 < Q^2 < 2.6 \text{ GeV}^2$ (concentrated at the lower values), while the Fomin data was taken at $Q^2 = 2.7 \text{ GeV}^2$. At $Q^2 = 1.5 \text{ GeV}^2$ and $1.5 \leq x_B \leq 2$, the minimum momentum of the struck nucleon ranges from 250 to 500 MeV/c, covering the expected region of tensor force dominance. However, at $Q^2 = 2.7 \text{ GeV}^2$, the minimum momentum of the struck nucleon ranges from 320 to 700 MeV/c, where central correlations could become important. It would be useful to measure the Q^2 dependence of the cross section ratios in future SRC measurements.

C. Exclusive Scattering

The study of SRCs using exclusive reactions has a long history that extends beyond the scope of this review. Here we focus only on exclusive measurements performed with high energy probes and large momentum transfer (hard reactions). See (Kelly, 1996) and references therein for a review of the older measurements. We use the term exclusive to refer to measurements in which, in addition to the scattered probe particle, two knocked-out nucleons are measured in the final state.

In the context of SRC studies, exclusive reactions are hard processes in which a probe scatters from one nucleon in an SRC pair and all particles emitted in the final state (e.g., the scattered probe and both nucleons of the pair) are detected. The energy of the probe and the momentum transfer are large enough so that the probe interacts with a single, high-momentum ($p_i > p_F$) nucleon in the pair. If the pair was at rest ($p_{cm} = 0$) and neither nucleon rescattered as it left the nucleus, then the struck nucleon’s correlated partner would recoil with momentum $\mathbf{p}_2 = -\mathbf{p}_i$. This back-to-back angular correlation between the initial momentum of the knocked out nucleon and the momentum of the recoil nucleon is

a clear experimental signature for exactly two nucleons being involved in the interaction.

However, other reaction mechanisms can also involve two nucleons, leaving the residual $A - 2$ nucleus almost at rest. The probe can scatter from one nucleon, which can rescatter from a second (FSI), the probe can scatter from a meson being exchanged between two nucleons (MEC), or the probe can excite the first nucleon which can then de-excite via interaction with a second nucleon (IC). Disentangling these competing and interfering effects can be difficult. However, the effects of MEC and IC can be dramatically decreased by choosing kinematics with $x_B > 1$ and with larger Q^2 . The effects of FSI can also be dramatically decreased by (a) choosing kinematics where the relative momentum of the two final-state nucleons is large and (b) avoiding kinematics where the opening angle between the two outgoing nucleons is $70 - 90^\circ$. (Nonrelativistically, when one billiard ball scatters from a second billiard ball at rest, the opening angle in the final state is 90° .)

The detection of the outgoing nucleons in exclusive reactions provides complementary information to the inclusive reactions discussed above. By detecting the struck nucleon at large p_{miss} and looking for the recoil partner nucleons, exclusive measurements can measure the fraction of high-momentum nucleons belonging to SRC pairs. They can also extract information on the SRC pair isospin structure and p_{cm} distribution, as well as their A and momentum dependence.

This additional information however comes at the price of increased sensitivity to FSI. FSI can be generally split into two main contributions: re-scattering between the nucleons of the pair, and re-scattering between the nucleons of the pair and the residual $A - 2$ system. Rescattering between the nucleons of the pair will alter the measured relative momentum but leave p_{cm} unchanged. Rescattering between the nucleons of the pair and the residual $A - 2$ system will change the momentum of the outgoing nucleons and “attenuate” them. The attenuation of the nucleons as they traverse the nucleus is usually referred to as the ‘nuclear transparency’ and limits the spatial region probed in the experiment to the outer part of the nucleus. It can be calculated in the Glauber approximation (for large enough nucleon momentum). The momentum changes also affect the measured kinematical distributions. Here the use of high momentum transfer, as required for hard reactions, also allows using the Glauber approximation to calculate to the effects of FSI and to select kinematics to minimize their effects, either in the measured cross sections or the kinematical distributions.

Specifically, at $Q^2 \geq 1.5 - 2 \text{ (GeV/c)}^2$ and $x_B \geq 1$ (or proton scattering experiments at $|t|, |u|, |s| \geq 2 \text{ GeV/c}^2$) Glauber calculations show that the outgoing nucleons predominantly rescatter from each other and not from the residual $A - 2$ system. This implies that certain

quantities such as the total pair momentum, p_{cm} , and pair isospin structure are insensitive to rescattering while other quantities like the pair relative momentum, p_{rel} , are very sensitive to rescattering and thus cannot be reliably extracted from the experimental data, see (Frankfurt *et al.*, 1997; Shneor *et al.*, 2007) for details. The contribution of Meson Exchange Currents (MEC) and Isobar Currents (IC) are also minimized at high Q^2 and $x_B \geq 1$.

The first exclusive hard two nucleon knockout experiments, measuring the $^{12}\text{C}(p, 2pn)$ and $^{12}\text{C}(e, e'pN)$ reactions, were done at BNL and JLab, respectively (Piasetzky *et al.*, 2006; Shneor *et al.*, 2007; Subedi *et al.*, 2008; Tang *et al.*, 2003). These experiments scattered 5 - 9 GeV/c protons (BNL) and electrons (JLab) off high initial momentum ($300 \leq p_i \leq 600$ MeV/c) protons in ^{12}C and looked for a correlated recoil nucleon emitted in the direction of the missing momentum. The JLab experiment measured both proton and neutron recoils, whereas the BNL experiment only measured recoiling neutrons. Both experiments measured at large momentum transfer ($Q^2 \approx 2$ (GeV/c) 2), which suppressed competing reaction mechanisms and largely confined FSI to be between the nucleons of the pair.

The main results of the ^{12}C measurements are shown in Figs. 10, 11 and 12. Figs. 10 and 11 show the angular correlation between the momentum vector of the recoil nucleons and the reconstructed initial momentum of the knocked-out proton. For the BNL data, the angle is shown as a function of the recoil neutron momentum. Two distinct regions are visible: below the Fermi momentum where no angular correlation is observed, and above the Fermi momentum where a clear back-to-back correlation is seen. The width of the recoil nucleon opening angle distribution allowed extracting the pair c.m. motion; this motion can be described by a Gaussian distribution in each direction, with $\sigma = 143 \pm 17$ (BNL) and $\sigma = 136 \pm 20$ (JLab). These values are also in overall agreement with theoretical calculations (Ciofi degli Atti and Simula, 1996b; Colle *et al.*, 2014). The electron and proton reactions are characterized by completely different operators and FSI mechanisms; therefore the agreement of their c.m. momentum distributions validates the consistent treatment of FSI in these measurements.

Fig. 12 shows the extracted ratio of two nucleon knockout (proton-neutron and proton-proton) to single proton knockout events and the ratio of proton-neutron to proton-proton two-nucleon knockout events. The ratios are all corrected for finite acceptance effects and shown as a function of p_{miss} , the reconstructed initial momentum of the knocked out protons for $300 \leq p_{miss} \leq 600$ MeV/c. The ratio of single proton knockout to two nucleon knockout is directly related to the fraction of high-momentum protons that are in SRC pairs. As can be seen, within statistical uncertainties of about 10%, all single nucleon knockout events at $300 \leq p_i \leq 600$ MeV/c were accompa-

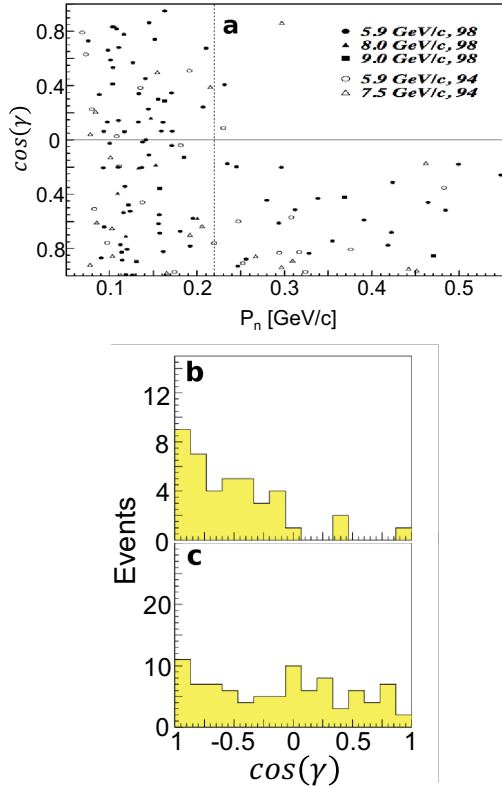


FIG. 10: Distributions of the relative angle (γ) between the reconstructed initial momentum of the knockout proton and the recoil nucleon. Results for $^{12}\text{C}(p, 2pn)$ events from BNL, shown as a function of the momentum of the recoil neutron (a) and for events with recoil neutron momentum greater than (b) and less than (c) $k_F = 225$ MeV/c. Note the transition from an isotropic distribution to a correlated one at about $k_F = 225$ MeV/c. Figures adapted from (Piasetzky *et al.*, 2006; Tang *et al.*, 2003).

nied by the emission of a recoil nucleon. The proton-to-neutron recoil ratio was found to be approximately 1:10, which corresponds to 20 times more np -SRC pairs than pp -SRC pairs in ^{12}C (Subedi *et al.*, 2008). This observed proton-neutron pair dominance was associated with the dominance of the tensor part of the nucleon-nucleon interaction at these initial moments (Sargsian *et al.*, 2005a; Schiavilla *et al.*, 2007).

A follow-up measurement of $^4\text{He}(e, e'pN)$ in similar kinematics set out to better constrain the importance of the tensor part of the NN interaction at short distance, and extend the experimental data to larger initial momenta, $400 \leq p_i \leq 800$ MeV/c (Korover *et al.*, 2014). At these higher momenta, the scalar repulsive core of the nucleon-nucleon interaction is expected to dominate over the tensor part, increasing the fraction of pp -SRC pairs. The ^4He nucleus was chosen to further reduce FSI and allow for comparisons with detailed ab-initio few-body

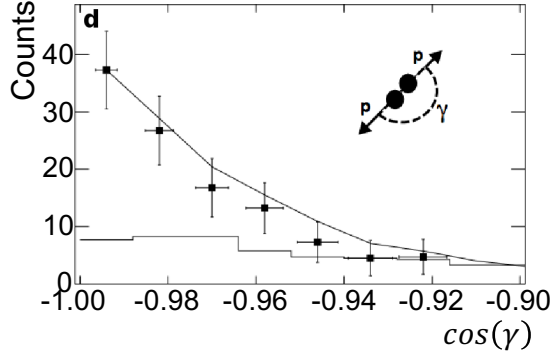


FIG. 11: Distributions of the relative angle (γ) between the reconstructed initial momentum of the knockout proton and the recoil nucleon. Results for $^{12}\text{C}(e, e'pp)$ events from JLab at kinematics corresponding to scattering off ~ 500 MeV/c initial momentum protons. Figure adapted from (Shneor *et al.*, 2007; Subedi *et al.*, 2008).

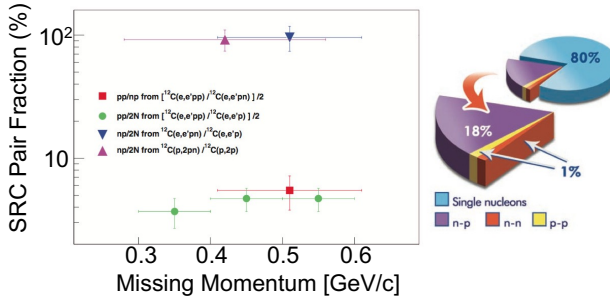


FIG. 12: The ratio of $^{12}\text{C}(e, e'pN)$ double knockout events to $^{12}\text{C}(e, e'p)$ single knockout events, shown as a function of the reconstructed initial (missing) momentum of the knocked-out proton from the $^{12}\text{C}(e, e'p)$ reaction. Triangles and circles mark $^{12}\text{C}(e, e'pn)$ and $^{12}\text{C}(e, e'pp)$ events, respectively. The square shows the $^{12}\text{C}(e, e'pp)/^{12}\text{C}(e, e'pn)$ ratio. A clear dominance of $^{12}\text{C}(e, e'pn)$ events is observed, evidence of the tensor nature of the nucleon-nucleon interaction in the measured momentum range. The pie chart on the right illustrates our understanding of the structure of ^{12}C , composed of 80% mean-field nucleons and 20% SRC pairs, where the latter is composed of $\sim 90\%$ np -SRC pairs and 5% pp and nn SRC pairs each. Figure adapted from (Subedi *et al.*, 2008).

calculations. The results of this measurement are shown in Figs. 13 and 14.

The two-nucleon opening angle distribution for ^4He (see Fig. 13) is very similar to that for C (see Fig. 11). The reconstructed missing mass distribution peaks at small missing mass for both pp - and np -SRC pair knockout. As can be seen, there is a peak at back angle, as

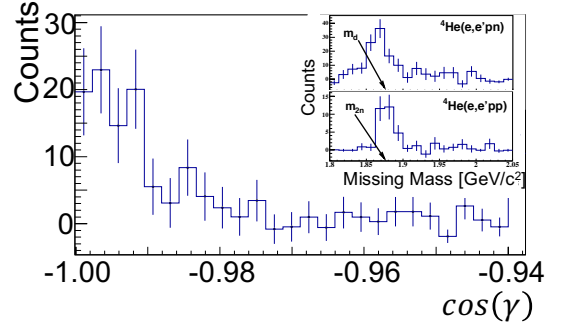


FIG. 13: (color online) The distribution of the cosine of the opening angle γ between \mathbf{p}_{miss} and \mathbf{p}_{recoil} for the $^4\text{He}(e, e'pn)$ reaction. The solid curve is a simulation of scattering off a moving pair with a c.m. momentum distribution having a width of 100 MeV/c. The insets show the missing-mass distributions. Figure adapted from (Korover *et al.*, 2014).

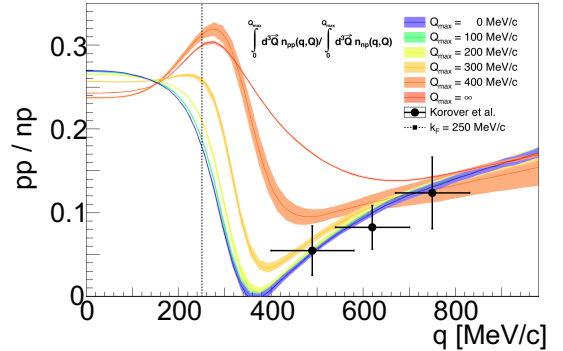


FIG. 14: (color online) The measured pp to pn ratio as function of the proton missing momentum (labelled q) (Korover *et al.*, 2014) compared to calculations of the two-nucleon momentum distribution (Wiringa *et al.*, 2014b) integrated over various ranges of the c.m. momentum (Cruz Torres, 2016). The data is shown as a function of the nucleon momentum and the calculations are shown as a function of the pair relative momentum. The two are equivalent for low c.m. momentum of the pair but differ at large c.m. momentum.

sociated with a breakup of ^4He into a SRC pair and a residual 2N system with low excitation energy. As with the ^{12}C measurements, the width of the opening angle distribution is due to the c.m. motion of the SRC pairs which was found to be consistent with a Gaussian in each direction with a width of 100 ± 20 MeV/c.

The extracted ^4He pp/np SRC pairs ratio increases with p_{miss} for $p_{miss} > 400$ MeV/c (see Fig. 14). The measured ratios are consistent with ab-initio Variational Monte Carlo (VMC) calculations of Ref. (Wiringa *et al.*, 2014b) integrated over c.m. momentum up to about 300

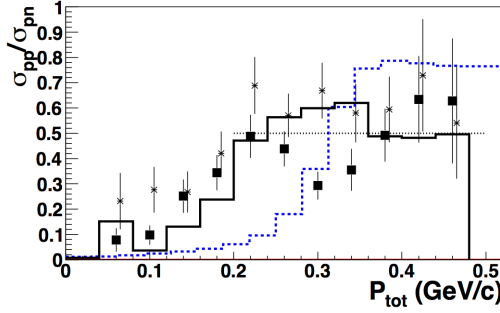


FIG. 15: The ratio of pp to pn pairs in ${}^3\text{He}(e, e'pp)n$. The solid and star points show the ratio for $300 \leq p_{rel} \leq 500$ MeV/c and for $400 \leq p_{rel} \leq 600$ MeV/c respectively, as a function of the total (e.g., center-of-mass) momentum of the pair. The pp/pn ratio is much less than one for small p_{tot} , increasing to the pair counting ratio of 0.5 at large p_{tot} . The ratio at small p_{tot} is about 0.1 for $300 \leq p_{rel} \leq 500$ MeV/c, increasing to about 0.25 for $400 \leq p_{rel} \leq 600$ MeV/c.

The solid line shows a calculation by Golak for $300 \leq p_{rel} \leq 500$ MeV/c which neglects rescattering of the struck nucleon but includes the reinteraction of the two nucleons in SRC pair. The dashed line (blue online) shows the ${}^3\text{He}$ momentum distribution integrated over the experimental acceptances. Figure adapted from (Baghdasaryan *et al.*, 2010).

The solid line shows a calculation by Golak for $300 \leq p_{rel} \leq 500$ MeV/c which neglects rescattering of the struck nucleon but includes the reinteraction of the two nucleons in SRC pair. The dashed line (blue online) shows the ${}^3\text{He}$ momentum distribution integrated over the experimental acceptances. Figure adapted from (Baghdasaryan *et al.*, 2010).

MeV/c, which is consistent with the measured width of the c.m. momentum distribution. At higher c.m. momentum, the two body momentum distribution is dominated by large contributions from un-correlated pairs. Similar results were also obtained by different calculations (Alvioli *et al.*, 2016; Ryckebusch *et al.*, 2015).

The importance of tensor correlations was further shown by measurements of the pp to pn ratio in ${}^3\text{He}(e, e'pp)n$ measured using the CLAS detector at JLab (Baghdasaryan *et al.*, 2010). They measured the relative and total momentum distribution of pp and pn pairs in ${}^3\text{He}$ by detecting events where the virtual photon was absorbed on one nucleon and the other two (spectator) nucleons were also detected. Fig. 15 shows the ratio of pp to pn pairs in ${}^3\text{He}$ as a function of the pair total (e.g., center-of-mass) momentum for two pair relative momentum ranges, $300 \leq p_{rel} \leq 500$ MeV/c and $400 \leq p_{rel} \leq 600$ MeV/c. The first range is centered at the s -wave minimum at 400 MeV/c where the effects of tensor correlations are expected to dominate; the second is not. For p_{rel} centered at 400 MeV/c, the pp to pn ratio is very small at $p_{tot} \leq 100$ MeV/c and consistent with the ${}^{12}\text{C}(e, e'pN)$ measurements discussed above. For p_{rel} centered at 500 MeV/c, the pp to pn ratio at $p_{tot} \leq 100$ MeV/c is significantly larger, consistent with the expected decreased dominance of tensor correlated pairs

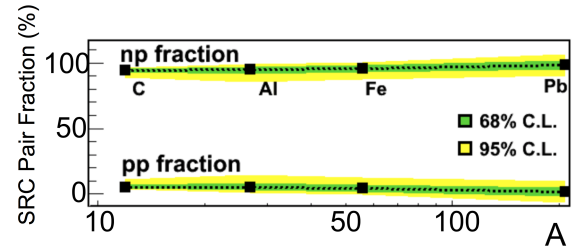


FIG. 16: The relative fraction of np and pp SRC pairs (excluding nn pairs) derived from $A(e, e'p)$ and $A(e, e'pp)$ measurements on a range of nuclei (Hen *et al.*, 2014c).

at this higher relative momentum. At large p_{tot} , the pp to pn ratio is 0.5, consistent with simple pair counting. The points at $300 \leq p_{rel} \leq 500$ MeV/c are consistent with a calculation by Golak (Golak *et al.*, 1995) which neglects rescattering of the struck nucleon but includes the reinteraction of the two nucleons in SRC pair.

The combined results of the ${}^3\text{He}$, ${}^4\text{He}$ and ${}^{12}\text{C}$ measurements indicate that for $300 \leq p_i \leq 500$ MeV/c, nucleons are predominantly part of pn -SRC pairs as predicted by dominance of the tensor part of the NN interaction at short distances. At higher initial momentum, the contribution of pp -SRC pairs seems to increase by a factor of 2 – 3, possibly due to larger contributions from the scalar repulsive core of the NN interaction.

Encouraged by these results, the latest exclusive measurements extended to medium and heavy nuclei (${}^{12}\text{C}$, ${}^{27}\text{Al}$, ${}^{56}\text{Fe}$, and ${}^{208}\text{Pb}$), where the persistence of np -SRC dominance was still unproven (Hen *et al.*, 2014c). In this experiment, the $A(e, e'pp)$ and $A(e, e'p)$ reactions were measured at similar kinematics to the previous ${}^4\text{He}$ and ${}^{12}\text{C}$ measurements, covering a reconstructed initial proton momentum range of $300 \leq p_i \leq 600$ MeV/c. The analysis assumed that, in these nuclei, the reaction is still dominated by scattering off SRC pairs and extracted the relative fraction of np - and pp -SRC pairs. Fig. 16 shows that SRC pairs are predominantly np -SRC pairs even in heavy neutron rich nuclei.

D. Universal Properties of Short Range Correlations in Nuclei

The combined results from the inclusive and exclusive measurements described in Sections II.B and II.C lead to a universal picture of SRC pairs in nuclei. In the conventional momentum space picture, the momentum distribution for all nuclei and nuclear matter can be divided into two regimes, above and below the Fermi-momentum (see Fig. 17). The region below the Fermi momentum accounts for about 80% of the nucleons in medium and heavy nuclei (i.e., $A \geq 12$) and can be described using

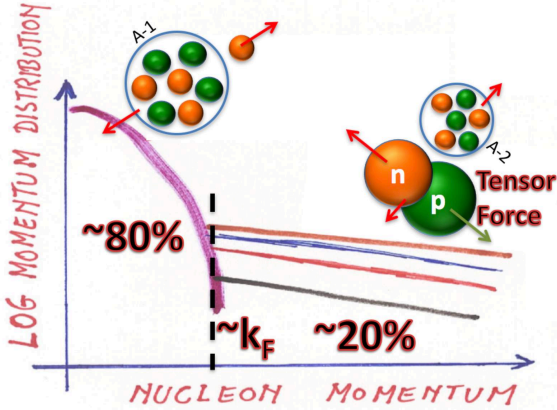


FIG. 17: A qualitative sketch of the dominant features of the nucleon momentum distribution in nuclei. At $k < k_F$, the nucleon momentum is balanced by that of the other $A - 1$ nucleons and can be described by mean field models. At $k > k_F$, the nucleon belongs to a pn -SRC pair and its momentum is balanced by that of one other nucleon.

mean-field approximations. The region with momenta greater than the Fermi momentum accounts for about 20–25% of the nucleons (see the pie chart in Fig. 12) and is dominated by nucleons belonging to NN -SRC, predominantly pn -SRC.

The SRC dominance of the high-momentum tail implies that the shape of the momentum distributions of all nuclei at high momenta is determined by the short range part of the fundamental NN interaction. The average number of SRC pairs is determined by the number of neutrons and protons in the nucleus.

The specific predominance of pn -SRC over pp - and nn -SRC is largely associated with the large contribution of the tensor part of the NN interaction at short-distances (Alvioli *et al.*, 2008; Sargsian *et al.*, 2005b; Schiavilla *et al.*, 2007), implying that the high-momentum distribution in heavier nuclei is approximately proportional to the deuteron momentum distribution. Experimental and theoretical studies of the latter show that, for $300 \leq k \leq 600$ MeV/c, $n(k) \propto 1/k^4$ (Hen *et al.*, 2015a). This specific functional form follows directly from the dominance of the tensor force acting in second order, see Section IX.A for details.

The predominance of np -SRC pairs implies that, even in asymmetric nuclei, the ratio of protons to neutrons in SRC pairs will equal 1. This, in turn, implies that in neutron rich nuclei, a larger fraction of the protons will be in an SRC pair (Hen *et al.*, 2014c; Sargsian, 2014a), i.e., that a minority nucleon (e.g., a proton) has a higher probability of belonging to a high-momentum SRC-pair than a majority nucleon (e.g., a neutron). This effect should grow with the nuclear asymmetry and could pos-

sibly invert the kinetic energy sharing such that the minority nucleons move faster on average than the majority. This asymmetry could have wide ranging implications for the NuTeV anomaly (Zeller *et al.*, 2002, 2003) (see Sects III.D.1, VI.A.5), the nuclear symmetry energy and neutron star structure and cooling rates (Hen *et al.*, 2016, 2015c), neutrino-nucleus interactions (Acciari *et al.*, 2014; Weinstein *et al.*, 2016) and more. The study of the nuclear asymmetry dependence of the number of SRC pairs and their isospin structure is an important topic that could be studied in future high-energy radioactive beam facilities.

III. Deep Inelastic Scattering (DIS) and the EMC effect

Basic models of nuclear physics describe the nucleus as a collection of free nucleons moving non-relativistically under the influence of two-nucleon and three-nucleon forces, which can be treated approximately as a mean field. In such a picture, the partonic structure functions of bound and free nucleons should be identical. Therefore, it was generally expected that, except for nucleon motion effects, Deep Inelastic Scattering (DIS) experiments which are sensitive to the partonic structure of the nucleon would give the same result for all nuclei.

Instead, the measurements (Arneodo, 1994; Aubert *et al.*, 1983; Frankfurt *et al.*, 2012; Geesaman *et al.*, 1995; Hen *et al.*, 2013a; Malace *et al.*, 2014; Norton, 2003; Piller and Weise, 2000) show a reduction of the structure function of nucleons bound in nuclei relative to nucleons bound in deuterium for the kinematics of the valence quark region. We term this reduction the EMC effect. Since its discovery, over 30 years ago, a large experimental and theoretical effort has been put into understanding the origin of the effect. While theorists have had no difficulty in creating models that qualitatively reproduce nuclear DIS data by itself, there has been generally accepted model. This is because the models are either not consistent with or do not attempt to explain other nuclear phenomena.

The nuclear deep inelastic scattering data also show a reduction in the small x_B region of the structure function, known as the shadowing region. The physics of shadowing has been well-reviewed (Frankfurt *et al.*, 2012) recently, and is not a subject of the present review.

Section I.B showed that the nucleon-nucleon interaction leads to the existence of Short-Range Correlated (SRC) pairs in nuclei and Section II showed the evidence for and our knowledge of the properties of these pairs.

This section will describe Deep Inelastic Scattering and its relationship to nucleon parton distributions. The EMC effect and the limitations of conventional nuclear physics to explain it will then be discussed. Section IV will present the phenomenological relationship between the number of SRC pairs in a nucleus and the strength

of the EMC effect and use that relationship to gain new insight into the origin of the EMC effect.

A. DIS and nucleon structure functions

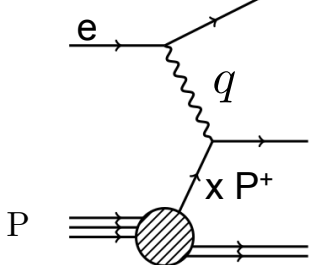


FIG. 18: Deep inelastic scattering at large values of Q^2 . A lepton (labelled ‘e’) scatters from a nucleon by emitting a space-like virtual photon with four-momentum q , which is absorbed on a single quark with momentum fraction $x_B P^+$. Only the outgoing lepton is subsequently detected.

We begin with a brief description of deep inelastic scattering on a nucleon. See one of the many texts for details, e.g., (Close, 1979; Halzen and Martin, 1984; Roberts, 1994; Thomas and Weise, 2001). The latest information is contained in the Particle Data Group tables (Olive *et al.*, 2014). The inclusive deep inelastic scattering process, (e, e') , involves a lepton scattering from a target, with only the final state lepton being detected. If spin variables are not observed, the process depends on only two variables, which are traditionally chosen to be the electron energy loss ν and negative of the four momentum transfer from the lepton to the target $Q^2 = \mathbf{q}^2 - \nu^2$, see Fig. 18. At large enough values of ν and Q^2 , conservation of momentum and energy leads to the result that the dynamical information, encoded in the structure functions $q(x_B)$, depends only on x_B , which is interpreted as the fraction of the target momentum carried by the struck quark.

Let’s see how this arises. Four-momentum conservation, and the idea that the quark is briefly free after absorbing the high-momentum photon gives

$$(k + q)^2 = m_q^2 \quad (16)$$

where k is the four-momentum of a quark in the target, and m_q is the quark mass. Let the spatial momentum of the photon lie in the negative z direction and using the light-front momentum variables, *e.g.* $P^\pm \equiv P^0 \pm P^3$, where P^μ is the target four-momentum, we have $q^- = \nu + \sqrt{\nu^2 + Q^2} = \nu + |\mathbf{q}|$, $q^+ = \nu - |\mathbf{q}|$, $q^- \gg q^+$, so that Eq. (16) can be re-written as

$$k^+ = \frac{Q^2 - k^2 - q^+ k^- + m_q^2}{\nu + \sqrt{\nu^2 + Q^2}}. \quad (17)$$

If the quark is on its mass shell (as is the case with light-front wave functions) then $k^2 = m_q^2$. Furthermore, if the quantity $q^+ k^- \ll Q^2$, the numerator becomes simply Q^2 . Then one defines a dimensionless, Lorentz invariant variable by dividing the resulting equation by P^+ , so that

$$\frac{k^+}{P^+} \approx \frac{Q^2}{P^+(\nu + \sqrt{\nu^2 + Q^2})} \equiv \xi, \quad (18)$$

where ξ is the Nachtmann variable. We see that the fraction of target momentum (plus-component) is simply ξ . This explains why deep inelastic scattering shows the scaling phenomenon. The relevant dynamical variable, $\frac{k^+}{P^+}$, depends only on one specific combination of ν and Q^2 . Note that this description is frame-independent. One need not go to the infinite momentum frame to understand scaling or the parton model.

If one further takes the Bjorken limit ($\nu^2 \gg Q^2$), then $\frac{k^+}{P^+} = \frac{Q^2}{2P^\mu q_\mu} \equiv x_B$. The dominant dependence on x_B is called Bjorken scaling, and its discovery, using hydrogen and deuteron targets (to obtain the neutron information), was the primary evidence for the existence of quarks within the nucleon.

Quarks are confined, so they are never on their mass shell. The off-mass shell effects, however, decrease with increasing values of Q^2 and are regarded as “higher twist”. Such effects could be important at Jefferson Lab energies. Effects of final state interactions (which depend on the kinematics of the probing beam) are not contained in the light-front wave function (Cosyn *et al.*, 2014).

Suppose the struck quark is confined in a nucleon of four-momentum p^μ that is bound within a nucleus of momentum P^μ . Then we have

$$\frac{k^+}{p^+} \frac{p^+}{P^+} = \xi. \quad (19)$$

This is the origin of the convolution model discussed in Sect. III.C.1. A nucleon in the nucleus of momentum p^+ contains a quark of momentum k^+ . A proper evaluation of deep inelastic scattering from nuclei therefore involves knowledge of the nuclear wave function, expressed in light-front variables.

More formally, one derives the expression for the momentum distribution (the probability that a quark has a given value of k^+/P^+), known as a quark distribution function, by starting with the square of the invariant scattering amplitude. The important part of this amplitude depends on the hadronic tensor $W^{\mu\nu}$, which is a matrix element of a commutator of electromagnetic current operators. After expanding in terms of the separation r of the spatial variable of the two current operators, the momentum distribution (for a specific flavor of quark) is given in the Bjorken scaling limit (in which the variable Q^2 is not explicit) by the Fourier transform (Thomas and Weise, 2001)

$$q(\xi) = \frac{1}{2\pi} \int dr^- e^{iq^+ r^-} \langle P | \psi_+^\dagger(r^-) \psi_+(0) | P \rangle_c, \quad (20)$$

where $|P\rangle_c$ is the proton wave function, the subscript c denotes a connected matrix element, ψ is the quark field-operator, the subscript $+$ denotes multiplication by the projection operator $(1 + \gamma^0 \gamma^3)/2$, and r^- is the minus-component of the separation distance. Notice that the expression Eq. (20) is independent of there is no need to work in the infinite momentum frame if appropriate light front coordinates are used.

Parton distributions are needed for a wide variety of applications in high-energy physics. $q(x_B, Q^2)$ has been determined for various flavors and for a wide range of values of x and Q^2 . Vast amounts of data are now codified as parton distributions, giving the probability as a function of Q^2 that a given flavor of quark carries a momentum fraction x_B , see Fig. 19.

This sub-section is concerned with nucleon targets, but (as mentioned above) we need to know how to evaluate a nuclear version of Eq. (20), which would involve nuclear wave functions expressed in terms of light front variables. This difficulty has been handled (Frankfurt and Strikman, 1981b, 1988a; Smith and Miller, 2002), (Blunden *et al.*, 1999; Miller and Machleidt, 1999b; Miller, 2000; Miller and Smith, 2002). One can implement light-front coordinates using a simple transformation. This works because the nucleus does not contain a significant $N\bar{N}$ content.

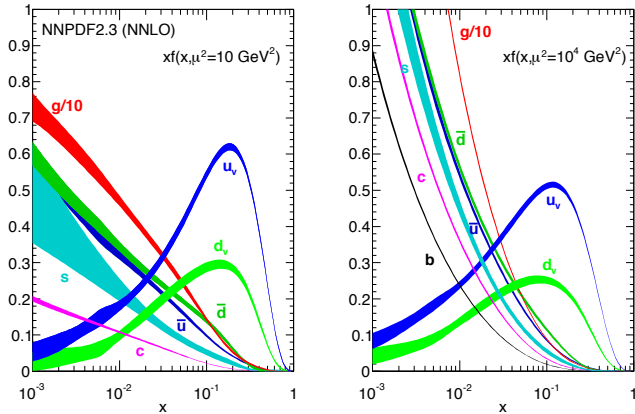


FIG. 19: The bands show x_B times the unpolarized parton distributions for the different parton flavors $\{u_v, d_v, u, d, s = \bar{s}, c = \bar{c}, b = \bar{b}, \text{ and } g\}$ obtained in NNLO NNPDF2.3 global analysis (Ball *et al.*, 2013), at $Q^2 = 10$ (GeV/c^2) and 10^4 (GeV/c^2), with $\alpha_s(M_Z^2) = 0.118$. From the PDG (Olive *et al.*, 2014). Here $x = x_B$.

B. The EMC effect

As stated, the discovery of Bjorken scaling was made using hydrogen and deuterium targets. It occurred to

many experimentalists that MeV-scale nuclear effects should be negligible at GeV-scale momentum and energy transfers and that therefore they could increase their experimental statistics by using nuclear targets. Surprisingly, the CERN European Muon Collaboration (EMC) found that the per-nucleon (e, e') cross section ratio of iron to deuterium was not unity (Aubert *et al.*, 1983), see Fig. 20. This surprising result, now called the EMC Effect, was confirmed by many groups, culminating with the high-precision electron and muon scattering data from SLAC, Fermilab, NMC at CERN, and Jefferson Lab (see Fig. 21). See one of the many EMC reviews for details (Arneodo, 1994; Geesaman *et al.*, 1995; Hen *et al.*, 2013a; Malace *et al.*, 2014; Norton, 2003; Piller and Weise, 2000).

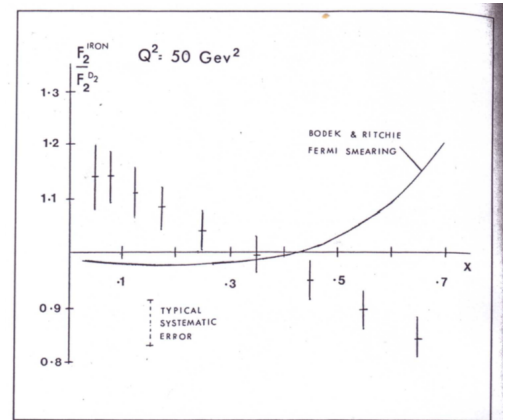


FIG. 20: Image of the EMC data as it appeared in the November 1982 issue of the CERN Courier. This image nearly derailed the refereed publication (Aubert *et al.*, 1983), as the editor argued that the data had already been published.

The conclusion from the combined experimental evidence was that the effect had a universal shape, was independent of the squared four momentum transfer Q^2 starting from remarkably small values of Q^2 (see Fig. 22), increased with nuclear mass number A , and increased with the average nuclear density.

One way to characterize the strength of the EMC effect is to measure the average slope of the cross section ratio for $0.35 \leq x_B \leq 0.7$. Plotting this slope versus the average nuclear density for light nuclei (see Fig. 23) shows that the EMC effect does not simply depend on average density. Since ${}^9\text{Be}$ can be described as a pair of tightly bound alpha particles plus one additional neutron, it has

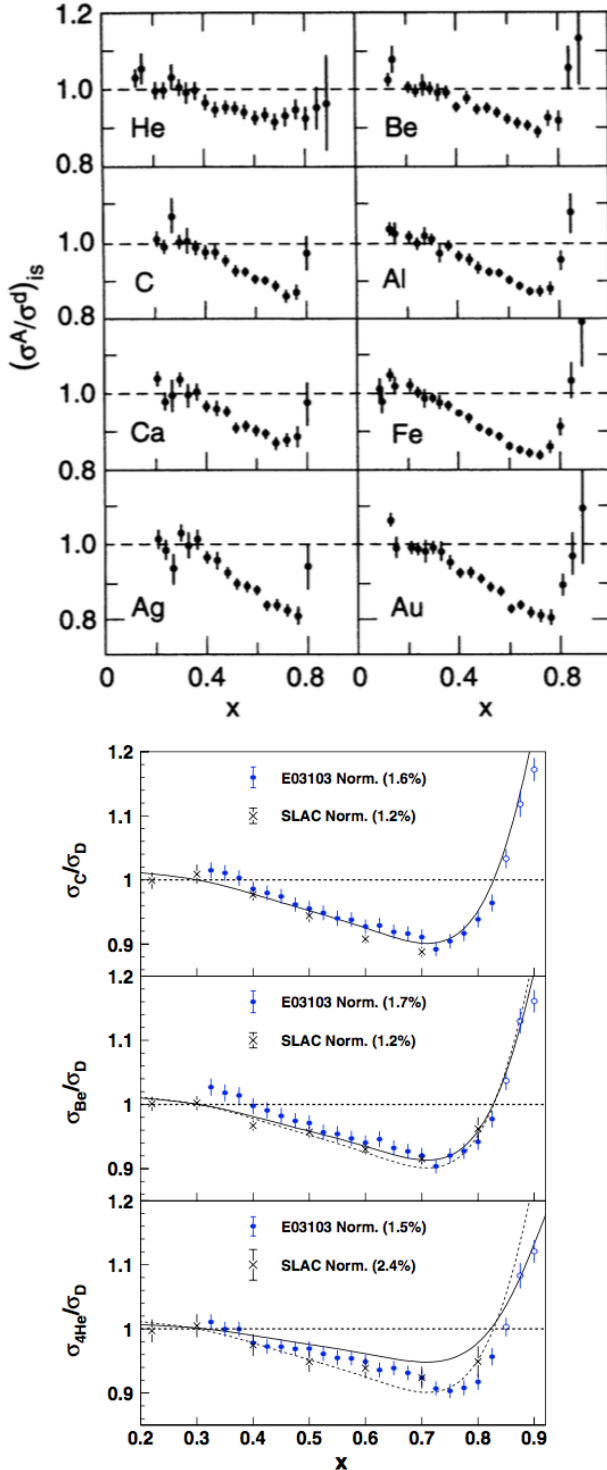


FIG. 21: The per nucleon cross section ratio of various nuclei to deuterium as measured at (top) SLAC (Gomez *et al.*, 1994) and (bottom) Jefferson Lab (Seely *et al.*, 2009a).

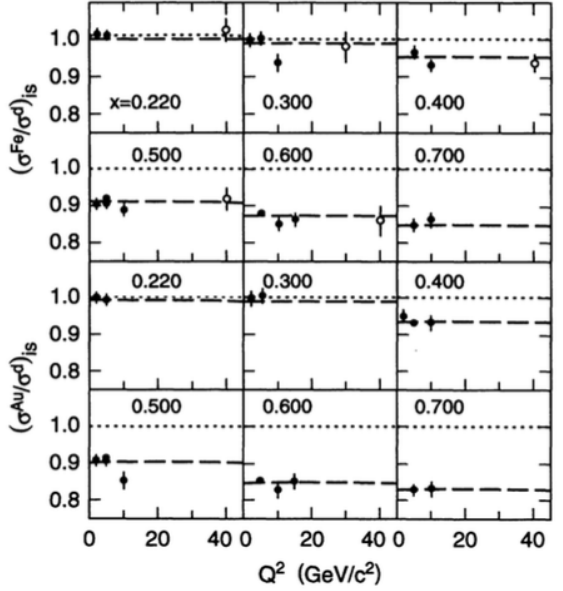


FIG. 22: The Q^2 dependence of the EMC ratio for iron at various values of x_B (Gomez *et al.*, 1994).

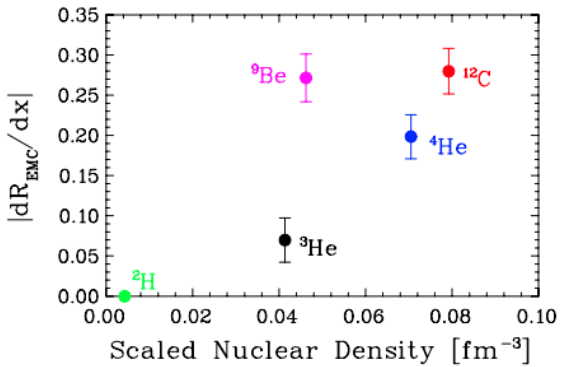


FIG. 23: The slope of the EMC effect for $0.35 \leq x_B \leq 0.7$ plotted versus the average nuclear density for various light nuclei as measured at Jefferson Lab (Seely *et al.*, 2009a).

been suggested that the local density is more important than the average density (Seely *et al.*, 2009a). See an early discussion in (Frankfurt and Strikman, 1981b).

The immediate parton model interpretation of the data at high x is that the valence quarks of a nucleon bound in a nucleus carry less momentum than those of free nucleons. This notion seems uncontested, but determining the underlying origin remained an elusive goal for a long time. The great number of models created to explain the EMC effect caused one of us to write in 1988 (Miller, 1988) that “EMC means Everyone’s Model is Cool”.

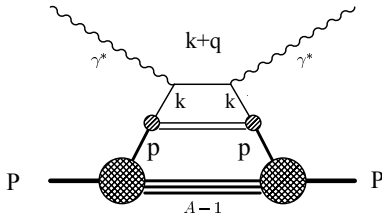


FIG. 24: Deep inelastic scattering diagram. A virtual photon, γ^* , of momentum q is absorbed on a quark of momentum k contained in a nucleon of momentum p in a nucleus of momentum P . The imaginary part of this diagram corresponds to the hadronic tensor $W^{\mu\nu}$.

C. Why Conventional nuclear physics cannot explain the EMC effect

1. Nucleons only

One must first try to explain the EMC effect using only the simple kinematic effects of binding energy and Fermi motion without modifying the bound nucleon structure. If the nucleon structure function is not modified and is the same on and off the energy shell (nucleon-only hypothesis) then evaluation of the diagram of Fig. 24 leads to the simple convolution formula:

$$\frac{F_{2A}(x_A)}{A} = \int_{x_A}^A dy f_N(y) F_{2N}(x_A/y), \quad (21)$$

where P is the total four momentum of the nucleus, and

$$x_A \equiv \frac{Q^2 A}{2P \cdot q} = \frac{x_B A M}{M_A}. \quad (22)$$

with M and M_A as the free nucleon and nuclear masses, respectively. x_A can be thought of as a version of x_B corrected for the average nucleon binding energy. The variable $y = Ap^+/P^+$ is the fraction of the nuclear momentum (per nucleon) carried by a single nucleon, and $f_N(y)$ is the corresponding probability distribution. The origin of the convolution formula can be understood using the simple terms of Sect. III.A. Suppose the struck quark is confined in a nucleon (of four-momentum p) that is bound within a nucleus of momentum P . Then from Eq. (19) we have

$$\xi \approx k^+/P^+ = (k^+/p^+)(p^+/P^+) = x_A/y. \quad (23)$$

This accounts for a nucleon in the nucleus of momentum p^+ that contains a quark of momentum k^+ . A proper evaluation of deep inelastic scattering from nuclei therefore involves knowledge of the nuclear wave function, expressed in light-front variables.

There were many attempts to explain the EMC effect without invoking medium modifications. We cite a few

of the references (Akulinichev and Shlomo, 1990; Benhar *et al.*, 1997, 1999; Benhar and Sick, 2012; Ciofi Degli Atti and Liuti, 1989; Dieperink and Miller, 1991; Jung and Miller, 1988, 1990; Marco *et al.*, 1996), with others to be found in the reviews.

The appeal of the nucleon-only idea can be understood using a simple caricature of the probability that the nucleon carries a momentum fraction y . The width of the function $f_N(y)$ is determined by the Fermi momentum divided by the nucleon mass, which is small. In the absence of interactions, $f_N(y)$ is peaked at $y = 1$. If the average separation energy $S \equiv \epsilon M$ (which for nuclear matter can be as large as 70 MeV), (Benhar *et al.*, 1997, 1999; Benhar and Sick, 2012; Dieperink and Miller, 1991) then $f_N(y)$ is peaked at about $y = 1 - \epsilon$. Taking for simplicity a zero width approximation

$$f_N(y) = \delta(y - (1 - \epsilon)), \quad (24)$$

then the convolution formula (Eq. (21)) tells us that

$$\frac{F_{2A}(x_A)}{A} \approx F_{2N} \left(\frac{x_A}{1 - \epsilon} \right). \quad (25)$$

As shown in Fig. 19 the structure function falls rapidly with increasing x_B , so that a slight increase in the argument leads to a significant decrease in the structure function. In particular,

$$\frac{F_{2A}(x_A)}{AF_{2N}(x_A)} \approx 1 + \epsilon \frac{F'_{2N}(x_A)}{F_{2N}(x_A)} \approx 1 - \gamma \epsilon, \quad (26)$$

where we have assumed $F_{2N}(x_B) \sim (1 - x_B)^\gamma$ at large x_B with $3 \leq \gamma \leq 4$.

Frankfurt and Strikman (Frankfurt and Strikman, 1987), using a more detailed calculation found that a value of $\epsilon = 0.04$ was sufficient to reproduce the early EMC data. However, we will show that the ideas of shifting the value of x_A based on binding energy or separation energy considerations violates rigorous (Collins, 2013) baryon and momentum sum rules, and therefore cannot be a viable explanation of the EMC effect. Consider a nuclear model in which nucleons are the only degrees of freedom. There will be a conserved baryon current and an energy-momentum tensor expressed in terms of these constituents. This means that in when expressed in terms of the convolution approach of the previous subsection we must have the momentum sum rule:

$$\int dy y f_N(y) = 1, \quad (27)$$

where the factor of y represents the momentum. The use of Eq. (24) in Eq. (27) leads immediately to a substantial violation of the momentum sum rule:

$$\int dy y f_N(y) = 1 - \epsilon. \quad (28)$$

Frankfurt and Strikman (Frankfurt and Strikman, 1987) also included an important relativistic correction known

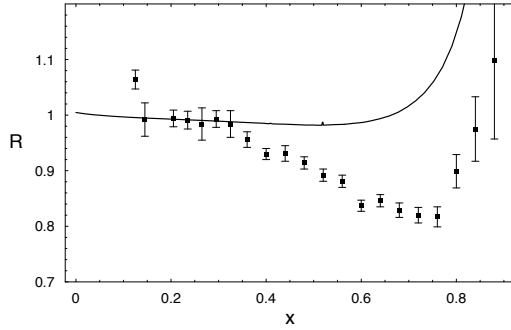


FIG. 25: The measured EMC effect in gold (Gomez *et al.*, 1994) compared to a nucleons-only calculation of the EMC effect in lead (Smith and Miller, 2002).

as the 'flux factor', which significantly reduces the effects of nuclear binding binding.

Going beyond the zero width approximation only makes this problem worse (Miller and Machleidt, 1999a). A violation of the sum rule by a few percent is actually a huge violation, because the EMC effect itself is only a 10-15% effect. Thus nucleon-only models must be regarded to be logically inconsistent and therefore wrong, even if they can be arranged to describe the data.

One might argue that sum rules can not be applied directly to the data because of the need to incorporate initial and final state interactions. Nevertheless, in using the convolution formalism in the nucleon-only approximation one must use a light-front wave function of the nucleus consistent with the conservation of baryon number and momentum, as discussed above. There is no way to avoid the constraints imposed by the sum rules.

Indeed, the application of sum rules and simple reasoning shows that Eq. (21) leads to the result that the nucleon-only hypothesis can not explain the EMC effect. Under the Hugenholtz van Hove theorem (Hugenholtz and van Hove, 1958; Miller and Smith, 2002; Smith and Miller, 2002) nuclear stability (pressure balance) implies (in the rest frame) that $P^+ = P^- = M_A$. But to an excellent approximation $P^+ = A(M_N - 8 \text{ MeV})$. Thus an average nucleon has $p^+ = M_N - 8 \text{ MeV}$. As caricatured in Eq. (24), the function $f_N(y)$ is narrowly peaked because the Fermi momentum is much smaller than the nucleon mass. This means that the value of y in the integral of Eq. (21) is constrained to be very near unity. Thus F_{2A}/A is well approximated by F_{2N} and one gets no substantial EMC effect this way (Miller and Smith, 2002; Smith and Miller, 2002). This is shown as the solid curve in Fig. 25.

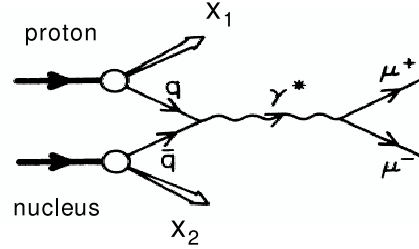


FIG. 26: The Drell-Yan process. A quark with momentum fraction x_1 from the incident proton annihilates with an anti-quark from the nuclear target with momentum fraction x_2 to form a time-like virtual photon which decays to a $\mu^+\mu^-$ pair.

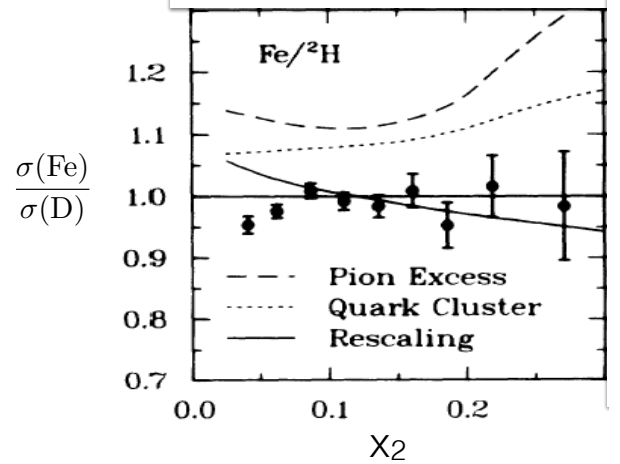


FIG. 27: Drell-Yan experimental results (Alde *et al.*, 1990) Ratio of Drell-Yan cross sections as a function of the momentum fraction x_2 of a quark in the nucleus. The version of the rescaling model shown in this figure does not reproduce the nuclear deep inelastic scattering data (Bickerstaff *et al.*, 1986).

2. Nucleons plus pions

Nucleons-only models fail, but it was natural to consider the idea that the missing momentum ϵ of Eq. (28) is carried by non-nucleonic degrees of freedom, e.g., pions (Ericson and Thomas, 1983; Llewellyn Smith, 1983). In

this case,

$$P^+ = P_N^+ + P_\pi^+ = M_A. \quad (29)$$

Many authors, see the reviews (Arneodo, 1994; Frankfurt and Strikman, 1988b; Geesaman *et al.*, 1995; Piller and Weise, 2000) found that using $P_\pi^+/M_A = 0.04$ is sufficient to account for the EMC effect. However, if nuclear pions carry 4% of the nuclear momentum (in the rest frame the plus component of momentum is the nuclear mass) then there should be more nuclear sea quarks (i.e., both quarks and anti-quarks). This enhancement should be observable in a nuclear Drell-Yan experiment (Bickerstaff *et al.*, 1984, 1986; Ericson and Thomas, 1984). The idea, see Fig. 26, is that a quark from an incident proton (defined by a large value of x_1) annihilates an anti-quark from the target nucleus (defined by a smaller value of x_2). A significant enhancement of pions would enhance the anti-quarks and enhance the nuclear Drell-Yan reaction. But no such enhancement was observed (Alde *et al.*, 1990) as shown in Fig. 27. This caused Bertsch *et al.* (Bertsch *et al.*, 1993) to announce “a crisis in nuclear theory” because conventional theory does not work. This statement is the verification of the title of this subsection.

The reader might ask at this stage, if the two-pion exchange effects discussed in the Appendix and Sects. I & II lead to a significant pion content and an enhanced sea in the nucleus. Explicit calculations show that the pionic content associated with the tensor potential is very small (Miller, 2014)

Subsequent work has confirmed that an intrinsic modification of the nucleon structure function is needed to explain the EMC effect (Frankfurt and Strikman, 2012; Hen *et al.*, 2013a; Kulagin and Petti, 2010, 2014). This result had been expected for some time, as stated explicitly “The change of the structure functions in nuclei (EMC effect) gives direct evidence for the modification of quark properties in the nuclear medium” (Walecka, 2005). The following sections discuss specific proposals for such modifications.

D. Beyond Conventional Nuclear Physics: Nucleon Modification

The failure of the nucleon-only or nucleon+pion models to explain the EMC and Drell-Yan data indicates that the structure of a nucleon bound in a nucleus significantly differs from that of a free nucleon. The medium modifies the nucleon.

This is not surprising, as there are evident simple examples. A free neutron undergoes β decay, so it can be thought of as having a $|pe^-\nu\rangle$ component. When bound in a stable nucleus, the neutron is stable. This “medium modification” suppresses the $|pe^-\nu\rangle$ component. Additionally, in the $(e, e'p)$ reaction shown in Fig. 28, four-momentum conservation shows that the square of the

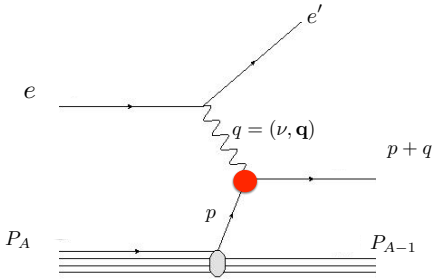


FIG. 28: The $A(e, e'p)$ reaction in the Plane Wave Impulse Approximation. A nucleus of four-momentum P emits a nucleon of four-momentum p that absorbs a virtual photon of four-momentum q to make a nucleon of four momentum $p + q$, with $(p + q)^2 = M^2$, where M is the nucleon mass. The blob represents the in-medium electromagnetic form factors.

1947- independent nucleons 1970 - independent 3-quark nucleons

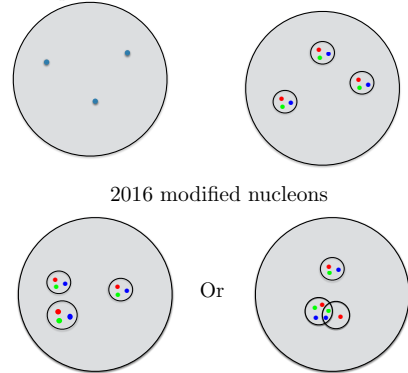


FIG. 29: Evolution of nuclear physics from structureless nucleons in the 1940s to independent 3-quark nucleons in the 1970s to the modified nucleons of today, either modified single-nucleons (left) or modified two-nucleon configurations (right).

initial four-momentum of the struck nucleon, p , cannot satisfy $p^2 = M^2$. Thus the form factor of a nucleon bound in the nucleus cannot be the same as that for a free nucleon; it is instead the amplitude for a transition between a virtual nucleon of mass $\sqrt{p^2}$ and a physical nucleon of mass M .

Now we must ask: what is the origin of the medium modification? This question is coupled to the broader questions listed in Sect. I, and more deeply to the very nature of confinement.

The parton model interpretation of the large- x_B part of the EMC effect is that the medium reduces the nuclear structure functions for large x_B , so that there are

fewer high-momentum quarks in a nucleus than in free space. This momentum reduction leads, via the uncertainty principle, to the notion that quarks in nuclei are confined in a larger volume than that of a free nucleon.

There are two general ways to realize this simple idea: mean-field effects cause bound nucleons to be larger than free ones, or nucleon-nucleon interactions at close range cause nucleon structure to be modified, by including either NN^* configurations or 6-quark configurations that are orthogonal to the two-nucleon wave functions. All of the papers seeking to explain the EMC effect using medium modification use one of the two ideas that are cartooned in Fig. 29).

One expects that the $\sim 80\%-20\%$ split between mean-field and correlated nucleons, Fig. (17), causes the necessary modifications associated with SRC to be about 5 times larger than for modifications associated with the mean-field. A phenomenological assessment of this idea in which the mean-field and SRC related origins of the EMC effect were treated phenomenologically was made in Ref. (Hen *et al.*, 2013a). The separation of the spectral function Eq. (7) into terms arising from low-lying excited states P_0 and higher-energy continuum states related to short-ranged correlation, P_1 was used. In the mean field model, a nucleus-independent modification of F_2 was included in the contribution to the nucleon distribution function, $f_N(y)$ Eq. (21) arising from P_0 . In the alternate model a much larger nucleus-independent modification of F_2 was included in the contribution to $f_N(y)$ arising from P_1 . Both approaches gave reasonably good descriptions of the nuclear DIS data.

We next describe specific models associated with the two different mechanisms.

1. Mean field

In mean-field models of nucleon modification, the interaction between nucleons occurs by the exchange of mesons between quarks confined in different nucleons. Four general models of the quarks confined in the nucleon have been used for this. The earliest model (quark meson coupling, QMC) used the MIT bag model to represent the three confined quarks in the proton (Guichon, 1988; Guichon *et al.*, 1996; Stone *et al.*, 2016). Later work used the QMC model with more general confinement mechanisms (Blunden and Miller, 1996), the covariant NJL model (Cloet *et al.*, 2009a, 2006, 2016) and the chiral quark soliton model (Diakonov *et al.*, 1996; Smith and Miller, 2003, 2004, 2005). In these models the attraction needed to produce a bound state is generated by the exchange of scalar quantum numbers (either by a scalar meson (Guichon, 1988; Guichon *et al.*, 1996; Stone *et al.*, 2016) or by pairs of pions (Smith and Miller, 2003, 2004, 2005)) and the repulsion needed to obtain nuclear saturation is caused by exchange of vector mesons.

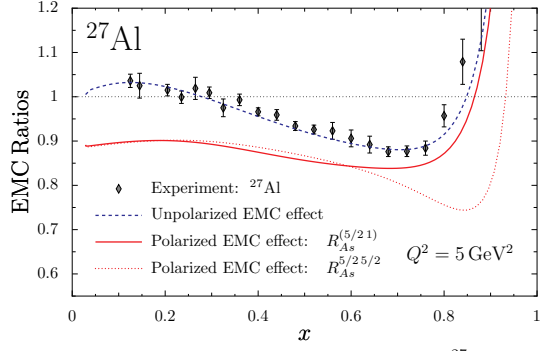


FIG. 30: (color online) The measured EMC effect for ^{27}Al (Gomez *et al.*, 1994) compared to QMC calculations of both the regular and the polarized EMC effect of Ref. (Cloet *et al.*, 2006).

We next explain two classes of models. The chiral quark soliton model (CWQSM) is based on the instanton-dominated nature of the vacuum (Negele, 1999). The coupling of quarks to vacuum instantons spontaneously generates a constituent quark mass of about 400 MeV. These quarks interact with pions through an effective CQSM Lagrangian. This model reproduces nucleon properties well, including structure functions which vanish at $x_B = 0$ and 1 (Diakonov *et al.*, 1996).

Nuclei are formed by collections of such nucleons exchanging scalar and vector mesons (Smith and Miller, 2003, 2004, 2005). Excellent saturation properties were obtained. The dominant effect of the medium is a slight broadening of the effective potential that binds the quarks in the nucleon. The use of the medium modified wave function to compute structure functions allows one to account for the EMC effect, while still agreeing with the Drell-Yan data. This indicates that the sea is not very modified.

The next model places an NJL-model nucleon in the medium (NJLMM) which is a relativistic extension of the earlier QMC including the effects of spontaneous symmetry breaking. Here the external scalar field enhances the lower component of the quark's Dirac wave function by about 15%. This model describes the EMC effect well (see Fig. 30). It also predicts an enhancement of the EMC Effect for spin structure functions (Cloet *et al.*, 2005b) in nuclei which could be measured at Jefferson Lab in experiment E12-14-001 (see Section VI.A.2).

The NJLMM predicts the effects of having different numbers of neutrons N and protons Z . Cloet and Thomas (Cloet *et al.*, 2009a) explained that a neutron or proton excess in nuclei leads to an isovector-vector mean-field which, through its coupling to the quarks in a bound nucleon, causes the quark distributions to be evaluated at a shifted value of the Bjorken scaling variable (Detmold

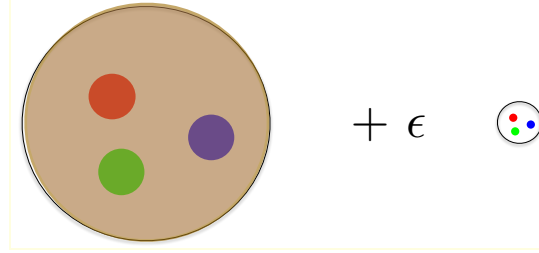


FIG. 31: Two component nucleon model: normal-sized component plus point-like configuration component.

et al., 2006; Mineo *et al.*, 2004). In relativistic mean-field models, the effect of a vector field is to shift the energy and therefore the value of the plus component of momentum of the single particle state. The isovector-vector mean field is represented by the ρ^0 , and in this work its strength is chosen to reproduce the nuclear symmetry energy. In a nucleus like ^{56}Fe or ^{208}Pb where $N > Z$, the ρ^0 field causes the u -quark to feel a small additional vector attraction and the d -quark to feel additional repulsion. This effect leads to an a significant correction to the NuTeV measurement of $\sin^2 \Theta_W$ (Zeller *et al.*, 2002, 2003). The sign of this correction is largely model independent, and it accounts for approximately two-thirds of the NuTeV anomaly. Thus the NuTeV measurement provides further evidence for the medium modification of the bound nucleon wave function.

Both sets of mean field models predict modification of nucleon electromagnetic form factors. The QMC model predicts modifications to both G_E and G_M (Lu *et al.*, 1999), while the chiral quark soliton model only modifies G_E (Smith and Miller, 2004). Both models predict the same ratio G_E/G_M .

However, because none of the mean-field models predicts significant extra high-momentum strength in the nuclear momentum distribution, it is very difficult to see how they could reproduce the plateaus observed in the cross section ratios at $x_B \geq 1.5$ seen in Section II.B.

2. Suppression of point-like configurations

We can also make a more general model of the nucleon as a superposition of various configurations or Fock states, each with a different quark-gluon structure. Fig. 31 shows a two-component nucleon where one component is “blob-like” (BLC) with the normal nucleon size and the other is “point-like” (PLC). The BLC can be thought of as an object that is similar to a nucleon. The PLC is meant to represent a three-quark system of small size that is responsible for the high- x behavior of the distribution function. The smaller the number of quarks, the more likely one can carry a large momentum fraction. Furthermore, because the PLC is smaller than the BLC,

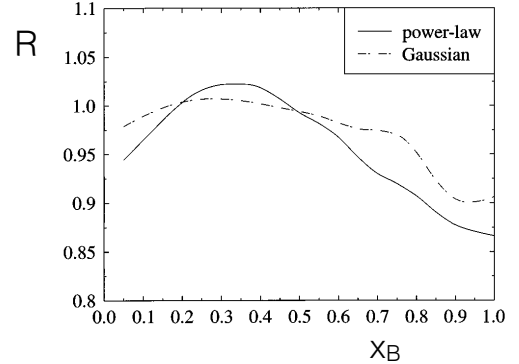


FIG. 32: The ratio of F_2 in the nucleus to the free F_2 (the EMC ratio) in the point-like configuration suppression model. (Frank *et al.*, 1996).

the uncertainty principle tells one that quarks confined in the PLC have higher momentum. The small-sized (with its small number of $q\bar{q}$ pairs) is very different than a low lying excitation.

When placed in a nucleus, the blob-like configuration feels the regular nuclear attraction and its energy decreases. The point-like-configuration feels far less nuclear-attraction because the effects of gluons emitted by small-sized configurations are cancelled in low-momentum transfer processes. This effect is termed color screening and has been verified in several different reactions (Dutta *et al.*, 2013; Frankfurt *et al.*, 1994). The nuclear attraction increases the energy difference between the BLCs and the PLCs, therefore reducing the PLC probability (Frankfurt and Strikman, 1985). The PLC is suppressed. Therefore, reducing the probability of PLCs in the nucleus reduces the quark momenta, in agreement with the EMC effect.

This idea was studied (Frank *et al.*, 1996) using a relativistic constituent quark model for the nucleon (Schlumpf, 1992, 1993). A nucleon is placed in the nucleus and therefore subject to a mean field that vanishes for configurations in which the three quarks are close together, see Fig. 32. The quark momentum distribution decreases for $x_B > 0.3$. The effects of nucleon motion are not included, so there is no rise for large values of x_B , and the dip at low values of x_B would be removed by such effects. It is also noteworthy that the PLC model, being a modification at large values of x_B , does not contradict the nuclear Drell-Yan data, Sect. III.

The notion that different constituents of the nucleon have different sizes and therefore different interaction strengths is directly related to medium modifications of all kinds. The main features of this idea can be understood using a simple schematic two-component model of the nucleon with a dominant normal-sized blob-like constituent (denoted by B) and a very small point-like con-

stituent (denoted by P). The Hamiltonian is given by the matrix

$$H_0 = \begin{bmatrix} E_B & V \\ V & E_P \end{bmatrix}, \quad (30)$$

where $E_P \gg E_B$. Because of the hard-interaction potential, V , that connects the two components, the eigenstates of H_0 are $|N\rangle$ and $|N^*\rangle$ rather than $|B\rangle$ and $|P\rangle$. In lowest-order perturbation theory, the eigenstates are given by

$$|N\rangle = |B\rangle + \epsilon|P\rangle, \quad (31)$$

$$|N^*\rangle = -\epsilon|B\rangle + |P\rangle, \quad (32)$$

with $\epsilon = V/(E_B - E_P)$. We assume $|V| \ll E_P - E_B$, so that the nucleon is mainly $|B\rangle$ and its excited state is mainly $|P\rangle$, and also take $V > 0$. We use the notation $|N^*\rangle$ to denote the state that is mainly a PLC, but the PLC, as discussed above, does not resemble a low-lying baryon resonance.

Now suppose the nucleon is bound to a nucleus. The nucleon feels an attractive nuclear potential H_1 :

$$H_1 = \begin{bmatrix} U & 0 \\ 0 & 0 \end{bmatrix} \quad (33)$$

to represent the idea that only the large-sized component of the nucleon feels the influence of the nuclear attraction. The treatment of the nuclear interaction, U , as a number is clearly a simplification. The interaction varies with the relevant kinematics, and this feature will be manifest in our model as a dependence on kinematics. We note that this model is similar to the model of (Frankfurt and Strikman, 1985), with the important difference that the medium effects will enter as an amplitude instead of as a probability. In (Frank *et al.*, 1996) the PLC is subject to a non-zero, but small, attractive potential that fluctuates with the nucleon configurations. The complete Hamiltonian $H = H_0 + H_1$ is now given by

$$H = \begin{bmatrix} E_B - |U| & V \\ V & E_P \end{bmatrix}, \quad (34)$$

in which the attractive nature of the nuclear binding potential is emphasized. Then interactions with the nucleus increase the energy difference between the BLC and the PLC, which decreases the PLC probability.

The medium-modified nucleon and its excited state, $|N\rangle_M$ and $|N^*\rangle_M$, are now using first-order perturbation theory

$$|N\rangle_M = |B\rangle + \epsilon_M|P\rangle \quad (35)$$

$$|N^*\rangle_M = -\epsilon_M|B\rangle + |P\rangle, \quad (36)$$

where

$$\epsilon_M = \frac{V}{E_B - |U| - E_P} = \epsilon \frac{E_B - E_P}{E_B - |U| - E_P} \quad (37)$$

so that PLC probability in the medium is suppressed. Both ϵ_M and ϵ are less than zero, so that $\epsilon_M - \epsilon > 0$.

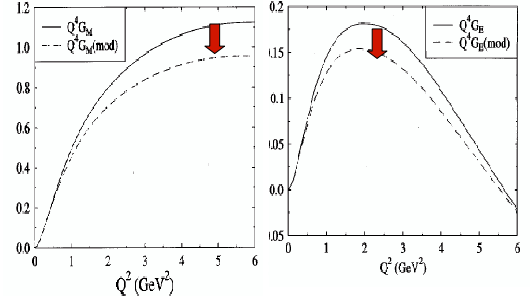


FIG. 33: Medium modification of form factors (Frank *et al.*, 1996).

The medium modified nucleon $|N\rangle_M$ may be expressed in terms of the unmodified eigenstates $|N\rangle, |N^*\rangle$ as

$$|N\rangle_M \approx |N\rangle + (\epsilon_M - \epsilon)|N^*\rangle. \quad (38)$$

Within this model the medium-modified nucleon contains a component that is an excited state of a free nucleon. The amount of modification, $\epsilon_M - \epsilon$, which gives a deviation of the EMC ratio from unity, is controlled by the potential U . A qualitative description of the EMC effect was obtained (Frankfurt and Strikman, 1985) (at $x_B = 0.5$, where effects of Fermi motion are small) using $U = -40$ MeV and $E_P - E_B \sim 500$ MeV. The present treatment differs from that on in that effects of the medium enter in the amplitude instead of the probability, so that the effects are generally larger for the present version. We will explore this further in Section IV.B.

The PLC suppression model also predicts changes to the elastic electric and magnetic form factors $G_{E,M}$. The electromagnetic form factor in free-space is obtained as

$$F = \frac{1}{1 + \epsilon^2} (\langle B|J|B\rangle + 2\epsilon\langle B|J|P\rangle + \epsilon^2\langle P|J|P\rangle), \quad (39)$$

where momentum and spin labels have been suppressed.

It is instructive to examine what to expect at both high and low momentum transfer. At low momentum transfer the first term dominates so that the spatial extent of the nucleon and its modification in the medium are important. Frankfurt and Strikman (Frankfurt and Strikman, 1985) estimated the value of $\langle r^2 \rangle$. Assuming that only the blob-like configuration $|B\rangle$ contributes to this long-ranged observable, one finds

$$\langle r^2 \rangle = \frac{\langle B|r^2|B\rangle}{1 + \epsilon^2}. \quad (40)$$

In the medium the potential U acts, so the value of ϵ is changed to ϵ_M . Since $\epsilon_M < \epsilon$, immersion of the nucleon in the medium suppresses the point-like components and increases $\langle r^2 \rangle$. The effect is of order $\epsilon(\epsilon_M - \epsilon)$, which was estimated to be between 2 and 5%.

At high momentum transfer, the term $2\epsilon\langle B|J|P\rangle$ becomes dominant. Then the change in the form factor is of order $\epsilon - \epsilon_M$, which is a larger effect.

The application of the PLC-suppression idea presented in the present two-state model is schematic: it does not distinguish between the electric, G_E , and magnetic, G_M , form factors.

A more detailed evaluation was included by (Frank *et al.*, 1996). Medium modifications of the proton form factors were predicted as shown in Fig. 33. The important modifications shown by the red arrow occur at larger values of momentum transfer than currently accessible experimentally. Fig 33 shows fairly significant effects, greater than about 10% (consistent with our present analysis) for the individual form factors. Experimentally it is easier to measure the medium modifications of the ratio G_E/G_M . The figure shows that since both G_E and G_M are decreased, the change in the ratio G_E/G_M is expected to be smaller.

In addition to the medium modifications, (Frank *et al.*, 1996) also predicted the more spectacular decrease (Gayou *et al.*, 2002; Jones *et al.*, 2000; Punjabi *et al.*, 2005) in the free-proton ratio G_E/G_M with increasing values of Q^2 .

3. Six-quark bags and the EMC Effect

One of the earliest attempts to understand the EMC effect (Bickerstaff *et al.*, 1984; Carlson and Havens, 1983; Jaffe, 1983) was to hypothesize that part of the time one nucleon is part of a six-quark configuration (Pirner and Vary, 1981) (who predicted the existence of plateaus in (e, e') cross section ratios) that is orthogonal to any two-nucleon wave function. Because a six-quark configuration is larger than a nucleon, the quarks are partially deconfined. Larger confinement volumes are associated with lower momenta, and therefore with a suppression of the structure function. The idea was usually implemented through the MIT bag model, or by guessing the related structure functions. Several reviews discuss this idea (Arneodo, 1994; Berger and Coester, 1987; Frankfurt and Strikman, 1988b; Geesaman *et al.*, 1995; Miller, 1984b; Mulders, 1990; Norton, 2003; Sloan *et al.*, 1988). It was relatively easy to use this idea to compute a wide variety of nuclear phenomena (Guichon and Miller, 1984; Koch and Miller, 1985; Miller, 1984a,b, 2014; Miller and Kisslinger, 1983). The use of 6-quark models that describe nuclear DIS led to predictions of large effects in the nuclear Drell-Yan process discussed in Sect. III.C, but little modification was seen, Fig. 27, severely limiting the applicability of six-quark bag models.

IV. The EMC - SRC Correlation

A. Experimental Overview

While there is no obvious connection between DIS scattering from quarks in the nucleus at $0.3 \leq x_B \leq 0.7$ and QE scattering from nucleons in the nucleus at $1.5 \leq x_B < 2$, analysis of world data showed a remarkable correlation (see Fig. 34) between the magnitude of the EMC effect in nucleus A and the probability that a nucleon in that nucleus is part of a 2N-SRC pair (Hen *et al.*, 2012; Weinstein *et al.*, 2011).

The strength of the EMC effect for nucleus A is characterized as the slope of the ratio of the per-nucleon deep inelastic electron scattering cross sections of nucleus A relative to deuterium, dR_{EMC}/dx , in the region $0.35 \leq x_B \leq 0.7$ (Seely *et al.*, 2009a). This slope is proportional to the value of the cross section ratio at $x_B \approx 0.5$, but is unaffected by overall normalization uncertainties that merely raise or lower all of the data points together. Table I shows data from the x_A corrected EMC data base of (Hen *et al.*, 2013b) which used the EMC data of (Gomez *et al.*, 1994; Seely *et al.*, 2009a).

The SRC scale factors were determined from the isospin-corrected per-nucleon ratio of the inclusive (e, e') cross sections on nucleus A and ${}^3\text{He}$ or deuterium. Columns two through four of Table I show the SRC scale factors measured by (Egiyan *et al.*, 2006a; Fomin *et al.*, 2012a; Frankfurt *et al.*, 1993) respectively. The large uncertainties in the SRC ratios of (Frankfurt *et al.*, 1993) are due to extrapolating data from different experiments measured at different kinematics. The SRC ratios measured by (Egiyan *et al.*, 2006a) were used in the original EMC-SRC analysis of (Weinstein *et al.*, 2011). The later results of (Fomin *et al.*, 2012a) include ${}^{63}\text{Cu}$ rather than ${}^{56}\text{Fe}$; the SRC scaling factor of ${}^{63}\text{Cu}$ is assumed to be the same as that of ${}^{56}\text{Fe}$. The values of ${}^9\text{Be}$ and ${}^{197}\text{Au}$ in the fifth column are those predicted by Ref. (Weinstein *et al.*, 2011) based on the measured EMC effect and the linear EMC-SRC correlation. These predictions are in remarkable agreement with the later results of (Fomin *et al.*, 2012a). Following (Hen *et al.*, 2012), the (Fomin *et al.*, 2012a) results are shown without the center of mass motion correction (i.e., including inelastic, radiative, and coulomb corrections only). Applying the SRC-pair center of mass motion correction decreases the ratios by 10% to 20%.

The EMC effect correlates imperfectly with other A -dependent quantities (see (Arrington *et al.*, 2012; Seely *et al.*, 2009b) and references therein). In general, nuclei with $A \geq 4$ fall on one straight line but deuterium and ${}^3\text{He}$ do not. This is true when the EMC effect is plotted versus A , $A^{-1/3}$, or the average nuclear separation energy. When plotting the EMC effect versus average nuclear density, ${}^9\text{Be}$ is a clear outlier (see Fig. 23). This indicates that the excellent correlation with the SRC

TABLE I: A compilation of world data on SRC scaling factors, $a_2(A)$ and EMC slopes dR_{EMC}/dx . Columns 2 through 4 show the SRC scaling factors extracted from various measurements. Column 5 shows the SRC scale factor prediction of (Weinstein *et al.*, 2011) based on the EMC-SRC correlation. Column 6 shows the world average of the EMC effect slope as compiled by (Weinstein *et al.*, 2011), using the data of (Gomez *et al.*, 1994; Seely *et al.*, 2009a). See text for details.

Nucleus	(Frankfurt <i>et al.</i> , 1993) $a_2(A)$	(Egiyan <i>et al.</i> , 2006a) $a_2(A)$	(Fomin <i>et al.</i> , 2012a) [excluding the CM motion correction] $a_2(A)$	(Weinstein <i>et al.</i> , 2011) EMC-SRC Prediction $a_2(A)$	(Weinstein <i>et al.</i> , 2011) EMC Slope $[dR_{EMC}/dx]$
column #	2	3	4	5	6
^3He	1.7 ± 0.3	1.97 ± 0.10	2.13 ± 0.04		-0.070 ± 0.029
^4He	3.3 ± 0.5	3.80 ± 0.34	3.60 ± 0.10		-0.197 ± 0.026
^9Be			3.91 ± 0.12	4.08 ± 0.60	-0.243 ± 0.023
^{12}C	5.0 ± 0.5	4.75 ± 0.41	4.75 ± 0.16		-0.292 ± 0.023
$^{56}\text{Fe}^{(63}\text{Cu)}$	5.2 ± 0.9	5.58 ± 0.45	5.21 ± 0.20		-0.388 ± 0.032
^{197}Au	4.8 ± 0.7		5.16 ± 0.22	6.19 ± 0.65	-0.409 ± 0.039
EMC-SRC slope $\frac{\sigma(n+p)}{\sigma_d} _{x_B=0.7}$		0.079 ± 0.006	0.084 ± 0.004		
χ^2/ndf		1.032 ± 0.004	1.034 ± 0.004		
		$0.7688/3$	$4.895/5$		

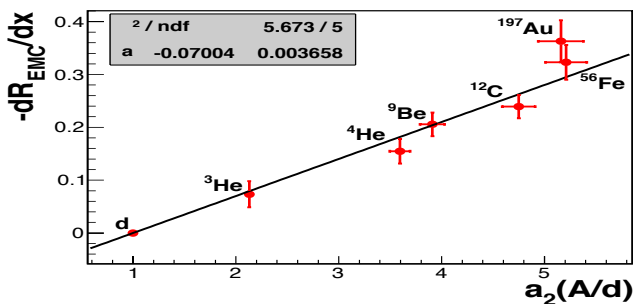


FIG. 34: The slope of the EMC effect (R_{EMC} , ratio of nuclear to deuteron cross section) for $0.35 \leq x_A \leq 0.7$ plotted vs. $a_2(A)$, the SRC scale factor (the relative probability that a nucleon belongs to an SRC NN pair) for a variety of nuclei (Hen *et al.*, 2013b). The fit parameter, $a = -0.070 \pm 0.004$ is the intercept of the line constrained to pass through the deuteron (and is therefore also the negative of the slope of that line).

scale factor is not just a trivial byproduct of their mutual A -dependence.

The correlation between the EMC effect and the SRC scale factor is robust (Hen *et al.*, 2012). It applies to

both SRC data sets of (Egiyan *et al.*, 2006b) and (Fomin *et al.*, 2012b). The quality of the correlation also does not depend on the corrections applied to the SRC data. These corrections include isoscalar cross section corrections, center-of-mass motion corrections, and isoscalar pair-counting corrections. The isoscalar correction to the SRC scale factors accounts for the different elementary electron-neutron and electron-proton cross sections. This has a negligible effect on the fit quality and the extracted fit parameter. Fomin *et al.* did not apply this correction, arguing that short range correlations are dominated by np pairs. Fomin *et al.* also argued that the SRC scale factors measured the relative probability of finding a high-momentum nucleon in nucleus A relative to deuterium and that these scale factors needed to be corrected for the center-of-mass (cm) motion of the pair in order to determine the relative probability that a nucleon in nucleus A belongs to an SRC pair. As shown in both (Hen *et al.*, 2012) and (Arrington *et al.*, 2012), including the pair c.m. motion correction improves the EMC-SRC correlation only slightly.

This EMC-SRC correlation gives new insight into the origin of the EMC effect. As discussed in Sect. III, many different explanations of the EMC effect have been proposed since 1983. After accounting for the standard nuclear effects of binding energy and Fermi motion, explanations for the EMC effect fall into two general categories, those that require modifications of mean-field nucleons and those that require modifications of high-momentum (large virtuality) nucleons.

The linear correlation between the strength of the EMC effect and the SRC scale factors indicates that possible modifications of nucleon structure occurs in nucleons belonging to SRC pairs.

This implies that the EMC effect, like short range correlations, is a short-distance, high virtuality, and high density phenomenon.

B. Theory Overview

1. High momentum nucleons and PLC suppression

Next we try to use the EMC-SRC correlation to better understand the relationship between short-ranged correlations measured in the $A(e, e')$ reaction and deep inelastic scattering reactions in a deeper manner. Both processes involve a probe that strikes a nucleon of four-momentum p in the nucleus, Fig. 28. It is natural to expect that the medium modification depends on the virtuality $v(\mathbf{p}, E)$ of the struck nucleon (C. Ciofi degli Atti, L.L. Frankfurt, L.P. Kaptari and M.I. Strikman, 2007):

$$v \equiv p^2 - M^2 = (P_A - P_{A-1})^2 - M^2. \quad (41)$$

In the $(e, e'p)$ reaction in PWIA (see Fig. 28), the nucleon initial momentum opposes the $A - 1$ recoil momentum $\mathbf{p} = -\mathbf{P}_{A-1}$. Using the recoil mass $M_{A-1} = M_A - M + E$, where $E > 0$ represents the excitation energy of the spectator nucleus (known as the removal energy (Ciofi degli Atti and Simula, 1996a)), we find

$$v(\mathbf{p}, E) = \left(M_A - \sqrt{(M_{A-1})^2 + \mathbf{p}^2} \right)^2 - \mathbf{p}^2 - M^2 \quad (42)$$

which reduces to

$$v(\mathbf{p}, E) \approx -2M \left(\frac{A}{A-1} \frac{\mathbf{p}^2}{2M} + E \right), \quad (43)$$

in the non-relativistic limit. The magnitude of the virtuality, $v(\mathbf{p}, E)$ increases with both the $A - 1$ excitation energy and the initial momentum of the struck nucleon.

(C. Ciofi degli Atti, L.L. Frankfurt, L.P. Kaptari and M.I. Strikman, 2007; Frankfurt and Strikman, 1985) obtained a relation between the potential U of Section III.D.2 and the virtuality $v(\mathbf{p}, E)$ by using the extension of the Schrödinger equation to an operator form:

$$\frac{\mathbf{p}^2}{2M_r} + U = -E, \quad (44)$$

where $M_r = M(A-1)/A$, and U is the interaction that both binds the nucleon to the nucleus and modifies its structure. The simple idea behind this equation is that, if the nucleon binding energy is fixed, then the NN interaction energy, U , must become more negative as the kinetic energy becomes more positive.

Comparing this equation with Eq. (42) one finds

$$U = \frac{v(\mathbf{p}, E)}{2M_r}, \quad (45)$$

so that the modification of the nucleon due to the PLC suppression is proportional to its virtuality. Potentially

large values of the virtuality greatly enhance the difference between ϵ_m and ϵ .

Now we need to understand how the structure function changes in the medium. In principle one needs to calculate the hadronic tensor $W^{\mu\nu}$ and $q(x)$ for the medium modified nucleon of Eq. (38) by replacing the state $|P\rangle$ in Eq. (20) by the state $|N\rangle_M$. To leading order, the change in the structure function will be linear in $\epsilon_M - \epsilon$. The hadronic part is an off-diagonal matrix element between a free physical nucleon, $|N\rangle$ and a free physical state $|N^*\rangle$. Thus the modification is the product of a coefficient that depends on the medium and a term that is independent of the medium.

These hadronic matrix elements have not yet been calculated. Instead we adopt a phenomenological approach, based on the suppression of point-like configurations (Frank *et al.*, 1996; Frankfurt and Strikman, 1985) where the medium modified quark structure function is given by the expression

$$q_M(x) = q(x) + (\epsilon_M - \epsilon) f(x) q(x), \quad (46)$$

with the suppression of point-like components manifest by the condition $df/dx < 0$. so that the ratio of structure functions is given by $R(x) = q_M(x)/q(x)$, so that

$$\frac{dR}{dx} = (\epsilon_M - \epsilon) \frac{df}{dx}. \quad (47)$$

This expression is only meaningful for $x_B < 0.7$ where Fermi motion effects can be ignored. Given that $\epsilon_M - \epsilon > 0$ (as discussed above), Eq. (47) shows that the slope of the EMC ratio is negative, consistent with observations.

(Ciofi degli Atti *et al.*, 2007) calculated the expected size of the modification of Eq. (45) using the spectral function $P(\mathbf{p}, E)$ of (Ciofi degli Atti and Simula, 1996b) (as discussed in Section I.B.3). The average values of the virtuality are quite large, as can be seen from Table II. The average kinetic and removal energies in channel 1 (high excitation final states) are much larger than the corresponding quantities in channel 0 (low excitation final states) and the high momentum components are linked to high removal energies (Ciofi degli Atti *et al.*, 1980). (Ciofi degli Atti *et al.*, 2007) shows that these values of the virtuality, for reasonable choices of E_B and E_P , can account for the EMC effect at $x_B \approx 0.5$.

This shows that high-momentum nucleons in nuclei can cause the EMC effect. Now we need to find a similar relation between these high-momentum nucleons and the plateaus observed at high x_B in inclusive (e, e') QE scattering. We first review the kinematics. We assume that the photon is absorbed by one of the baryons contained in an interacting system of two baryons $M_2 \approx M_d$. The photon hits a baryon of momentum p in a ‘deuteron’ of momentum P , and the second, spectator baryon has momentum $p_s = P - p$. The struck nucleon has final momentum $p_f = p + q$. Let the plus-component of p be

TABLE II: The virtualities (in MeV) for channels 0 and 1 (see Eq. (7)) and their sum (Ciofi degli Atti *et al.*, 2007).

A	$\langle v_0(\mathbf{p}, E) \rangle / 2M$	$\langle v_1(\mathbf{p}, E) \rangle / 2M$	$\langle v(\mathbf{p}, E) \rangle / 2M$
^3He	-7.15	-27.44	-34.59
^4He	-26.82	-42.58	-69.40
^{12}C	-33.17	-49.11	-82.28
^{16}O	-31.40	-48.28	-79.68
^{40}Ca	-35.00	-49.54	-84.54
^{56}Fe	-31.66	-50.76	-82.44
^{208}Pb	-32.87	-59.33	-92.20

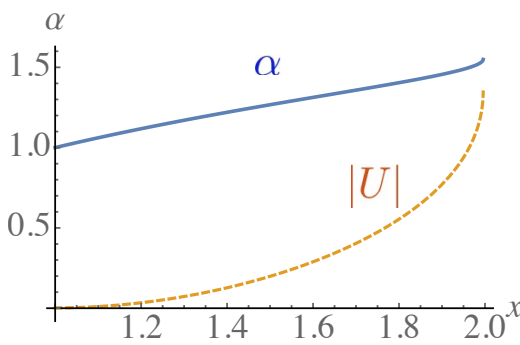


FIG. 35: (color online) α solid, $|U|$ dashed for $Q^2 = 2.7$ GeV^2 and $p_\perp = 0$. The quantity $|U|$ is presented in units of the nucleon mass M and is proportional to the virtuality $v(\mathbf{p}, E)$ via Eq. (45)

given as aM_d . The light-front fraction a is related to the Frankfurt-Strikman variable α by $a = \alpha \frac{M}{M_d}$. Then

$$p_f^- = \frac{p_\perp^2 + M^2}{aM_d + q^+} > 0 \quad (48)$$

$$p_s^- = \frac{p_\perp^2 + M^2}{(1-a)M_d} > 0. \quad (49)$$

In our convention $q^+ < 0$ so that Eq. (48) tells us that $a > 0$ and Eq. (49) tells us that $a < 1$. Conservation of energy tells us that $p_f^+ + p_f^- + p_s^+ + p_s^- = 2(M_d + \nu)$, which leads to a quadratic equation for a :

$$(aM_d + q^+)(1-a)M_d = \frac{M_d + q^+}{M_d + q^-}(p_\perp^2 + M^2). \quad (50)$$

The condition that this equation for a has real roots leads to limits on the value of p_\perp .

Fig. (35) shows the results of a specific example using $Q^2 = 2.7 \text{ GeV}^2$ and $p_\perp = 0$. Solving Eq. (50) gives the resulting values of α as a function of x_B . We see that α is considerably greater than one for $1.5 < x_B < 2$, corresponding to the plateau region of Fig. 9. Using the displayed values of α we can calculate $v(\mathbf{p}, E = p^0)$:

$$v(\mathbf{p}, p^0) = p^+ p^- - p_\perp^2 - M^2 \quad (51)$$

where $p^+ = aM_d$, $p^- = \frac{M^2 + p_\perp^2}{aM_d + q^+} - q^-$. Then the use of Eq. (45) gives the values shown in Fig. (35). This procedure gives values of $|U| \approx 0.7M$ in the plateau region. Thus, for $1.5 < x_B < 2$, we have

$$270 \text{ MeV} < |U| < 600 \text{ MeV}. \quad (52)$$

Such large values of $|U|$ can only arise from hard interactions of two nucleons, i.e., at short range.

Thus (e, e') at high x_B is associated with short-ranged correlations. Next we relate the virtuality to the observed plateaus in the cross section ratios. (Ciofi degli Atti and Simula, 1996b) showed that, for large values of $|\mathbf{p}|$:

$$n_A(\mathbf{p}) \approx n_A^{(1)}(\mathbf{p}) \approx a_2(A) n_D(\mathbf{p}). \quad (53)$$

This relation is explained in Sect. IX.

To summarize: there is a consistent picture in which short-ranged correlations are involved with significant modification of the nuclear quark distribution function by suppressing the point-like configurations. The key feature is that larger values of the nuclear excitation energy E , associated with the short-ranged correlations, correspond to larger values of virtuality and therefore to more significant deformations of the nucleon. These very same short-ranged correlations are also responsible for the validity of Eq. (53) for large values of momentum (where the virtuality is large), which via the logic of (Frankfurt and Strikman, 1981a, 1988a; Frankfurt *et al.*, 1993) is responsible for the cross section ratio plateaus. The spectral function $P(\mathbf{p}, E)$ contains the information necessary to compute both the virtuality needed to understand the DIS EMC effect and the momentum probability $n_A(\mathbf{p})$ needed to understand the plateaus.

2. Effective Field Theory

It is not necessary that the suppression of point-like configurations for off-shell nucleons be the sole origin of the EMC effect. Indeed another dynamical idea could also account for the experimental findings. For example, the presence of non-nucleonic 6-quark clusters (Sect. III D) in nuclei could be important. A more general approach, using effective field theory (EFT), which is not specific as to the underlying mechanism of medium modification has been presented (Beane and Savage, 2005; Chen and Detmold, 2005; Chen *et al.*, 2016). The authors (Chen *et al.*, 2016) show that the empirical linear relation between the magnitude of the EMC effect in deep inelastic scattering on nuclei and the short range correlation scaling factor a_2 extracted from high-energy quasi-elastic scattering at $x_B \geq 1$ is a natural consequence of scale separation and derive the relationship using effective field theory.

Their EFT Analysis proceeds by studying the dominant (leading-twist) parton distributions determined by

target matrix elements of bilocal light-cone operators. Applying the operator product expansion, the Mellin moments of the parton distributions,

$$\langle x_B^n \rangle_A(Q) = \int_{-A}^A x_B^n q_A(x_B, Q) dx_B, \quad (54)$$

are determined by matrix elements of local operators. Each of the QCD operators is matched to hadronic operators (Chen and Detmold, 2005). The relative importance of the hadronic operators in a nuclear matrix element can be systematically estimated from EFT power counting. The nuclear matrix element is given by

$$\langle x_B^n \rangle_A(Q) = \langle x_B^n \rangle_N(Q) \left[A + \alpha_n(\Lambda, Q) \langle A | (N^\dagger N)^2 | A \rangle_\Lambda \right], \quad (55)$$

where α_n depends on Λ but not A and is completely determined by the two-nucleon system. This relation is valid for all n , so after an inverse Mellin transform, the isoscalar PDFs satisfy

$$\frac{1}{A} F_2^A(x_B, Q) = F^N(x_B, Q) + g_2(A, \Lambda) \tilde{f}_2(x_B, Q, \Lambda) \quad (56)$$

where

$$g_2(A, \Lambda) = \frac{1}{A} \langle A | (N^\dagger N)^2 | A \rangle_\Lambda, \quad (57)$$

and $f_2(x_B, Q, \Lambda)$ is an unknown function independent of A . This feature is similar to that of our Eq. (47). Indeed, Equation (56) was also obtained phenomenologically in Ref. (Frankfurt and Strikman, 1981a, 1988a) using the impulse approximation. The factorization scale of the PDF is $\mu_f = Q$, while Λ is the nuclear physics “ultraviolet” cut-off that separates the high energy parton physics from lower energy hadronic and nuclear effects. The two scales must be significantly separated for the EFT description to be valid.

The second term on the right-hand side of Eq. (56) is the nuclear modification of the structure function. The shape of distortion, i.e., the x_B dependence of f_2 , which is due to physics above the scale Λ , is A independent and hence universal among nuclei. The magnitude of distortion, g_2 , which is due to physics below the scale Λ , depends only on A and Λ .

At smaller values of Q^2 , the previous analysis was generalized to apply to the (e, e') cross section at large x_B , so that

$$\sigma_A/A = \sigma_N + g_2(A, \Lambda) \sigma_2(\Lambda), \quad (58)$$

where the E_0 (incident electron energy), x_B and Q^2 dependence of σ_i is suppressed. With σ_N vanishing for $x_B > 1$, for both DIS and QE,

$$a_2(A, x_B > 1) = \frac{g_2(A, \Lambda)}{g_2(2, \Lambda)}. \quad (59)$$

In principle, a_2 could depend on E , x_B and Q^2 , however the EFT factorization shows that this dependence cancels at this order in the EFT yielding a plateau in a_2 as observed experimentally at $1.5 < x_B < 2$. The influence of Fermi motion, extends the contribution of the single nucleon PDF to x_B slightly above 1, pushing the onset of the plateau to larger values of x_B .)

Eq. (56) and the definition $R(A, x_B) \equiv F_2^A/(AF_2^N)$, lead to the result that

$$\frac{dR(A, x_B)}{dx_B} = C(x_B) [a_2(A) - 1], \quad (60)$$

has a linear relation with a_2 , with $C(x_B) = g_2(2)[f'_2 F_2^N - f_2 F_2^{N'}]/[F_2^N + g_2(2)f_2]^2$ independent of A and Λ (here, $f' = df/dx_B$). This means that EFT naturally accounts for the linear relation between the EMC slope and the height of the plateau. The function a_2 was also computed using the Green’s Function Monte Carlo method (Carlson *et al.*, 2015) and good agreement with the empirical findings is obtained.

3. The Isovector EMC Effect

This SRC-related PLC suppression model also leads to an explanation of the NuTeV anomaly (Sargsian, 2014c). We have discussed the dominance of the pn SRCs, relative to the pp and nn correlations, for nuclear internal momenta between 300 and 600 MeV/c, that is caused by the effects of the tensor force. The pp and nn components of the NN SRC are strongly suppressed since they are dominated by the central NN potential with relative $L = 0$. The resulting picture for nuclear matter consisting of protons and neutrons at densities in which inter-nucleon distances are about 1.7 fm is rather unique: it represents a system with suppressed pp and nn but enhanced pn interactions. Using this idea Sargsian (Sargsian, 2014b) predicted two new properties for the nuclear momentum distributions for momenta between the Fermi momentum and about 600 MeV/c. There is an approximate equality of p - and n - momentum distributions weighted by their relative fractions in the nucleus $x_p = Z/A$ and $x_n = (A - Z)/Z$:

$$x_p n_p^A(p) \approx x_n n_n^A(p) \quad (61)$$

with $\int d^3 p n^A(p) = 1$. The probability of a proton being in a high momentum NN SRC is inversely proportional to its relative fraction, x_p , and can be related to the momentum distribution in the deuteron $n_D(p)$:

$$n_p^A(p) = \frac{1}{2x_p} a_2(A, N) n_D(p) \quad (62)$$

and similarly for neutrons. The main predictions of Eq. (62) is that high momentum protons and neutrons became increasingly unbalanced as the ratio $(N -$

$Z)/(N+Z)$ increases. Using this equation one can calculate the fraction of the protons having momenta greater than the Fermi momentum as

$$P_p(A, N) \approx \frac{1}{2x_p} a_2(A, N) \int d^3p n_D(p) \Theta(p - k_F), \quad (63)$$

and similarly for neutrons. For example in Iron, $P_p = 23\%$, and $P_n = 20\%$.

The energetic protons in neutron rich nuclei will result also in the stronger nuclear modification of u -quarks as compared to d -quarks and the effect grows with A . The predicted effects also can be checked in parity violating deep inelastic scattering off heavy nuclei (Cloet *et al.*, 2012; Souder, 2016) (see Section VI.A.5).

4. Summary

In summary, driven by the short-range correlations between two nucleons, the strong connection between the EMC effect and the plateaus observed in (e, e') scattering at high x_B is both a natural consequence of the impulse approximation of scattering theory, and also of effective field theory. In the impulse approximation the relevant ratio is that of momentum-space densities, in the EFT the relevant ratio is that of coordinate space densities. Sect. IX shows that ratios of these are the same as long as large values of momenta are used in the impulse approximation and small values of relative distance are used in the EFT. This means that the relation shown in Fig. 34 is derived using two very different technical techniques. The fact that using two different technical approaches, each driven by short-range physics, gives the same result, gives significant credence to the interpretation that the same short-range physics accounts for both the EMC effect and the QE cross section plateaus.

The underlying mechanism of the distortion of the nucleon structure is not yet established, and could occur from PLC suppression or from other mechanisms. Nevertheless, it is very clear that the relation shown in Fig. 34 is no accident. There is a true underlying cause of the EMC effect and the observed plateaus in ratios of (e, e') scattering cross sections.

C. Are the nucleons in the correlated pair really nucleons?

According to the logic presented here, most of the correlated pair consists of nucleons, but the part that is responsible for the EMC effect consists of non-nucleonic configurations. These could be NN^* or N^*N^* configurations or more complex 6-quark configurations.

D. Determining the structure function of a free neutron

Determining the structure function of the neutron is challenging because a free neutron target does not exist. Experimentalists have therefore used deuteron or ^3He targets to extract the neutron structure which implies that our knowledge of the neutron structure function is intimately connected with the need to understand medium effects in light targets. As we shall see, medium effects in the deuteron must be accounted for accurately if one hopes to correctly understand the free neutron structure function.

1. The Deuteron IMC Effect

The deuteron In Medium Correction (IMC) effect was first introduced in Ref. (Weinstein *et al.*, 2011) and refers to the difference between the DIS cross section for the deuteron and the sum of the DIS cross sections for a free proton and neutron. One can use the EMC-SRC correlation as a phenomenological tool to constrain the deuteron IMC effect, and thus extract the free neutron structure function. Following Weinstein *et al.* (Weinstein *et al.*, 2011), we can extrapolate the linear fit to the EMC-SRC correlation to the limit of $a_2(A) \rightarrow 0$. This is the limit of no correlations, which is equivalent to a free proton-neutron pair. The intercept of this limit with the y -axis is therefore the IMC ratio of the free proton-neutron pair to the deuteron.

The $a_2(A) \rightarrow 0$ extrapolation to the y -axis of the EMC-SRC correlation gives $dR_{\text{EMC}}/dx_{a_2(A)=0} = -0.070 \pm 0.004$. Since the EMC effect is linear for $0.3 \leq x_A \leq 0.7$ for all nuclei with $A > 2$, we assume that the EMC effect is also linear in this region for the deuteron. This implies that the EMC effect for the deuteron relative to a free proton plus neutron can be written as:

$$\frac{\sigma_d}{\sigma_p + \sigma_n} = 1 - a(x_B - b) \quad \text{for } 0.3 \leq x_B \leq 0.7,$$

where σ_d and σ_p are the measured DIS cross sections for the deuteron and free proton, σ_n is the free neutron DIS cross section that we want to extract, $a = |dR_{\text{EMC}}/dx|_{a_2(A)=0} = 0.070 \pm 0.004$, and $b = 0.34 \pm 0.02$ is the average value of x_B where the EMC ratio is unity¹. This implies that $\sigma_d/(\sigma_p + \sigma_n)$ decreases linearly from 1 to 0.97 as x_B increases from 0.3 to 0.7. We can then use this relationship to extract the free neutron cross section in this x_B range, as shown in the next section below.

It should be noted that the uncertainty quoted above for the IMC slope is due to the EMC and SRC data and the

¹ The x_A correction does not significantly change the slope, a , of the EMC-SRC correlation, and it increases, the b parameter, by less than the uncertainty from reported in Ref. (Weinstein *et al.*, 2011)

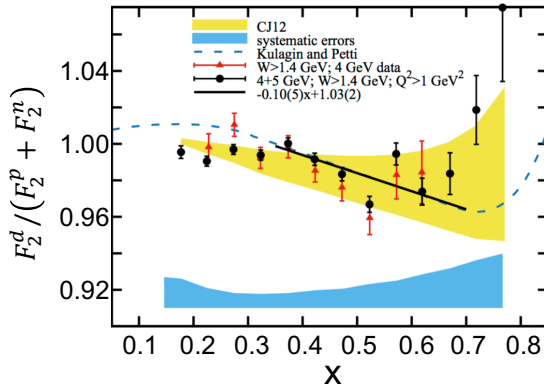


FIG. 36: The deuteron IMC ratio $R_{EMC}^d = F_2^d / (F_2^n + F_2^p)$ as extracted from the BONuS data. Total systematic uncertainties are shown as a band arbitrarily positioned at 0.91 (blue). The yellow band shows the CJ12 (Owens *et al.*, 2013) limits expected from their nuclear models. The black points are the combined 4- and 5-GeV data, whereas the red points are the 4-GeV data alone. The dashed blue line shows the calculations of Ref. (Kulagin and Petti, 2006). The solid line (black) is the fit to the black points for $0.35 < x_B < 0.7$. Figure adapted from (Griffioen *et al.*, 2015).

fit. It does not include any uncertainty due to corrections applied to the EMC and SRC data. As stated above, if we include the proposed correction for $a_2(A)$ due to the c.m. motion of the correlated pair, then the fit parameter increases by 25% and so does the free proton plus neutron EMC effect. These effects are discussed in detail in (?).

Following the prediction of the IMC effect, the BONuS collaboration (Tkachenko *et al.*, 2014) published their experimental extraction of the IMC effect, measured at $Q^2 > 1 \text{ GeV}^2$ and $W > 1.4 \text{ GeV}$, see Fig. 36 (Griffioen *et al.*, 2015). A linear fit for $0.35 < x < 0.7$ yields $dR_{EMC}^d/dx = -0.1 \pm 0.05$ where the uncertainties come from the fit. This result is consistent with the IMC prediction of -0.07 . For $x < 0.5$ the EMC ratios R_{EMC}^d agree within uncertainties with those obtained using more stringent cuts in W . The ratio for $x_B > 0.5$ continues the trend of the lower- x_B data, with a hint of the expected rise above $x_B = 0.7$ as seen in R_{EMC}^A for heavier nuclei, but these high- x_B values are more uncertain because there are fewer data points for resonance averaging.

2. The Free Neutron Structure Function

If the structure function F_2 is proportional to the DIS cross section (*i.e.*, if the ratio of the longitudinal to trans-

verse cross sections is the same for n, p and d [see discussion in (Geesaman *et al.*, 1995)]), then the free neutron structure function, $F_2^n(x_B, Q^2)$, can also be deduced from the measured deuteron and proton structure functions and from the deuteron IMC effect:

$$F_2^n(x_B, Q^2) = \frac{2F_2^d(x_B, Q^2) - [1 - a(x_B - b)]F_2^p(x_B, Q^2)}{[1 - a(x_B - b)]} \quad (64)$$

which leads to

$$\frac{F_2^n(x_B, Q^2)}{F_2^p(x_B, Q^2)} = \frac{2\frac{F_2^d(x_B, Q^2)}{F_2^p(x_B, Q^2)} - [1 - a(x_B - b)]}{[1 - a(x_B - b)]} \quad . \quad (65)$$

This is only valid for $0.35 \leq x_B \leq 0.7$.

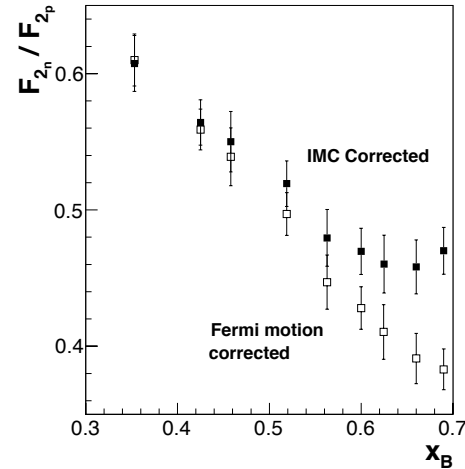


FIG. 37: The ratio of neutron to proton structure functions, $F_2^n(x_B, Q^2)/F_2^p(x_B, Q^2)$ as extracted from the measured deuteron and proton structure functions, F_2^d and F_2^p . The filled symbols show F_2^n/F_2^p extracted by (Weinstein *et al.*, 2011) from the deuteron In Medium Correction (IMC) ratio and the world data for F_2^d/F_2^p at $Q^2 = 12 \text{ GeV}^2$ (Arrington *et al.*, 2009). The open symbols show F_2^n/F_2^p extracted from the same data correcting only for nucleon motion in deuterium using a relativistic deuteron momentum density (Arrington *et al.*, 2009). Figure adapted from (Weinstein *et al.*, 2011).

Fig. 37 shows the ratio of F_2^n/F_2^p extracted by (Weinstein *et al.*, 2011) using the IMC-based correction and the $Q^2 = 12 \text{ GeV}^2$ ratio F_2^d/F_2^p from Ref. (Arrington *et al.*, 2009). Note that the ratio F_2^d/F_2^p is Q^2 -independent from $6 \leq Q^2 \leq 20 \text{ GeV}^2$ for $0.4 \leq x_B \leq 0.7$ (Arrington *et al.*, 2009). The dominant uncertainty in this extraction is the uncertainty in the measured F_2^p/F_2^d . The

IMC-based correction increases the extracted free neutron structure function (relative to that extracted using the deuteron momentum density (Arrington *et al.*, 2009)) by an amount that increases with x_B . This is qualitatively similar to the recent extraction of (Cosyn and Sargsian, 2016). Thus, the IMC-based F_2^n strongly favors model-based extractions of F_2^n that include nucleon modification in the deuteron (Melnitchouk and Thomas, 1996a).

The IMC based extraction of F_2^n/F_2^p , extrapolated in the region of $x_B < 0.3$, is compared in Fig. 38, to several other experimental and phenomenological extractions of this ratio. Also shown are several QCD predictions. see (Holt, 2013; Roberts *et al.*, 2013) for details.

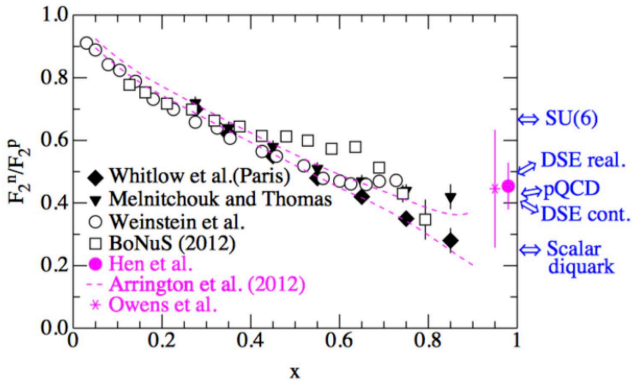


FIG. 38: F_2^n/F_2^p as a function of x_B . Results from the IMC and other phenomenological extractions are compared to selected theoretical predictions. See (Holt, 2013; Roberts *et al.*, 2013) for details.

3. The d/u ratio at large x_B

The ratio of the neutron structure function, F_2^n , to the proton structure function, F_2^p , is particularly interesting as it can be related, within the parton model, to the ratio of the d-quark and u-quark distributions. The latter provides a unique opportunity for studying the flavor and spin dynamics of quarks in the nucleon, with the d/u quark distribution ratio in particular being very sensitive to different mechanisms of spin-flavor symmetry breaking (Holt and Roberts, 2010; Melnitchouk and Thomas, 1996b).

Historically, proton DIS data placed strong constraints on the u -quark distribution, while neutron structure functions were used to constrain the d -quark distribution and form the d/u ratio. Specifically, the d/u ratio in the far valence quark dominance domain (i.e., at large

x_B) was extracted from the F_2^n/F_2^p strcute funciton ratio using:

$$F_2^n/F_2^p = [1 + 4(d_v/u_v)]/[4 + (d_v/u_v)],$$

where the absence of free neutron targets meant that the neutron straucture function used was not measured directly, but instead extracted from deuterium DIS data. However, uncertainties in the nuclear corrections in the deuteron, such as those associated with nucleon off-shell effects and the large-momentum components of the deuteron wave function, give rise to significant uncertainties in the resulting d/u ratio for $x_B \gtrsim 0.5$ (Accardi *et al.*, 2011).

To rectify the situation, Hen *et al.*, (Hen *et al.*, 2011a) used the the phenomenological IMC corrected extraction of F_2^n/F_2^p discussed above as an added constraint on the extraction of the d/u ratio in the global analysis of the CTEQ-JLab collaboration (Accardi *et al.*, 2011).

Recently, new data on charged lepton and W boson asymmetry measured at the Tevatron were published (Abazov *et al.*, 2013, 2014, 2015). These data are sensitive to the large-x d/u ratio with no nuclear uncertainties (Accardi *et al.*, 2016).

Fig. 39 shows the d/u ratio at large-x extracted from global QCD analysis using DIS data without (CJ11, (Accardi *et al.*, 2011)) and with (CJ11+IMC, (Hen *et al.*, 2011a)) the IMC constraint and using the new asymmetry data, with no nuclear corrections applied (CJ15, (Accardi *et al.*, 2016) and CT14, (Dulat *et al.*, 2016)). As can be seen, while the various extractions somewhat differ at lage-x, the IMC costraint on the CJ11 analysis constrain the distributoin in a way that is consistent with the effect of the new asymmetry data.

To summarize, the use of the IMC-extracted neutron structure function directly constrains the d -quark PDF for $x \lesssim 0.7$, and indirectly for $x \rightarrow 1$. We find the d/u ratio in the limit $x \rightarrow 1$ to be 0.23 ± 0.09 at the 90% confidence level, in overall agreement with new extractions using charged lepton and w boson asymmetry and with agreement with the models of (Cloet *et al.*, 2005a; Farrar and Jackson, 1975) which predict intermediate values of d/u between the SU(6) symmetry and scalar diquark dominance limits.

V. Existing electromagnetic form factor searches

We have shown that the experimental and theoretical evidence indicates that the structure of the nucleon is modified by its immersion in a nucleus. The only models that account for the EMC effect, the plateaus of the high x_B (e, e') reaction and the lack of a medium effect in the nuclear Drell-Yan data are those involving short-ranged correlations. Nevertheless, the task of understanding the EMC and SRC effects is not complete. The available models need to be improved in a technical tense (to be

discussed in Sect. VI.B). We need models that are sufficiently complete that they can explain both the EMC effect, the nuclear Drell-Yan data and also predict and account for new independent phenomena.

If the nuclear medium modifies the bound nucleon structure functions (and thus their wave functions), then it almost certainly will modify their electromagnetic form factors. All of the medium modification models predict that the existence of medium-modified bound electromagnetic form factors, see Sect. III. These effects could be manifest in the quasi-elastic nucleon knockout ($e, e'N$) cross sections, and the longitudinal response of the nucleus in the inclusive (e, e') process. The influence of nucleon modification on the nuclear elastic form factor can not be detected because the nuclear charge distribution is the convolution of the imprecisely known distribution of nucleons within the nucleus with the smaller-sized charge distribution of the nucleon.

This section will discuss the experimental evidence for modification of bound nucleon form factors.

A. Polarization transfer in the $(\vec{e}, e' \vec{p})$ reaction

Polarization transfer in the $H(\vec{e}, e' \vec{p})$ reaction allowed measurement of the ratio of the free proton electromagnetic form factors G_E/G_M with much smaller systematic uncertainties than previous methods (Perdrisat *et al.*, 2007). This technique was then applied to measure the ratio of bound proton electromagnetic form factors using the quasielastic $A(\vec{e}, e' \vec{p})$ reaction (Dieterich *et al.*, 2001; Malace *et al.*, 2011; Paolone *et al.*, 2010; Strauch *et al.*, 2003; Strauch, 2012). The ratio of the

longitudinal and transverse polarization transfers is proportional to the ratio of G_E/G_M for the free proton, $P'_x/P'_z \propto G_E/G_M$ (Perdrisat *et al.*, 2007). For a bound proton, one must also correct for the effects of meson exchange currents, isobar configurations, and especially final state interactions. After using a model to correct for these effects, the polarization double ratio

$$R \equiv \left(\frac{P'_x}{P'_z} \right)_A / \left(\frac{P'_x}{P'_z} \right)_{^1H} \quad (66)$$

should be sensitive to medium modification of the form factor ratio. The induced polarization P_y measured in the $(e, e' \vec{p})$ reaction should be more sensitive to final state interactions and much less sensitive to medium modification effects.

Fig. 40 shows the ${}^4He(\vec{e}, e' \vec{p}){}^3H$ double ratio R and the induced polarization, P_y , measured at small values of missing momentum ($p_{miss} < 150$ MeV/c) over a range of Q^2 . Relativistic distorted-wave-impulse approximation (rDWIA) calculations by the Madrid group (Cabanturo *et al.*, 1998; Udias *et al.*, 1999; Udias and Vignote, 2000) can only explain the data if they include medium-modified form factors. They calculated the induced polarization and the polarization transfer ratio using the unmodified but offshell cc1 and cc2 (De Forest, 1983b) current operators and the optical potentials of (Horowitz, 1985; Murdock and Horowitz, 1987) to account for final state interactions. No charge exchange effects (photon knocks out neutron, which undergoes a charge exchange reaction) were included. This unmodified calculation agreed with the induced polarization data when using the cc1 current operator. However, good agreement with the measured value of R was only achieved by including either the QMC (Lu *et al.*, 1999) or CQS (Smith and Miller, 2004) medium modified form factors.

Schiavilla *et al.* (Schiavilla *et al.*, 2005) calculated P_y and R using DWIA. However, they computed the final state interactions using an optical potential that includes both spin-independent and spin-dependent charge exchange terms. They updated their calculation in 2010 with new parameters. They updated their calculation in 2010 with new parameters. While their calculation describes both P_y and R without medium modified form factors, its significance is decreased because they did not follow the standard procedure (Austern, 1970) of independently constraining the parameters of the optical potential they used to describe the final state interactions. Thus our view is that the results of the nuclear polarization experiments strongly indicate that medium effects do influence electromagnetic form factors. We eagerly await new experiments with improved precision and also at larger values of p_{miss} which would confirm or rule out this interpretation.

Experiments performed at the Mainz Microtron (MAMI) using the A1 beam-line (Yaron *et al.*, 2016) measured the polarization transfer ratio R for deuterium and

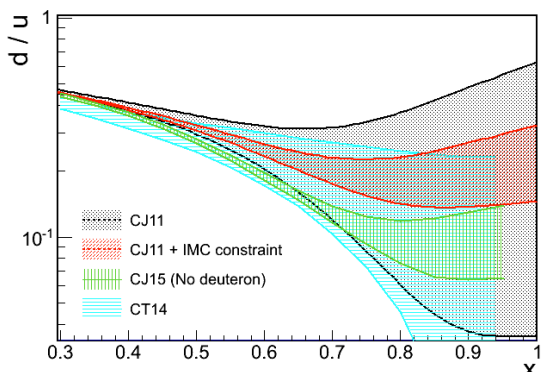


FIG. 39: d/u ratio at $Q^2 = 12$ GeV 2 with the full theoretical uncertainty from Ref. (Accardi *et al.*, 2011) (black) and with the IMC constraint at the 90% C. L. (red). Figure adapted from (Hen *et al.*, 2011a).

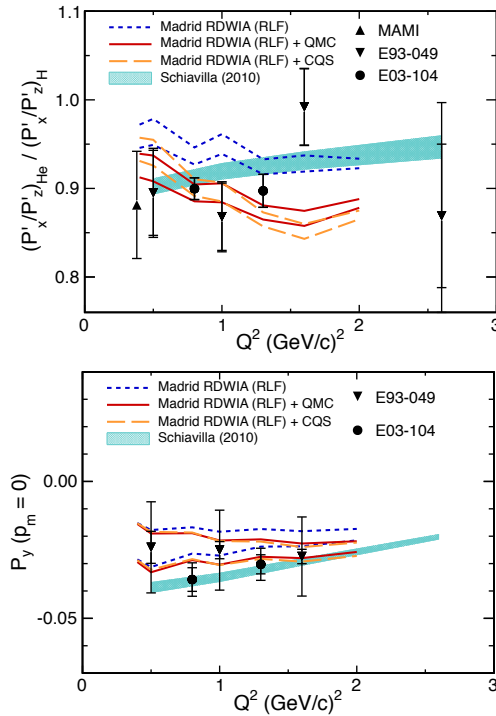


FIG. 40: The measured ${}^4\text{He}(\vec{e}, e' \vec{p}){}^3\text{H}$ polarization-transfer double ratio R (upper panel) and induced polarization P_y (lower panel) as a function of Q^2 : open symbols: (Dieterich *et al.*, 2001; Strauch *et al.*, 2003) and filled circles: (Malace *et al.*, 2011; Paolone *et al.*, 2010). The data are compared to DWIA calculations from (Schiavilla *et al.*, 2005) (updated in 2010) using unmodified form factors and from the Madrid group (Caballero *et al.*, 1998; Udiás *et al.*, 1999; Udiás and Vignote, 2000) using the cc1 (lower set of curves) and cc2 (upper set of curves) off-shell current operators in combination with unmodified (black dashed line), QMC modified (red solid line) and CQS modified (red dashed line) in medium form factors. See text for details. Figure adapted from (Strauch, 2012).

${}^{12}\text{C}$ at lower Q^2 ($Q^2 = 0.175$ and 0.4 GeV 2) but twice the virtuality than at Jefferson Lab. For deuterium, the ratio R decreases significantly with virtuality and is consistent with that previously measured on ${}^4\text{He}$. This indicates that the effect in nuclei is due to the virtuality of the knocked-out proton and not due to the average nuclear density. The deuteron calculations (Arenhövel *et al.*, 2005) predict the deviation and associate most of it with FSI (Yaron *et al.*, 2016). The $\approx 10\%$ differences between the data and calculations may indicate the need for in-medium modifications. The carbon data is still under analysis.

Jefferson Lab experiment E12-11-002 will measure polarization-transfer observables as a function of virtuality for both ${}^4\text{He}$ and ${}^2\text{H}$ and will measure the proton

recoil polarization at $Q^2 = 1.8$ GeV 2 to help us understand whether the observed difference in the ratio R can be attributed to medium modifications or merely to FSI.

B. Polarization transfer in the $(\vec{e}, e' \vec{n})$ reaction

A complementary experiment would be the measurement of polarization transfer to the neutron in quasielastic scattering in the $(\vec{e}, e' \vec{n})$ reaction. Cloët *et al.* (Cloët *et al.*, 2009c) studied possible in-medium changes of the bound neutron electromagnetic form-factor ratio with respect to the free ratio, the superratio $(G_E^*/G_M^*) / (G_E/G_M)$. At small values of Q^2 this superratio depends on the in-medium modifications of the neutron magnetic moment and the effective electric and magnetic radii. The superratio of the neutron is dominated by the expected increase of the electric charge radius in the nuclear medium and is found to be greater than one. In contrast, the proton superratio is predicted to be smaller than one. A comparison of high-precision measurements of the reactions ${}^2\text{H}(\vec{e}, e' \vec{n})p$ and ${}^4\text{He}(\vec{e}, e' \vec{n}){}^3\text{H}$ would test these predictions.

However, a very major drawback to nuclear polarization transfer measurements, no matter whether the proton or neutron is detected, is that medium modifications that affect both G_E and G_M will tend to cancel in the ratio. See Fig. 33, for example.

C. The (e, e') reaction and the Coulomb Sum Rule (CSR)

This sum rule (De Forest and Walecka, 1966; McVoy and Van Hove, 1962) states that the integral of the longitudinal response function at fixed momentum transfer over all possible energy transfers should equal the total charge of the nucleus, Z . The first measurement of the CSR (Altemus *et al.*, 1980) found a smaller result than that—quenching was observed. This indicated that the cross section for scattering from a bound nucleon was significantly less than the free cross section. Thus, (Cloët *et al.*, 2016) say that the first hints of QCD effects in nuclei came from quasielastic electron scattering on nuclear targets (Altemus *et al.*, 1980; Meziani *et al.*, 1984; Noble, 1981). However, later work cast doubt on this result.

The (e, e') inclusive cross section can be written as

$$\frac{d^2\sigma}{d\Omega d\nu} = \sigma_{Mott} \left[\frac{Q^4}{|\mathbf{q}|^4} R_L(\nu, |\mathbf{q}|) + \left(\frac{Q^2}{2|\mathbf{q}|^2} + \tan^2 \frac{\theta}{2} \right) R_T(\nu, |\mathbf{q}|) \right] \quad (67)$$

where σ_{Mott} is the Mott cross section, R_L and R_T are the longitudinal and transverse response functions, and θ is the electron scattering angle. In the non-relativistic limit of the impulse approximation (Bertozzi *et al.*, 1972;

De Forest and Walecka, 1966) one has

$$R_L(\omega, \mathbf{q}) = \langle A | \sum_{i=1}^Z e^{i\mathbf{q} \cdot \mathbf{r}_i} \delta(\omega - H) \sum_{j=1}^Z e^{-i\mathbf{q} \cdot \mathbf{r}_j} | A \rangle G_E^2(q^2),$$

where H is the nuclear Hamiltonian, the ground state energy is taken as 0, and for simplicity we assume that neutrons do not contribute. The non-relativistic formulation is only valid when $\mathbf{q}^2 \approx Q^2$. Since R_L is proportional to the square of G_E , its sensitivity to medium effects is greater than the polarization transfer measurements.

The Coulomb sum is the integral over *all* values of ν (including the inaccessible time-like regime where $\nu > |\mathbf{q}|$):

$$\frac{R_L(q)}{G_E^2(q^2)} = \frac{\int d\nu R_L(\nu, \mathbf{q})}{G_E^2(q^2)} = \langle A | \sum_{i,j=1}^Z e^{i\mathbf{q} \cdot (\mathbf{r}_i - \mathbf{r}_j)} | A \rangle. \quad (68)$$

Splitting Eq. (68) into terms with $i = j$ and $i \neq j$ we get:

$$\frac{R_L(q)}{G_E^2(q^2)} = Z + Z(Z-1) \int d^3r d^3r' e^{i\mathbf{q} \cdot (\mathbf{r} - \mathbf{r}')} \rho_2(\mathbf{r}, \mathbf{r}'), \quad (69)$$

where ρ_2 is the two proton density function, see Eq. (80). At large enough momentum transfer the second term vanishes as $1/\mathbf{q}^4$, so that one finds the CSR:

$$\lim_{Q^2 \rightarrow \infty} \frac{R_L(q)}{G_E^2(q^2)} = Z. \quad (70)$$

Since electron scattering doesn't measure the cross section in the time-like region, the Coulomb sum is properly defined (Cloet *et al.*, 2016) as an integral over ν from energies just above the elastic peak to $|\mathbf{q}|$:

$$S_L(|\mathbf{q}|) = \int_{\nu^+}^{|\mathbf{q}|} d\nu \frac{R_L(\nu, |\mathbf{q}|)}{Z G_{Ep}^2(Q^2) + N G_{En}^2(Q^2)}, \quad (71)$$

where G_{Ep} and G_{Mp} are the free nucleon Sachs electric form factors. The quantity S_L can be correctly be compared with the results obtained from electron scattering.

The initial motivation to measure the Coulomb Sum Rule (De Forest and Walecka, 1966) was to learn about ρ_2 . However, the recent focus has been to learn about nucleon medium modification at large values of the momentum transfer where the effect of ρ_2 is negligible.

(Cloet *et al.*, 2016) discuss the interesting history of the theory. Calculations (Horikawa and Bentz, 2005; Saito *et al.*, 1999), in which the internal structural properties of bound nucleons are self-consistently modified by the nuclear medium unsurprisingly predict significant quenching of the CSR. However, calculations that assume an unmodified nucleon electromagnetic current (Carlson *et al.*, 2002; Do Dang *et al.*, 1987; Kim *et al.*, 2006; Mihaila and Heisenberg, 2000), including the state-of-the-art Green function Monte Carlo (GFMC) result for ^{12}C

from Ref. (Lovato *et al.*, 2013, 2016), find modest or no quenching of the CSR. Most recently (Cloet *et al.*, 2016) used an NJL model in an to find a dramatic reduction of the Coulomb sum rule for $|\mathbf{q}| \gtrsim 0.5$ GeV, driven by changes to the bound-proton Dirac form factor.

The experimental status of the CSR is unclear. The initial measurements found quenching of the CSR for ^{12}C , ^{40}Ca and ^{56}Fe (Altemus *et al.*, 1980; Meziani *et al.*, 1984). However, a reanalysis of these data (Jourdan, 1995, 1996), utilizing an alternative prescription for the Coulomb corrections, concluded that there is no quenching. The analysis of the Coulomb corrections in those works was later challenged (Aste *et al.*, 2005; Aste, 2008; Wallace and Tjon, 2008) and quenching of the CSR over a wider range of nuclei was reported in Ref. (Morgenstern and Meziani, 2001). This impasse over the CSR should be resolved by forthcoming results at high momentum transfer and on a variety of nuclear targets from Jefferson Lab Experiment E05-110 (Choi *et al.*, 2005). Verification or disproof of the CSR quenching should reveal critical aspects of nucleon modification in nuclei.

VI. Future directions in nuclear deep inelastic scattering and detecting short-ranged correlations

A. Experiment

There are several different promising experimental approaches to understanding the EMC-SRC correlation and the origin of the EMC effect. The most promising approach is to directly test the EMC-SRC correlation by measuring the change in bound nucleon structure function with nucleon momentum using tagged structure function measurements.

The second approach is to test other predictions of models of the EMC effect by measuring other quantities related to nucleon modification, including measuring the bound ratio of electric to magnetic elastic form factors using polarization transfer $A(\vec{e}, e' \vec{p})$ and measuring the Coulomb Sum Rule.

Lastly, we can learn more about SRC and about the EMC effect individually in several ways. The first way is to extend EMC and SRC inclusive measurements to more nuclei over a wider range of momentum transfer. We can also extend semi-exclusive and exclusive SRC measurements. We can select the nucleons we study by measuring the polarized EMC effect and we can measure the isospin dependence of the EMC effect in asymmetric nuclei by measuring parity violating deep inelastic scattering.

1. Inclusive EMC and SRC Measurements

The inclusive EMC and SRC measurements described in sections III and II were performed on a limited number of nuclei and, in the case of SRC measurements and the

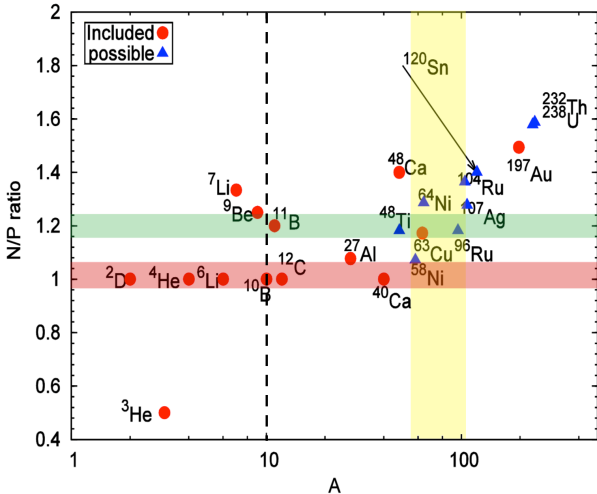


FIG. 41: Phase-space of nuclei considered for future EMC/SRC measurements at Jefferson Lab as a function of their mass number (A) and nuclear asymmetry (N/Z). The vertical dashed line at $A = 10$ separates light and medium / heavy nuclei. Red points mark nuclei planned to be measured and blue triangles mark nuclei that could also be measured. Horizontal and vertical bands mark nuclei with similar asymmetries and different mass numbers and vice-versa.

JLab EMC measurements, in a limited kinematic range. Therefore, it is natural to extend both EMC and SRC measurements to additional nuclei over a wider kinematical range.

Fig. 41 shows the nuclei that can or will be measured at Jefferson Lab as a function of their mass number (A) and nuclear asymmetry (N/Z). As indicated by the horizontal and vertical bands, a wise selection of nuclei allows for a systematical experimental study of SRC and the EMC effect for fixed nuclear asymmetry as a function of mass number and for fixed mass number as a function of asymmetry. The planned Jefferson Lab measurements (Arrington and Day, 2006; Arrington *et al.*, 2010; Petratos *et al.*, 2010; Solvignon-Slifer and Arrington, 2011) will cover a wide range of mass numbers and asymmetries. Measurements with unstable nuclei at other laboratories could significantly extend the available range of nuclear asymmetry.

Light and heavy nuclei can exhibit significantly different nuclear effects. Medium and heavy nuclei ($A \geq 10$) exhibit properties of nuclear saturation and can be relatively well described using effective theories for strongly interacting many-body Fermi systems. However, light nuclei span a wide range of nuclear densities and asymmetries, with some nuclei exhibiting a rich cluster-like substructure.

An additional advantage of light-nuclei studies is the

ability to compare the experimental results with detailed ab-initio nuclear structure calculations. Assuming reaction mechanisms such as FSI, MEC and others are under control, such comparisons of experiment and theory can offer significant insight into the underlying microscopic physics. For heavy nuclei, such ab-initio calculations of short-range nuclear structure are still limited, but rapid progress is being made (Hagen *et al.*, 2015; Wiringa *et al.*, 2014b).

In addition to extending the range of nuclei measured, it is also important to extend the measured Q^2 range. This is especially important for SRC studies where the minimum initial momentum depends strongly on Q^2 (see Fig. 6). The SRC cross section ratios of (Egiyan *et al.*, 2003) were measured at $1.4 \leq Q^2 \leq 2.6 \text{ GeV}^2$ with most of the data at $Q^2 < 2 \text{ GeV}^2$ (see Fig. 9a). They observed flat plateaus in the cross section ratio for $1.5 \leq x_B \leq 1.9$, which corresponds to $250 \leq p_{min} \leq 500 \text{ MeV}/c$ which is where we expect tensor correlations to dominate. By contrast, the SRC cross section ratios of (Fomin *et al.*, 2012a) which were measured at $Q^2 = 2.7 \text{ GeV}^2$ exhibit “plateaus” that are not quite as flat, especially for heavier nuclei (see Fig. 9a). At $Q^2 = 2.7 \text{ GeV}^2$, $1.5 \leq x_B \leq 1.9$ corresponds to $325 \leq p_{min} \leq 700 \text{ MeV}/c$, which extends beyond the tensor correlations region into the central correlations region. Measuring the Q^2 dependence of the SRC plateaus will help us quantitatively relate the experimental results to detailed ab-initio nuclear structure calculations.

The Q^2 -dependence of the EMC effect has been studied over a wide kinematical regime. However, there are still several intriguing questions about higher twist effects that should be studied systematically. The Jefferson Lab 6 GeV EMC effect measurements included data with invariant mass, $W > 1.4 \text{ GeV}$, a region that is dominated by resonance production rather than DIS. The fact that the measured EMC ratios agreed with the SLAC data, measured at higher W , showed that resonance contributions cancel to a large extent in the A/d ratio. By covering a broader kinematic range, the future 12 GeV measurements will help quantify this issue.

2. Polarized EMC Measurements

Motivated by open questions about the EMC effect and the “proton spin crisis”, Jefferson Lab will perform the first measurement of the spin-dependent EMC effect utilizing CLAS12 in Hall B with 11 GeV polarized electrons and polarized targets (Kuhn and Brooks, 2014). They will determine the ratio of the double-spin asymmetries measured on ^7Li (using ^7LiD) in which a highly polarized proton is embedded in the nuclear medium and on the proton (using ^6LiH). The double spin asymmetry is

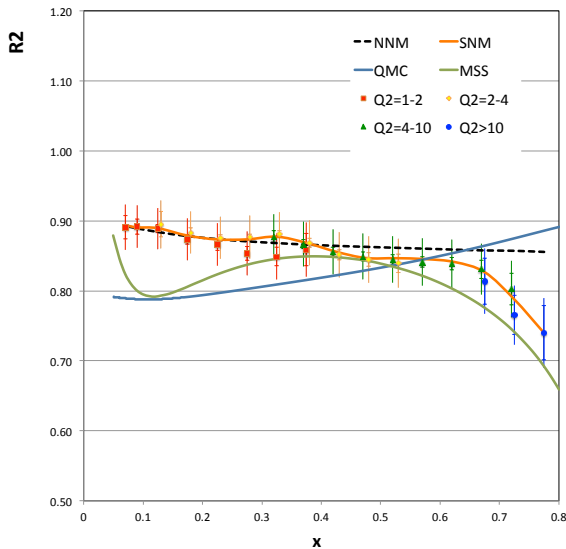


FIG. 42: The expected results of the polarized EMC effect measurement at Jefferson Lab. The ratio of the parallel double spin asymmetry $A_{||}$ for ${}^7\text{Li}(\vec{e}, e')$ to $\vec{p}(\vec{e}, e')$, normalized by multiplying it with the “naive” unpolarized structure function ratio for ${}^7\text{Li}$ over hydrogen, plotted vs x_B . The models are NNM (naive nuclear model with no fermi motion), SNM (standard nuclear model with fermi motion and kinematical binding energy effects), QMC (Quark-Meson Coupling model), and MSS (x-rescaling (Fanchiotti *et al.*, 2014)). Figure adapted from (Kuhn and Brooks, 2014).

measured as

$$A_{||} = \frac{d\sigma_{\downarrow\uparrow} - d\sigma_{\uparrow\uparrow}}{d\sigma_{\downarrow\uparrow} + d\sigma_{\uparrow\uparrow}}$$

and is approximately equal to the ratio of polarized to unpolarized structure functions: $g_1^{{}^7\text{Li}}/F_1^{{}^7\text{Li}}$. Many systematic uncertainties will cancel in the asymmetries and in the ratios of asymmetries. Together with the unpolarized structure function (also to be measured at Jefferson Lab), they will also extract $g_1^{{}^7\text{Li}}$ and, using a sophisticated modern wave function model, extract the in-medium proton spin structure function function $g_1^{p||{}^7\text{Li}}$ for a proton bound in ${}^7\text{Li}$. They will cover a kinematic range of $1 < Q^2 < 15 \text{ GeV}^2$ and $0.06 < x_B < 0.8$.

Mean field models of nucleon modification predict stronger effects than in the unpolarized structure functions. On the other hand, since nucleons in tensor correlations tend to have opposite spin to the overall nuclear spin, the EMC effect could be minimal or even in the opposite direction. These data will provide new constraints on models for the EMC effect, some of which predict that medium modifications of quark distributions depend strongly on the quark helicities (see Fig. 42).

3. Semi-Inclusive and Exclusive SRC Measurements

We can learn more about high momentum nucleons and SRC in nuclei by scattering an electron or other probe from a nucleus and detecting one or more of the ejected nucleons. $A(e, e'p)$ experiments can measure the amounts of high momentum nucleons in different nuclei. One Jefferson Lab experiment (?) will measure ${}^3\text{H}$ and ${}^3\text{He}(e, e'p)$ as a function of p_{miss} in kinematics where FSI are small in order to determine the ratio of the ${}^3\text{He}$ and ${}^3\text{H}$ momentum distributions. In the naive SRC picture, this ratio should be two at low p_{miss} because there are twice as many protons in ${}^3\text{He}$ as in ${}^3\text{H}$ and it should decrease to one at high p_{miss} because there are two pn pairs each in ${}^3\text{He}$ and ${}^3\text{H}$. Similar experiments could measure how the number of high momentum protons changes as you add eight *neutrons* from ${}^{40}\text{Ca}$ to ${}^{48}\text{Ca}$ (Cohen *et al.*, 2016).

We can gain more information about SRC pairing in nuclei by knocking out a high-initial momentum nucleon and detecting its correlated partner, either with electron or proton probes, $A(e, e'pN)$ or $A(p, 2pN)$. By extending the range of missing momentum we can study the transition from tensor dominance (at $300 \leq p_{miss} \leq 500 \text{ MeV}/c$) to the scalar repulsive core (at higher p_{miss}). By focusing on lower p_{miss} , we can map the transition from the mean-field to the SRC-dominated domain (the nuclear “Migdal jump”). By extending the A -dependence of SRC pair abundancies and properties we can learn about SRC-pair quantum numbers and provide data for a quantitative theory of SRCs.

4. Tagged Structure function Measurements

The EMC Effect is measured in inclusive (e, e') DIS from a nucleon in a nucleus. In order to learn more about the DIS reaction, we can “tag” the reaction by detecting a recoiling nuclear fragment in coincidence with the scattered electron. By choosing the nuclear fragment and kinematics wisely, we can restrict the initial state of the struck nucleon (the nucleon that absorbed the virtual photon), and thereby learn more about the microscopic origin of the EMC effect.

The simplest example for such a process is DIS on the deuteron. If we can detect a nucleon with momentum \mathbf{p} that did not interact in the DIS reaction and did not have a final state interaction (i.e., a spectator), then we know that the struck nucleon had initial momentum $-\mathbf{p}$. We can then measure the cross section for scattering from a nucleon in the nucleus as a function of its initial momentum. This will allow us to extract F_2 and hence the quark distributions.

This was initially studied with 5.7 GeV electrons incident on deuterium, measuring the scattered electron and the recoil proton with the CLAS spectrometer (Klimenko

et al., 2006). While this measurement did not have the kinematic reach to unambiguously measure a change in the nucleon structure function, they did show that protons emitted at large angles, $\theta_{pq} > 120^\circ$ (where θ_{pq} is the angle between the proton and the virtual photon), were predominantly spectators. Later theoretical works support this observation (Cosyn and Sargsian, 2011; Palli *et al.*, 2009).

In practice, experiments will measure the ratio of cross sections at fixed recoil momentum and different values of x'_B where

$$x'_B = \frac{Q^2}{2p_\mu q^\mu} = \frac{Q^2}{2[(M_d - E_S)\nu + \mathbf{p}_S \cdot \mathbf{q}]}$$

is the value of x_B in the frame of the struck nucleon, M_d is the deuteron mass, and E_S and \mathbf{p}_S are the energy and momentum of the spectator nucleon. They will measure

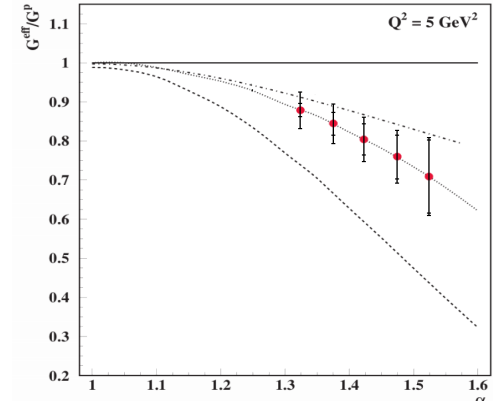
$$\frac{F_2^{bound}(x'^{hi}_B, Q_1^2, \mathbf{p}_S)}{F_2^{free}(x'^{hi}_B, Q_1^2)} = \frac{\sigma_{DIS}(x'^{hi}_B, Q_1^2, \mathbf{p}_S)}{\sigma_{DIS}(x'^{low}_B, Q_2^2, \mathbf{p}_S)} \cdot \frac{\sigma_{DIS}^{free}(x'^{low}_B, Q_2^2)}{\sigma_{DIS}^{free}(x'^{hi}_B, Q_1^2)} \cdot R_{FSI} \quad (72)$$

where σ_{DIS}^{free} is the free-nucleon DIS cross section, R_{FSI} is a correction factor for the effects of final state interactions, $x'^{low}_B \approx 0.3$ where the EMC effect is very small (i.e., where the EMC ratio is very close to 1), and $x'^{hi}_B > 0.45$.

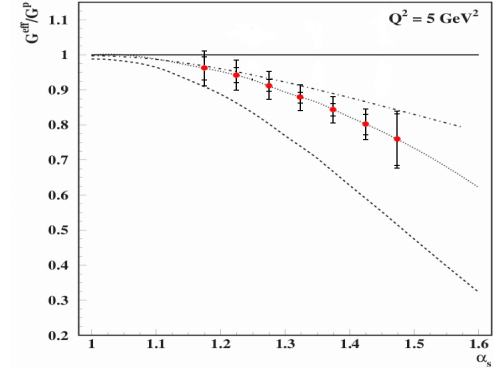
By measuring the ratio of the bound to free nucleon structure functions as a function of spectator momentum (i.e., of nucleon initial momentum), these experiments will answer the crucial question of which nucleons are modified. Little momentum dependence would imply that the mean-field nucleons are modified and large momentum dependence would imply that SRC nucleons are modified.

There are two approved Jefferson Lab experiments to measure this reaction. Experiment E12-11-107 (Hen *et al.*, 2011b) will measure neutron modification by detecting the scattered electrons in the Hall C magnetic spectrometers and the spectator protons in a set of GEM detectors and scintillators covering scattering angles from about 80° to 170° . The expected results are shown in Fig. 43b. Experiment E12-11-003A (Hen *et al.*, 2014a) will measure proton modification by detecting the scattered electrons in the CLAS12 forward and the spectator neutrons in a large scintillator array covering scattering angles from 160° to 170° . The expected results are shown in Fig. 43a.

A second category of experiments consists of measuring the tagged EMC ratio. We can “tag” different reaction mechanisms by detecting either a spectator nucleon or a recoil $A - 1$ nucleus. The main idea is that the electron scatters from a quark in one nucleon. If that nucleon belongs to an SRC NN pair, then its partner nucleon



(a) Bound proton structure via $d(e, e' n_{recoil})X$ scattering



(b) Bound neutron structure via $d(e, e' p_{recoil})X$ scattering

FIG. 43: The expected results from future Jefferson Lab tagged DIS measurements (Hen *et al.*, 2014a, 2011b).

will leave the nucleus. If that nucleon does not belong to an NN SRC pair, then the $A - 1$ nucleus is much more likely to recoil intact. In either case, we will need to fully account for FSI effects. Instead of the inclusive cross section ratio, the tagged EMC ratio is

$$R = \frac{\sigma_A(e, e' p_S)/A}{\sigma_d(e, e' p_S)/2}$$

integrated over spectator momenta and angles. Typically, backward angles, $\theta_{pq} > 120^\circ$, are chosen to minimize FSI.

If the spectator is a proton and has momentum greater than 300 MeV/c, then it almost certainly belonged to an np SRC pair. If nucleon modification is due to nucleons belonging to SRC pairs, then nucleon modification should be the same in deuterium and in the heavier nucleus and

therefore the tagged EMC ratio should be independent of x_B and should be equal to $a_2(A)$, the relative probability of finding a nucleon in an SRC pair in nucleus A relative to d .

The biggest uncertainty in interpreting these tagged EMC measurements is the possibility that the fragments of the struck nucleon will break up another SRC pair as they exit the nucleus, significantly increasing the number of backward nucleons.

If the spectator is an $A - 1$ nucleus, then the struck nucleon almost certainly did not belong to an SRC pair. By comparing the tagged EMC ratio for ${}^4\text{He}$ with spectator protons and spectator ${}^3\text{He}$, we can see whether nucleon modification depends on the struck nucleon momentum or on the struck nucleon SRC pairing.

5. Parity Violating Deep Inelastic Scattering

There is some evidence that u - and d -quark distributions are modified differently in asymmetric nuclei. Theoretically, since protons move faster than neutrons in neutron-rich nuclei, if nucleon modification depends on nucleon virtuality (as in the PLC model), then we expect protons, with 2 u - and 1 d -quarks, to be more modified than neutrons.

Experimentally, the NuTeV experiment compared neutrino and anti-neutrino DIS off an Iron target and extracted a value of the Weinberg mixing angle that differs from the standard model by about 3σ (Zeller *et al.*, 2002, 2003). While this led to much excitement and attempts to relate it to physics beyond the standard model, recently it was shown that an isospin dependent EMC effect that affects protons more than neutrons could resolve the anomaly (Cloet *et al.*, 2009b).

A measurement of parity violation in $A(e, e')$ DIS would directly measure the $d - u$ difference as a function of x_B (Riordan *et al.*, 2016). The difference in the left-right asymmetry for helicity +1 and -1 electrons is proportional to the product of the photon and Z amplitudes divided by the square of the photon amplitude. This asymmetry will be 10^2 to 10^3 parts per million for DIS scattering from a heavy nucleus:

$$A_{PV} \approx -\frac{G_F Q^2}{4\sqrt{2}\pi\alpha} \left[a_1(x) + \frac{1 - (1 - y)^2}{1 + (1 - y)^2} a_3(x) \right]$$

where $y = 1 - E/E'$, and a_1 and a_2 depend on the quark distributions. In the symmetric nucleus limit

$$a_1 \simeq \frac{9}{5} - 4 \sin^2 \theta_W - \frac{12}{25} \frac{u_A^+ - d_A^+}{u_A^+ + d_A^+} + \dots$$

where u_A refers to all the up quarks in the nucleus and the superscript + refers to the sum of the quark and anti-quark distributions. Thus the parity violating asymmetry is sensitive to the difference between the u and d quark distributions in the nucleus.

B. Theory

The review of the theory presented here shows that there is a strong connection between the cause of the EMC effect and the short-ranged correlations that cause the high x_B plateau in (e, e') scattering on nuclei. Nevertheless, there are gaps in almost every part of the theory, from the initial state wave function, to the modification of nucleon structure, to the need to include the effects of final state interactions. We therefore present an outline of the necessary improvements.

The EMC effect is a modification of nucleon structure functions. Obtaining an understanding of this effect therefore requires a working understanding of the valence sector of the free nucleon wave function, so that the effects of the medium on the relevant components can be correctly included. Lattice calculations, *e.g.* (Ji, 2013; Lin *et al.*, 2015), and the Dyson-Schwinger approach (Cloet and Roberts, 2014) are making progress on computing free nucleon parton distributions. It also would be necessary to build nucleon models that are easily related to the output of these Euclidean-space theories. One would also need to build models that can easily be related to these theories *e.g.* (Burkardt *et al.*, 1997; Hobbs *et al.*, 2016). A twenty-first century calculation of medium modifications cannot be made without inputs from such models.

The calculation of deep inelastic scattering from nuclei needs to be improved in several different manners. For example, the calculations using the PLC-suppression model have been made mainly for $x_B = 0.5$ (C. Ciofi degli Atti, L.L. Frankfurt, L.P. Kaptari and M.I. Strikman, 2007), where effects of Fermi motion nearly vanish. To understand the EMC ratios, R , discussed above it is necessary to be able to make accurate calculations for a range of values of $0.3 \leq x_B \leq 0.7$. Calculations generally need to be extended to handle finite-sized nuclei without resorting starting with infinite nuclear matter calculations and using a local density approximation. Carrying out such a program would require computations of nuclear spectral functions for finite-sized nuclei. This would involve intensive numerical work, so it would be important to present such spectral functions in an easily accessible manner.

We have seen that only models with medium modification arising from short-ranged effects can handle both the EMC effect and high x_B (e, e') scattering. However models in which the medium modification is driven by mean-field effects give an excellent description of the EMC effect, see *e.g.* (Cloet *et al.*, 2009a, 2005b, 2006). It would not be realistic to think that the ultimate accurate description would make use of only one of the two possible ideas. Therefore it is important to build models of medium modifications of nucleon wave functions that includes both mean-field effects and the effects of correlations. The necessary model of nuclei would need to

be consistent with nuclear saturation properties, include non-nucleonic degrees of freedom and have those relativistic effects needed to compute nuclear deep inelastic scattering cross sections.

Many treatments of final state interactions for exclusive reactions (e.g., $(e, e'p)$ and $(e, e'pN)$) use complex optical potentials, which automatically violate current conservation (CC). To fully understand spectroscopic factors and nucleon-nucleon correlations it is necessary to insure that CC is respected in the reaction theory models. A related more general need is to better understand electromagnetic current operators in models of the nucleon-nucleon interactions that employ low-momentum cutoffs.

There is a need to understand higher twist effects in nuclei, with the aim of understanding why it is that EMC ratios measured at JLab are nearly the same as those measured by the much higher energy machines at SLAC and CRRN.

In addition to improving our understanding of the theoretical underpinnings of the causes of the EMC-SRC correlation, it is necessary to explore the implications of the EMC-SRC correlations and of pn dominance in SRC. The possible inversion of the kinetic energy sharing in asymmetric nuclei could significantly affect several sub-fields of physics. In astrophysics the nuclear symmetry energy is of fundamental importance. It describes the change in energy of a nuclear system when a proton is replaced by a neutron. np -SRC dramatically reduce the kinetic part of the symmetry energy (Hen *et al.*, 2015c) and work is ongoing to understand other effects. Additional implications of SRCs on nuclear systems include the nuclear response to neutrino scattering (Fields *et al.*, 2013; Fiorentini *et al.*, 2013), cooling rates of neutron stars, contact interactions in fermi systems (Hen *et al.*, 2015a) and more. While the discussion of these effects extends beyond the scope of this review, they are extensively discussed in the literature.

VII. The way we think it is and the ways to check

This article has focused on explaining two seemingly unrelated phenomena: lepton-nucleus deep inelastic scattering (DIS) and quasi-elastic (QE) electron-nucleus scattering at large values of x_B , and their surprising relation. DIS from a nucleus is very different than DIS from a collection of free nucleons; this is the EMC effect which is parameterized in terms of the slope of the EMC ratio, R , of bound to “free” cross sections. This slope cannot be explained unless the internal quark structure of a bound nucleon differs from that of a free nucleon.

Quasi-elastic scattering, in which a nucleon is knocked out of the nucleus intact, reveals plateaus in the cross section ratios of nuclei to deuterium at large values of x_B that correspond to scattering from short range correlated (SRC) two-nucleon pairs. Different experiments

show that the slope of the EMC effect is linearly proportional to the height of the plateaus! Further studies showed that, for present experiments, the two-nucleon pairs consist of a neutron and a proton.

A review of the available experimental and theoretical evidence shows that the relation between the EMC slope, dR/dx_B , and the SRC plateau height is no accident. There is an underlying cause of both effects: the influence of strongly correlated neutron-proton pairs is largely responsible for both effects. This conclusion needs to be quantified by future experiments and improved theoretical analyses that are discussed in this article.

The connection between the EMC effect and nucleon-nucleon correlations is very profound. Although the binding energy of a nucleon is less than a percent of its mass, the fact that the nucleon is made of quarks and gluons is manifest in two distinct sets of phenomena, via experiments that have been repeated several times. The direct influence of the quark presence in nuclei is now established.

This presence is a subtle effect as it must be, given the generally small deviation of R from unity, and does not arise via the usual low-energy, low momentum transfer nuclear physics observables: binding energy, spectra, radii, electroweak transition rates, *etc.* Nonetheless, the quark presence cannot be denied. We expect that a deeper understanding of the EMC/SRC connection will ultimately lead to an improved understanding of the nature of confinement of light quarks.

VIII. Acknowledgments

We thank our many colleagues for their efforts in accomplishing the research discussed in this review and also for the many insights that they have provided through discussions. This work was supported in part by the U.S. Department of Energy Office of Science, Office of Basic Energy Sciences program under Award Numbers DE-FG02-97ER-41014, DE-FG02-94ER40818 and DE-FG02-96ER-40960 and by the Israel Science Foundation (Israel) under Grants Nos. 136/12 and 1334/16.

IX. Appendix

A. Understanding the np relative wave function

The aim of this Appendix is to provide a qualitative explanation that the momentum space wave function of the deuteron, a very weakly bound system, has a significant high momentum k tail. Indeed one sees an approximate k^{-4} behavior of the deuteron density for large values of k . This tail persists in nuclei because of short ranged correlations between nucleons.

A $1/k^4$ density comes from $1/k^2$ in the wave function

which can be obtained if the nucleon-nucleon interaction is a delta function in coordinate space, as occurs in leading order EFT or in the effective range expansion behavior. Such approximations are valid only at very small values of momentum $1/r_e \gg k \gg 1/a$, where there is approximate scale invariance, where a is the scattering length of about 5 fm and r_e is the effective range of about 2 fm. The $1/k^2$ behavior of the wave function emerges at large values of k due to the second-order effects of the one pion exchange (OPE) contribution to the tensor potential V_T . The Schrödinger equation for the spin-one two-nucleon system, which involves S and D state components, can be expressed as an equation involving the S state only by using $(-B - H_0)|\Psi_D\rangle = V_T|\Psi_S\rangle$, where B is the binding energy of the system and H_0 is the Hamiltonian excluding the tensor potential. Thus one obtains an effective S -state potential: $V_{00} = V_T(-B - H_0)^{-1}V_T$, Eq. (4), where V_T connects the S and D states. The intermediate Hamiltonian H_0 is dominated by the effects of the centrifugal barrier and can be approximated by the kinetic energy operator (Brown and Jackson, 1976). This second-order term is large because it contains an isospin factor $(\tau_1 \cdot \tau_2)^2 = 9$, and because $S_{12}^2 = 8 - 2S_{12}$. Evaluation of the S -state potential, neglecting the small effects of the central potential in the intermediate D -state, yields

$$V_{00}(k, k') \approx -M \frac{32f^4}{\mu^4\pi^2} \int \frac{p^2 dp}{MB + p^2} I_{02}(k, p) I_{20}(p, k'), \quad (73)$$

where M is the nucleon mass, $f^2 \approx 0.08$ is the square of the πN coupling constant, μ is the pion mass, and $I_{LL'}$ are partial wave projections of the OPEP extensor interaction in momentum space. These are evaluated in (Haftel and Tabakin, 1970)

$$I_{02}(p, k) = I_{20}(p, k) = \frac{k^2 Q_2(z) + p^2 Q_0(z)}{2pk} - Q_1(z), \quad (74)$$

with $z \equiv (p^2 + k^2 + \mu^2)/(2pk)$, and Q_i are Legendre functions of the second kind in the conventions of that reference. The result, Eq. (73) corrects errors in (Hen *et al.*, 2015b). The errors do not affect the qualitative statements made in the cited paper, as we now demonstrate.

We use Eq. (73) to estimate quantities of interest. We note the asymptotic property: $\lim_{p \rightarrow \infty} I_{02}(p, k) = 1 - (k^2 + \mu^2)/p^2 + \dots$. Thus the integrand of Eq. (73) is dominated by large values of p and diverges unless there is a cutoff. This means that $V_{00}(k', k)$ is approximately a constant, independent of k and k' . This is the signature of a short ranged interaction. We expose this feature in more detail by assuming that for the important regions of the integral appearing in Eq. (73) by treating the variables k, k' as small compared to the cutoff momentum.

Then $I_{02}(0, p) \approx \frac{p^2}{p^2 + \mu^2}$, and

$$V_{00}(k, k') \approx -M \frac{32f^4}{\mu^4\pi^2} \int_0^M \frac{p^2 dp}{MB + p^2} \left(\frac{p^2}{p^2 + \mu^2} \right)^2 (1 + \dots), \quad (75)$$

where we have cut off the linearly divergent integral for momenta $p > M$ and \dots represents terms of $\mathcal{O}(\frac{k^2 + k'^2}{M^2})$. All realistic models of the NN interaction employ some sort of a cutoff, and a mass scale of the nucleon mass is typical of one-boson exchange potentials (Machleidt, 1989; Machleidt *et al.*, 1987). Thus $V_{00}(k, k')$ is approximately independent of its momentum arguments, the hallmark of short-ranged interactions. The use of Eq. (75) provides an approximate upper limit.

The resulting asymptotic $1/k^4$ dependence of the square of the wave function can be seen by using the Lippmann-Schwinger equation in the form

$$\begin{aligned} \langle k|\psi_S\rangle &\approx \langle k|(-B - H_0)^{-1} \int d^3k' V_{00}(k, k') \langle k'|\psi_S\rangle \rangle (76) \\ &\approx \frac{-V_{00}(0, 0)}{B + \frac{k^2}{M}} \int d^3k' \psi_S(k') = \frac{-V_{00}(0, 0)}{B + \frac{k^2}{M}} (2\pi)^{3/2} \psi_S(r = 0) \end{aligned}$$

where the subscript S refers to the S -state and the integral over all momenta, k' leads to a proportionality to the coordinate-space wave function at the origin. In terms of the usual S -state radial wave function $u(r)$ we have

$$\psi_S(r = 0) = \lim_{r \rightarrow 0} \frac{u(r)}{r} \frac{1}{\sqrt{4\pi}}. \quad (77)$$

Using known wave functions, we find $\lim_{r \rightarrow 0} \frac{u(r)}{r} = (0.0267, 0.0584, 0.0792) \text{ fm}^{-3/2}$ for the Nijmegen, Reid93 (Stoks *et al.*, 1994a), and Argonne V18 (Wiringa *et al.*, 1995b) potentials respectively. The result Eq. (75) shows the $1/k^2$ dependence of the wave function, with overall strength determined by the detailed potential models. The density is the square of the wave function $\sim 1/k^4$ with an overall strength varying by a factor of 9, depending on the potential used. Thus we find a high momentum $1/k^4$ behavior far beyond the validity of the effective range approximation. Potentials without this high-momentum density either have a very weak tensor force or a cutoff at low momenta.

We may check the rough validity of these findings by computing the D state probability, P_D :

$$\begin{aligned} P_D &= \langle \psi_S | V_T \frac{1}{(B + H_0)^2} V_T | \psi_S \rangle \\ &\approx \frac{32f^4}{\mu^4\pi^2} (2\pi)^3 \psi^2(r = 0) \int_0^M \frac{p^2 dp}{(B + \frac{p^2}{M})^2} \left(\frac{p^2}{p^2 + \mu^2} \right)^2 \end{aligned} \quad (78)$$

We evaluate P_D using $u(r = 0)$ for each of the Nijmegen, Reid93 (Stoks *et al.*, 1994a), and Argonne V18 (Wiringa *et al.*, 1995b) potentials respectively. Numerical evaluation of Eq. (78) equation yields $P_D = (2, 10, 18) \%$ for the three potentials respectively. The actual value for all of these potentials is about $P_D = 6\%$. These results show that qualitative treatment here is adequate only for

rough estimates that maintain the qualitative idea that the iterated effects of OPEP produce the $1/k^4$ behavior of the deuteron density. The results of this sub-section depend on the chosen scale (M here). Choosing a sufficiently softer scale would modify the high-momentum dependence of the wave function. A detailed comparison of the momentum dependence of known deuteron wave functions is presented in (Hen *et al.*, 2015b).

B. Basic terminology

We define some basic terms. The probability to find a nucleon at a coordinate \mathbf{x} (where this notation includes spatial position, nucleon spin and isospin) is given by

$$\rho(\mathbf{x}) = \frac{1}{A} \langle \Psi | \sum_{i=1}^A \delta(\mathbf{x} - \mathbf{x}_i) | \Psi \rangle, \quad (79)$$

where $|\Psi\rangle$ is the relevant nuclear wave function. The quantity $\rho(\mathbf{x})$ is known as the density. The normalization is $\int d\mathbf{x} \rho(\mathbf{x}) = 1$, where the integral includes a sum over nucleon spin and isospin.

The two-body density in coordinate space is given by

$$\rho^{(2)}(\mathbf{x}, \mathbf{y}) = \frac{1}{A(A-1)} \langle \Psi | \sum_{i \neq j} \delta(\mathbf{x} - \mathbf{x}_i) \delta(\mathbf{y} - \mathbf{y}_j) | \Psi \rangle. \quad (80)$$

The integral of the two-body density over \mathbf{x} yields the density $\rho(\mathbf{y})$. The correlation function $C(\mathbf{x}, \mathbf{y})$ is the deviation of the two-body density from the mean field approximation:

$$C(\mathbf{x}, \mathbf{y}) = \rho^{(2)}(\mathbf{x}, \mathbf{y}) - \rho(\mathbf{x})\rho(\mathbf{y}). \quad (81)$$

The quantity $C(\mathbf{x}, \mathbf{y})$ vanishes if the wave function $|\Psi\rangle$ can be represented as a product of single-nucleon wave functions. Furthermore the stated normalization conditions lead to the result

$$\int d\mathbf{x} C(\mathbf{x}, \mathbf{y}) = 0, \quad \int d\mathbf{y} C(\mathbf{x}, \mathbf{y}) = 0. \quad (82)$$

It is useful to also define the probability $\rho_{2,1}(r)$ that if a nucleon is at a given position, another one is separated by a distance r .

$$\begin{aligned} \rho_{2,1}(r) &\equiv \frac{1}{4\pi r^2 A} \langle \Psi | \sum_{i \neq j} \delta(r - |\mathbf{r}_i - \mathbf{r}_j|) | \Psi \rangle \\ &= \int d^3 R \rho_2(\mathbf{R} + \mathbf{r}/2, \mathbf{R} - \mathbf{r}/2). \end{aligned} \quad (83)$$

where \mathbf{R} is the center of mass position of the two-nucleon system.

The same kind of analysis can be done in momentum space. Evaluation of $\rho(\mathbf{x})$ requires the square of the coordinate-space representation of $|\Psi\rangle$, while that of $n(\mathbf{k})$ requires the momentum-space representation of the same wave function. The probability for a nucleon to have a momentum \mathbf{k} is given by

$$n(\mathbf{k}) = \frac{1}{A} \langle \Psi | \sum_{i=1}^A \delta(\mathbf{k} - \mathbf{k}_i) | \Psi \rangle. \quad (84)$$

It is convenient to define a two-body density $n_2(\mathbf{K}, \boldsymbol{\kappa})$ in momentum space, which gives the probability of two nucleons having a total momentum of \mathbf{K} and a relative momentum $\boldsymbol{\kappa}$:

$$\begin{aligned} n_2(\mathbf{K}, \boldsymbol{\kappa}) &= \\ &\frac{1}{A(A-1)} \langle \Psi | \sum_{i \neq j} \delta(\mathbf{K}/2 + \boldsymbol{\kappa} - \mathbf{k}_i) \delta(\mathbf{K}/2 - \boldsymbol{\kappa} - \mathbf{k}_j) | \Psi \rangle \end{aligned} \quad (85)$$

Experimentalists defined a correlation as existing if the system has $\boldsymbol{\kappa} \gg \mathbf{K}$, with $\boldsymbol{\kappa} > k_F$ and $\mathbf{K} < k_F$.

It is also useful to consider the integrated quantity:

$$\begin{aligned} n_{2,1}(\boldsymbol{\kappa}) &\equiv \int d^3 K n_2(\mathbf{K}, \boldsymbol{\kappa}) \\ &= \frac{2}{A(A-1)} \langle \Psi | \sum_{i \neq j} \delta(\mathbf{k}_i - \mathbf{k}_j - 2\boldsymbol{\kappa}) | \Psi \rangle, \end{aligned} \quad (86)$$

which is the momentum space version of Eq. (83).

A specific model for the two-nucleon density is used in the analysis of the data relevant to this review. For small relative distances r one writes the two-nucleon wave function $\Psi(\mathbf{R}, \mathbf{r})$ in the following form

$$\Psi(\mathbf{R}, \mathbf{r}) = F_A(R) \psi_D(r), \quad r \ll R_A, \quad (87)$$

where R_A is the radius of the nucleus, and the often used assumption is that at short distances all relative wave functions are the same as that of the deuteron D . In this model

$$\rho_{2,1}^A(r) = \int d^3 R F_A^2(R) \psi_D^2(r) \equiv a_2(A) \psi_D^2(r), \quad r \ll R_A \quad (88)$$

In momentum space

$$\tilde{\Psi}(\mathbf{K}, \mathbf{k}) = \widetilde{F_A}(K) \widetilde{\psi_D}(k), \quad k \gg 1/R_A \quad (89)$$

where the tilde denotes Fourier transform and the momentum variables are canonically conjugate to \mathbf{R} and \mathbf{r} . The one-body density $n_A(\mathbf{k}_1)$ is given by

$$\begin{aligned} n_A(\mathbf{k}_1) &= \int d^3 k_2 \left| \tilde{\Psi}(\mathbf{K}, \mathbf{k}) \right|^2 \\ &= \int d^3 P \widetilde{F_A}^2(P) \left| \widetilde{\psi_D}(\mathbf{k}_1 - \mathbf{P}/2) \right|^2 \end{aligned} \quad (90)$$

$$\approx \int d^3 P \widetilde{F_A}^2(P) \left| \widetilde{\psi_D}(\mathbf{k}_1) \right|^2 = a_2(A) \left| \widetilde{\psi_D}(\mathbf{k}_1) \right|^2, \quad (91)$$

where $k_1 \gg 1/R_A$ is assumed and the relation in terms of $a_2(A)$ is an example of Parceval's theorem.

The next step is to relate the quantities $n_A(k_1)$ and $\rho_{2,1}(r)$. The use of Eq. (88) and Eq. (91) leads immediately to the result

$$a_2(A) = \frac{\rho_{2,1}^A(r)}{r_{2,1}^D(r)} = \frac{n_A(k)}{n_D(k)}, \quad (r \ll R_A, k > 1/R_A) \quad (92)$$

The early workers (Frankfurt *et al.*, 1993) used the ratio of momentum-space densities, and recent workers (Chen *et al.*, 2016) use the coordinate space version, but both are the same in the leading-order approximation of each approach.

C. Why center-of-mass and relative coordinates factorize

We provide a qualitative explanation of the factorization inherent in Eq. (87). Start with the non-relativistic nuclear Hamiltonian with only two-nucleon forces, and consider infinite nuclear matter. The basic assumption is the independent pair approximation. The idea is that the average separation between nucleons $d = 1.7$ fm, so that when one of the nucleons of the pair makes a close encounter with a third particle the collision occurs under conditions such that the original pair had no interactions at all (Gomes *et al.*, 1958). This idea was formally codified by Bethe and co-workers (Bethe, 1971), such that the results of the independent pair approximation appear as the first term in the hole-line expansion.

We explain how this works. Consider two-nucleons in nuclear matter, which interact independently of the other nucleons (except for the influence of the Pauli principle). The two-nucleon Hamiltonian, h , is given by

$$h = h_0 + h_1 \quad (93)$$

$$h_0 = \frac{P^2}{4M}, \quad h_1 = \frac{p^2}{M} + Qv, \quad (94)$$

where \mathbf{P} is the center-of-mass momentum operator, \mathbf{p} is the relative momentum operator, v is the two-nucleon potential, and Q is an operator that projects both nucleon momenta to be greater than the Fermi momentum, k_F . Since the two-nucleon Hamiltonian is a sum of two terms, $h = h_0 + h_1$, that commute the solution to the Schrödinger equation, $h|\psi\rangle = E|\psi\rangle$, is a product:

$$\psi(\mathbf{R}, \mathbf{r}) = F(\mathbf{R})\chi(\mathbf{r}) \quad (95)$$

where

$$h_0 F(\mathbf{R}) = E_{\text{cm}} F(\mathbf{R}), \quad h_1 \chi(\mathbf{r}) = \epsilon \chi(\mathbf{r}), \quad E = E_{\text{cm}} + \epsilon \quad (96)$$

with

$$\psi(\mathbf{R}, \mathbf{r}) = e^{i\mathbf{K}\cdot\mathbf{R}}\chi(\mathbf{r}), \quad (97)$$

where we suppress notations regarding spin and isospin to simplify the discussion. In general the function $\chi(\mathbf{r})$ contains all values of angular momentum and has both short ranged and long-ranged aspects. The essence of Eq. (87) is that for small values of $|\mathbf{r}|$ all relative wave functions look like the deuteron wave function:

$$\lim_{r \ll d} \chi(\mathbf{r}) = \gamma \psi_D(r), \quad (98)$$

where γ represents the probability amplitude that the wave function χ corresponds to the deuteron quantum numbers.

It is necessary to introduce a single-particle, mean-field operator U to extend this idea to finite-sized nuclei. In that case, Eq. (97) is often replaced (see *e.g.* (Haxton *et al.*, 1980) by

$$\psi(\mathbf{R}, \mathbf{r}) = \sum_{\alpha\beta} C_{\alpha\beta} \phi_{\alpha}(\mathbf{r}_1) \phi_{\beta}(\mathbf{r}_2) \chi(\mathbf{r}), \quad (99)$$

where $\phi_{\alpha\beta}$ are solutions of the single-particle equation, $C_{\alpha\beta}$ are coefficients computed using the shell model. The single-particles vary over the size of the nucleus, while the variations of $\chi(\mathbf{r}) - 1$ occur over the range of the nucleon-nucleon interaction. If the size of the nucleus is much larger than this range Eq. (95) remains true. In these applications the Miller-Spencer correlation function (Miller and Spencer, 1976) has often been used to represent $\chi(\mathbf{r})$.

References

Abazov, Victor Mukhamedovich, *et al.* (D0) (2013), “Measurement of the muon charge asymmetry in $p\bar{p} \rightarrow W+X \rightarrow \mu\nu + X$ events at $\sqrt{s}=1.96$ TeV,” *Phys. Rev.* **D88**, 091102, arXiv:1309.2591 [hep-ex].

Abazov, Victor Mukhamedovich, *et al.* (D0) (2014), “Measurement of the W Boson Production Charge Asymmetry in $p\bar{p} \rightarrow W + X \rightarrow e\nu + X$ Events at $\sqrt{s} = 1.96$ TeV,” *Phys. Rev. Lett.* **112** (15), 151803, [Erratum: *Phys. Rev. Lett.* 114,no.4,049901(2015)], arXiv:1312.2895 [hep-ex].

Abazov, Victor Mukhamedovich, *et al.* (D0) (2015), “Measurement of the electron charge asymmetry in $p\bar{p} \rightarrow W + X \rightarrow e\nu + X$ decays in $p\bar{p}$ collisions at $\sqrt{s} = 1.96$ TeV,” *Phys. Rev.* **D91** (3), 032007, [Erratum: *Phys. Rev.* D91,no.7,079901(2015)], arXiv:1412.2862 [hep-ex].

Accardi, A, L. T. Brady, W. Melnitchouk, J. F. Owens, and N. Sato (2016), “Constraints on large- x parton distributions from new weak boson production and deep-inelastic scattering data,” *Phys. Rev.* **D93** (11), 114017, arXiv:1602.03154 [hep-ph].

Accardi, A, W. Melnitchouk, J. F. Owens, M. E. Christy, C. E. Keppel, L. Zhu, and J. G. Morfin (2011), “Uncertainties in determining parton distributions at large x ,” *Phys. Rev. D* **84**, 014008.

Acciarri, R, *et al.* (ArgoNeuT) (2014), “Detection of back-to-back proton pairs in charged-current neutrino interactions with the ArgoNeuT detector in the NuMI low energy beam line,” *Phys. Rev.* **D90** (1), 012008, arXiv:1405.4261 [nucl-ex].

Akulinichev, S V, and S. Shlomo (1990), “Nuclear Binding Effect in Deep Inelastic Lepton Scattering,” *Phys. Lett.* **B234**, 170–174.

Alde, D M, *et al.* (1990), “Nuclear dependence of dimuon production at 800-GeV. FNAL-772 experiment,” *Phys. Rev. Lett.* **64**, 2479–2482.

Altemus, R, A. Cafolla, D. Day, J. S. McCarthy, R. R. Whitney, and J. E. Wise (1980), “LONGITUDINAL AND TRANSVERSE INELASTIC ELECTRON SCATTERING FROM FE-56,” *Phys. Rev. Lett.* **44**, 965–968.

Alvioli, M, C. Ciofi degli Atti, L. P. Kaptari, C. B. Mezzetti, and H. Morita (2013), “Nucleon momentum distributions, their spin-isospin dependence, and short-range correlations,” *Phys. Rev. C* **87**, 034603.

Alvioli, M, C. Ciofi degli Atti, and H. Morita (2008), “Proton-neutron and proton-proton correlations in medium-weight nuclei and the role of the tensor force,” *Phys. Rev. Lett.* **100**, 162503.

Alvioli, Massimiliano, Claudio Ciofi degli Atti, and Hiko Morita (2016), “Universality of nucleon-nucleon short-range correlations: the factorization property of the nu-

clear wave function, the relative and center-of-mass momentum distributions, and the nuclear contacts," Phys. Rev. **C94** (4), 044309, arXiv:1607.04103 [nucl-th].

Anastasio, M R, L. S. Celenza, W. S. Pong, and C. M. Shakin (1983), "RELATIVISTIC NUCLEAR STRUCTURE PHYSICS," Phys. Rept. **100**, 327–401.

Anderson, E R, S. K. Bogner, R. J. Furnstahl, and R. J. Perry (2010), "Operator Evolution via the Similarity Renormalization Group I: The Deuteron," Phys. Rev. **C82**, 054001, arXiv:1008.1569 [nucl-th].

Arenhövel, Hartmut, Winfried Leidemann, and Edward L. Tomusiak (2005), "General survey of polarization observables in deuteron electrodisintegration," Eur. Phys. J. **A23**, 147–190, arXiv:nucl-th/0407053 [nucl-th].

Arneodo, Michele (1994), "Nuclear effects in structure functions," Phys. Rept. **240**, 301–393.

Arrington, J, F. Coester, R.J. Holt, and T.-S. H. Lee (2009), "Neutron structure functions," J. Phys. G **36**, 025005.

Arrington, J, A. Daniel, D. B. Day, N. Fomin, D. Gaskell, and P. Solvignon (2012), "Detailed study of the nuclear dependence of the emc effect and short-range correlations," Phys. Rev. C **86**, 065204.

Arrington, J, and D. Day (2006), "Inclusive Scattering from Nuclei at $x > 1$ in the quasielastic and deeply inelastic regimes, Jefferson Lab Experiment E12-06-105,"

Arrington, J, D. Gaskell, and A. Daniel (2010), "Detailed studies of the nuclear dependence of F_2 in light nuclei, Jefferson Lab Experiment E12-10-008,"

Aste, Andreas, Cyrill von Arx, and Dirk Trautmann (2005), "Coulomb distortion of relativistic electrons in the nuclear electrostatic field," Eur. Phys. J. **A26**, 167–178, arXiv:nucl-th/0502074 [nucl-th].

Aste, Andreas W (2008), "Coulomb distortion effects in quasi-elastic (e,e') scattering on heavy nuclei," Nucl. Phys. **A806**, 191–215, arXiv:0710.1261 [nucl-th].

Ciofi degli Atti, C, L. L. Frankfurt, L. P. Kaptari, and M. I. Strikman (2007), "On the dependence of the wave function of a bound nucleon on its momentum and the EMC effect," Phys. Rev. **C76**, 055206, arXiv:0706.2937 [nucl-th].

Ciofi degli Atti, C, E. Pace, and G. Salme (1980), "Realistic nucleon-nucleon interactions and the three-body electrodisintegration of H-3," Phys. Rev. **C21**, 805–815.

Ciofi degli Atti, C, E. Pace, and G. Salmè (1991a), " y -scaling analysis of quasielastic electron scattering and nucleon momentum distributions in few-body systems, complex nuclei, and nuclear matter," Phys. Rev. C **43**, 1155–1176.

Ciofi degli Atti, C, and S. Simula (1996a), "Realistic model of the nucleon spectral function in few- and many-nucleon systems," Phys. Rev. C **53**, 1689.

Ciofi degli Atti, C, S. Simula, L.L. Frankfurt, and M.I. Strikman (1991b), "Two-nucleon correlations and the structure of the nucleon spectral function at high values of momentum and removal energy," Phys. Rev. C **44**, R7.

Ciofi degli Atti, Claudio (2015), "In-medium short-range dynamics of nucleons: Recent theoretical and experimental advances," Phys. Rept. **590**, 1–85.

Ciofi degli Atti, Claudio, and S. Simula (1996b), "Realistic model of the nucleon spectral function in few and many nucleon systems," Phys. Rev. C **53**, 1689, arXiv:nucl-th/9507024 [nucl-th].

Aubert, JJ, et al. (1983), Phys. Lett. B **123**, 275.

Austern, N (1970), *Direct Nuclear Reaction Theories* (Wiley-Interscience).

Baghdasaryan, H, et al. (CLAS Collaboration) (2010), "Ten-

sor correlations measured in $^3he(e, e' pp)n$," Phys. Rev. Lett. **105** (22), 222501.

Ball, Richard D, et al. (2013), "Parton distributions with LHC data," Nucl. Phys. **B867**, 244–289, arXiv:1207.1303 [hep-ph].

Beane, Silas R, and Martin J. Savage (2005), "Dvcs-dissociation of the deuteron and the EMC effect," Nucl. Phys. **A761**, 259–268, arXiv:nucl-th/0412025 [nucl-th].

Bedaque, Paulo F, and Ubirajara van Kolck (2002), "Effective field theory for few nucleon systems," Ann. Rev. Nucl. Part. Sci. **52**, 339–396, arXiv:nucl-th/0203055 [nucl-th].

Benhar, O, A. Fabrocini, and S. Fantoni (1989), "The Nucleon Spectral Function in Nuclear Matter," Nucl. Phys. **A505**, 267–299.

Benhar, O, V. R. Pandharipande, and I. Sick (1997), "Nuclear binding and deep inelastic scattering," Phys. Lett. **B410**, 79–85.

Benhar, O, V. R. Pandharipande, and I. Sick (1999), "Density dependence of the EMC effect," Phys. Lett. **B469**, 19–24.

Benhar, Omar, and Ingo Sick (2012), "Nuclear binding, correlations and the origin of EMC effect," arXiv:1207.4595 [nucl-th].

Berger, Edmond L, and F. Coester (1987), "Nuclear Effects in Deep Inelastic Lepton Scattering," Ann. Rev. Nucl. Part. Sci. **37**, 463–491.

Bertozzi, W, J. Friar, J. Heisenberg, and J. W. Negele (1972), "Contributions of neutrons to elastic electron scattering from nuclei," Phys. Lett. **B41**, 408–414.

Bertsch, G F, L. Frankfurt, and M. Strikman (1993), "Where are the nuclear pions?" Science **259**, 773–774.

Bethe, HA (1971), "Theory of nuclear matter," Ann. Rev. Nucl. Part. Sci. **21**, 93–244.

Bickerstaff, R P, M. C. Birse, and G. A. Miller (1984), "DISENTANGLING EXPLANATIONS OF DEEP INELASTIC LEPTON NUCLEUS SCATTERING BY LEPTON PAIR PRODUCTION," Phys. Rev. Lett. **53**, 2532–2535.

Bickerstaff, R P, M. C. Birse, and G. A. Miller (1986), "PARTONS IN NUCLEI," Phys. Rev. **D33**, 3228–3245.

Blunden, P G, M. Burkhardt, and G. A. Miller (1999), "Light front nuclear physics: Mean field theory for finite nuclei," Phys. Rev. **C60**, 055211, arXiv:nucl-th/9906012 [nucl-th].

Blunden, Peter G, and Gerald A. Miller (1996), "Quark - meson coupling model for finite nuclei," Phys. Rev. **C54**, 359–370, arXiv:nucl-th/9602031 [nucl-th].

Bogner, S K, R. J. Furnstahl, and A. Schwenk (2010), "From low-momentum interactions to nuclear structure," Prog. Part. Nucl. Phys. **65**, 94–147, arXiv:0912.3688 [nucl-th].

Bogner, S K, A. Schwenk, R. J. Furnstahl, and A. Nogga (2005), "Is nuclear matter perturbative with low-momentum interactions?" Nucl. Phys. **A763**, 59–79, arXiv:nucl-th/0504043 [nucl-th].

Brockmann, R, and R. Machleidt (1984), "NUCLEAR SATURATION IN A RELATIVISTIC BRUCKNER-HARTREE-FOCK APPROACH," Phys. Lett. **B149**, 283.

Brown, G E (1967), *Unified Theory of Nuclear Models and Forces* (North-Holland Publishing Company, Amsterdam).

Brown, G E, and A. D. Jackson (1976), *The Nucleon-Nucleon Interaction* (North-Holland Publishing Company, Amsterdam).

Burkhardt, M, M. R. Frank, and K. L. Mitchell (1997), "On the calculation of hadron form-factors from Euclidean Dyson-Schwinger equations," Phys. Rev. Lett. **78**, 3059–3062, arXiv:hep-ph/9611256 [hep-ph].

C. Ciofi degli Atti, (2015), "In-medium short-range dynam-

ics of nucleons: Recent theoretical and experimental advances," *Phys. Rep.* **590**, 1.

Ciofi degli Atti, L.L. Frankfurt, L.P. Kaptari and M.I. Strikman, (2007), "On the dependence of the wave function of a bound nucleon on its momentum and the emc effect," *Phys. Rev. C* **76** (5), 055206.

Caballero, J A, T. W. Donnelly, E. Moya de Guerra, and J. M. Udias (1998), "Analysis of factorization in (e, e-prime p) reactions: A Survey of the relativistic plane wave impulse approximation," *Nucl. Phys.* **A632**, 323–362, arXiv:nucl-th/9710038 [nucl-th].

Carlson, C E, and T. J. Havens (1983), "Quark Distributions in Nuclei," *Phys. Rev. Lett.* **51**, 261.

Carlson, J, S. Gandolfi, F. Pederiva, Steven C. Pieper, R. Schiavilla, K. E. Schmidt, and R. B. Wiringa (2015), "Quantum Monte Carlo methods for nuclear physics," *Rev. Mod. Phys.* **87**, 1067, arXiv:1412.3081 [nucl-th].

Carlson, J, J. Jourdan, R. Schiavilla, and I. Sick (2002), "Longitudinal and transverse quasielastic response functions of light nuclei," *Phys. Rev. C* **65**, 024002, arXiv:nucl-th/0106047 [nucl-th].

Chen, Jiunn-Wei, and William Detmold (2005), "Universality of the EMC effect," *Phys. Lett.* **B625**, 165–170, arXiv:hep-ph/0412119 [hep-ph].

Chen, Jiunn-Wei, William Detmold, Joel E. Lynn, and Achim Schwenk (2016), "Short Range Correlations and the EMC Effect in Effective Field Theory," arXiv:1607.03065 [hep-ph].

Choi, S, J.P. Chen, and Z.E. Meziani (2005), "Precision measurement of longitudinal and transverse response functions of quasi-elastic electron scattering in the momentum transfer range 0.55 gev/c \pm q \pm 0.9 gev/c, jefferson lab experiment e05-110,".

Ciofi Degli Atti, Claudio, and S. Liuti (1989), "On the Effects of Nucleon Binding and Correlations in Deep Inelastic Electron Scattering by Nuclei," *Phys. Lett.* **B225**, 215–221.

Cloet, I C, W. Bentz, and A. W. Thomas (2009a), "Isovector EMC effect explains the NuTeV anomaly," *Phys. Rev. Lett.* **102**, 252301, arXiv:0901.3559 [nucl-th].

Cloet, I C, W. Bentz, and A. W. Thomas (2009b), "Isovector EMC effect explains the NuTeV anomaly," *Phys. Rev. Lett.* **102**, 252301, arXiv:0901.3559 [nucl-th].

Cloet, I C, W. Bentz, and A. W. Thomas (2012), "Parity-violating DIS and the flavour dependence of the EMC effect," *Phys. Rev. Lett.* **109**, 182301, arXiv:1202.6401 [nucl-th].

Cloet, I C, Wolfgang Bentz, and Anthony William Thomas (2005a), "Nucleon quark distributions in a covariant quark-diquark model," *Phys. Lett.* **B621**, 246–252, arXiv:hep-ph/0504229 [hep-ph].

Cloet, I C, Wolfgang Bentz, and Anthony William Thomas (2005b), "Spin-dependent structure functions in nuclear matter and the polarized EMC effect," *Phys. Rev. Lett.* **95**, 052302, arXiv:nucl-th/0504019 [nucl-th].

Cloet, I C, Wolfgang Bentz, and Anthony William Thomas (2006), "EMC and polarized EMC effects in nuclei," *Phys. Lett.* **B642**, 210–217, arXiv:nucl-th/0605061 [nucl-th].

Cloet, I C, Gerald A. Miller, E. Piasetzky, and G. Ron (2009c), "Neutron Properties in the Medium," *Phys. Rev. Lett.* **103**, 082301, arXiv:0903.1312 [nucl-th].

Cloet, Ian C, Wolfgang Bentz, and Anthony W. Thomas (2016), "Relativistic and Nuclear Medium Effects on the Coulomb Sum Rule," *Phys. Rev. Lett.* **116** (3), 032701, arXiv:1506.05875 [nucl-th].

Cloet, Ian C, and Craig D. Roberts (2014), "Explanation and Prediction of Observables using Continuum Strong QCD," *Prog. Part. Nucl. Phys.* **77**, 1–69, arXiv:1310.2651 [nucl-th].

Close, F E (1979), *An Introduction to Quarks and Partons* (Academic Press, London).

Cohen, E, O. Hen, D.W. Higinbotham, and L.B. Weinstein (2016), "The CaFe Experiment: Short-Range Pairing Mechanisms in Heavy Nuclei, Jefferson Lab Proposal E12-16-004,".

Colle, C, et al. (2015), "Extracting the mass dependence and quantum numbers of short-range correlated pairs from $a(e, e' p)$ and $a(e, e' pp)$ scattering," *Phys. Rev. C* **92**, 024604.

Colle, Camille, Wim Cosyn, Jan Ryckebusch, and Maarten Vanhalst (2014), "Factorization of exclusive electron-induced two-nucleon knockout," *Phys. Rev. C* **89** (2), 024603, arXiv:1311.1980 [nucl-th].

Collins, John (2013), *Foundations of perturbative QCD* (Cambridge University Press).

Cosyn, Wim, Wally Melnitchouk, and Misak Sargsian (2014), "Final-state interactions in inclusive deep-inelastic scattering from the deuteron," *Phys. Rev. C* **89** (1), 014612, arXiv:1311.3550 [nucl-th].

Cosyn, Wim, and Misak Sargsian (2011), "Final-state interactions in semi-inclusive deep inelastic scattering off the Deuteron," *Phys. Rev. C* **84**, 014601, arXiv:1012.0293 [nucl-th].

Cosyn, Wim, and Misak M. Sargsian (2016), "High x Structure Function of the Virtually Free Neutron," *Phys. Rev. C* **93** (5), 055205, arXiv:1506.01067 [hep-ph].

Cruz Torres, R (2016), "Private communication,".

Day, D B, J. S. McCarthy, T. W. Donnelly, and I. Sick (1990), *Annu. Rev. Nucl. Part. Sci.* **40**, 357.

Day, D B, et al. (1987), "y scaling in electron-nucleus scattering," *Phys. Rev. Lett.* **59** (4), 427.

De Forest, T (1983a), *Nucl. Phys.* **A392**, 232.

De Forest, T (1983b), "Off-Shell electron Nucleon Cross-Sections. The Impulse Approximation," *Nucl. Phys.* **A392**, 232–248.

De Forest, Jr, T, and J. D. Walecka (1966), "Electron scattering and nuclear structure," *Adv. Phys.* **15**, 1–109.

Detmold, W, G. A. Miller, and Jason Robert Smith (2006), "Role of the nuclear vector potential in deep inelastic scattering," *Phys. Rev. C* **73**, 015204, arXiv:nucl-th/0509033 [nucl-th].

Diakonov, Dmitri, V. Petrov, P. Pobylitsa, Maxim V. Polyakov, and C. Weiss (1996), "Nucleon parton distributions at low normalization point in the large N(c) limit," *Nucl. Phys.* **B480**, 341–380, arXiv:hep-ph/9606314 [hep-ph].

Dieperink, A E L, and G. A. Miller (1991), "Nucleon binding corrections to lepton nucleus deep inelastic scattering: Use of a realistic spectral function," *Phys. Rev. C* **44**, 866–869.

Dieterich, S, et al. (2001), "Polarization transfer in the He-4(polarized-e, e-prime polarized-p)H-3 reaction," *Phys. Lett.* **B500**, 47–52, arXiv:nucl-ex/0011008 [nucl-ex].

Do Dang, G, M. L'Huillier, Nguyen Van Giai, and J. Wallace Van Orden (1987), "Coulomb sum rules in the relativistic Fermi gas model," *Phys. Rev. C* **35**, 1637–1645.

Dulat, Sayipjamal, Tie-Jiun Hou, Jun Gao, Marco Guzzi, Joey Huston, Pavel Nadolsky, Jon Pumplin, Carl Schmidt, Daniel Stump, and C. P. Yuan (2016), "New parton distribution functions from a global analysis of quantum chromo-

dynamics,” Phys. Rev. **D93** (3), 033006, arXiv:1506.07443 [hep-ph].

Dutta, D, K. Hafidi, and M. Strikman (2013), “Color Transparency: past, present and future,” Prog. Part. Nucl. Phys. **69**, 1–27, arXiv:1211.2826 [nucl-th].

Egiyan, K, *et al.* (CLAS Collaboration) (2003), “Observation of nuclear scaling in the $a(e, e')$ reaction at x_b greater than 1,” Phys. Rev. C **68**, 014313.

Egiyan, K, *et al.* (CLAS Collaboration) (2006a), “Measurement of 2- and 3-nucleon short range correlation probabilities in nuclei,” Phys. Rev. Lett. **96**, 082501.

Egiyan, K, *et al.* (CLAS Collaboration) (2006b), “Measurement of 2- and 3-nucleon short range correlation probabilities in nuclei,” Phys. Rev. Lett. **96**, 082501.

Epelbaum, Evgeny, Hans-Werner Hammer, and Ulf-G. Meissner (2009), “Modern Theory of Nuclear Forces,” Rev. Mod. Phys. **81**, 1773–1825, arXiv:0811.1338 [nucl-th].

Ericson, Magda, and Anthony William Thomas (1983), “Pionic Corrections and the EMC Enhancement of the Sea in Iron,” Phys. Lett. **B128**, 112–116.

Ericson, Magda, and Anthony William Thomas (1984), “Evidence for an Enhanced Nuclear Sea From the Proton - Nucleus Drell-Yan Process,” Phys. Lett. **B148**, 191–193.

Fanchiotti, Huner, Carlos A. García Canal, Tatiana Tarutina, and Vicente Vento (2014), “Medium effects in dis from polarized nuclear targets,” The European Physical Journal A **50** (7), 1–5.

Farrar, Glennys R, and Darrell R. Jackson (1975), “Pion and nucleon structure functions near $x = 1$,” Phys. Rev. Lett. **35**, 1416–1419.

Feldmeier, H, W. Horiuchi, T. Neff, and Y. Suzuki (2011), “Universality of short-range nucleon-nucleon correlations,” Phys. Rev. **C84**, 054003, arXiv:1107.4956 [nucl-th].

Fields, L, *et al.* (MINERvA Collaboration) (2013), “Measurement of muon antineutrino quasielastic scattering on a hydrocarbon target at $E_\nu \sim 3.5$ GeV,” Phys. Rev. Lett. **111**, 022501.

Fiorentini, G A, *et al.* (MINERvA Collaboration) (2013), Phys. Rev. Lett. **111**, 022501.

Fissum, KG, *et al.* (Jefferson Lab Hall A Collaboration) (2004), “The Dynamics of the quasielastic O-16(e, e-prime p) reaction at $Q^{**2} = 0.8$ (GeV/c)**2,” Phys. Rev. **C70**, 034606, arXiv:nucl-ex/0401021 [nucl-ex].

Fomin, N, *et al.* (2012a), “New measurements of high-momentum nucleons and short-range structures in nuclei,” Phys. Rev. Lett. **108**, 092502.

Fomin, N, *et al.* (2012b), “New measurements of high-momentum nucleons and short-range structures in nuclei,” Phys. Rev. Lett. **108**, 092502.

Frank, M R, B. K. Jennings, and G. A. Miller (1996), “The Role of color neutrality in nuclear physics: Modifications of nucleonic wave functions,” Phys. Rev. **C54**, 920–935, arXiv:nucl-th/9509030 [nucl-th].

Frankfurt, L, V. Guzey, and M. Strikman (2012), “Leading Twist Nuclear Shadowing Phenomena in Hard Processes with Nuclei,” Phys. Rept. **512**, 255–393, arXiv:1106.2091 [hep-ph].

Frankfurt, L L, G. A. Miller, and M. Strikman (1994), “The Geometrical color optics of coherent high-energy processes,” Ann. Rev. Nucl. Part. Sci. **44**, 501–560, arXiv:hep-ph/9407274 [hep-ph].

Frankfurt, L L, M. M. Sargsian, and M. I. Strikman (1997), “Feynman graphs and Gribov-Glauber approach to high-energy knockout processes,” Phys. Rev. **C56**, 1124–1137, arXiv:nucl-th/9603018 [nucl-th].

Frankfurt, L L, and M. I. Strikman (1981a), “High-energy phenomena, short-range nuclear structure and qcd,” Phys. Rep. **76** (4), 215.

Frankfurt, L L, and M. I. Strikman (1981b), “High-Energy Phenomena, Short Range Nuclear Structure and QCD,” Phys. Rept. **76**, 215–347.

Frankfurt, L L, and M. I. Strikman (1985), “Point-like CONFIGURATIONS IN HADRONS AND NUCLEI AND DEEP INELASTIC REACTIONS WITH LEPTONS: EMC AND EMC LIKE EFFECTS,” Nucl. Phys. **B250**, 143–176.

Frankfurt, L L, and M. I. Strikman (1987), “On the Normalization of Nucleus Spectral Function and the EMC Effect,” Phys. Lett. **B183**, 254.

Frankfurt, L L, and M. I. Strikman (1988a), “Hard Nuclear Processes and Microscopic Nuclear Structure,” Phys. Rept. **160**, 235–427.

Frankfurt, Leonid, Misak Sargsian, and Mark Strikman (2008), “Recent observation of short range nucleon correlations in nuclei and their implications for the structure of nuclei and neutron stars,” Int. J. Mod. Phys. **A23**, 2991–3055, arXiv:0806.4412 [nucl-th].

Frankfurt, Leonid, and Mark Strikman (1988b), “Hard nuclear processes and microscopic nuclear structure,” Phys. Rep. **160** (5-6), 235 – 427.

Frankfurt, Leonid, and Mark Strikman (2012), “QCD and QED dynamics in the EMC effect,” Int. J. Mod. Phys. **E21**, 1230002, arXiv:1203.5278 [hep-ph].

Frankfurt, LL, M.I. Strikman, D.B. Day, and M. Sargsyan (1993), “Evidence for short-range correlations from high q^2 (e, e') reactions,” Phys. Rev. C **48**, 2451.

Frullani, S, and J. Mougey (1984), “Single particle properties of nuclei through (e, e') reactions,” Adv. Nucl. Phys. **14**, 1.

Gao, J, *et al.* (2000), “Dynamical relativistic effects in quasielastic 1p-shell proton knockout from ^{16}O ,” Phys. Rev. Lett. **84**, 3265.

Gayou, O, *et al.* (Jefferson Lab Hall A) (2002), “Measurement of $G(\text{Ep}) / G(\text{Mp})$ in polarized-e p —> e polarized-p to $Q^{**2} = 5.6\text{-GeV}^{**2}$,” Phys. Rev. Lett. **88**, 092301, arXiv:nucl-ex/0111010 [nucl-ex].

Geesaman, DF, K. Saito, and A.W. Thomas (1995), “The Nuclear EMC Effect,” Ann. Rev. Nucl. and Part. Sci. **45**, 337.

Gezerlis, A, I. Tews, E. Epelbaum, M. Freunek, S. Gandolfi, K. Hebeler, A. Nogga, and A. Schwenk (2014), “Local chiral effective field theory interactions and quantum Monte Carlo applications,” Phys. Rev. **C90** (5), 054323, arXiv:1406.0454 [nucl-th].

Golak, J, H. Kamada, H. Witala, W. Glockle, and S. Ishikawa (1995), “Electron induced pd and ppn breakup of ^{3}He with full inclusion of final-state interactions,” Phys. Rev. C **51** (4), 1638–1647.

Gomes, L C, J. D. Walecka, and V. F. Weisskopf (1958), “Properties of nuclear matter,” Annals Phys. **3**, 241–274.

Gomez, J, *et al.* (1994), “Measurement of the a dependence of deep-inelastic electron scattering,” Phys. Rev. D **49**, 4348.

Gribov, V N, B. L. Ioffe, and I. Ya. Pomeranchuk (1966), “What is the range of interactions at high-energies,” Sov. J. Nucl. Phys. **2**, 549, [Yad. Fiz. 2, 768 (1965)].

Griffoen, K A, *et al.* (2015), “Measurement of the EMC Effect in the Deuteron,” Phys. Rev. **C92** (1), 015211, arXiv:1506.00871 [hep-ph].

Gross, Franz, and D. O. Riska (1987), "Current Conservation and Interaction Currents in Relativistic Meson Theories," *Phys. Rev. C* **36**, 1928.

Guichon, Pierre A M (1988), "A Possible Quark Mechanism for the Saturation of Nuclear Matter," *Phys. Lett. B* **200**, 235–240.

Guichon, Pierre A M, and Gerald A. Miller (1984), "Quarks and the Deuteron Asymptotic D State," *Phys. Lett. B* **134**, 15–20.

Guichon, Pierre A M, Koichi Saito, Evgenii N. Rodionov, and Anthony William Thomas (1996), "The Role of nucleon structure in finite nuclei," *Nucl. Phys. A* **601**, 349–379, arXiv:nucl-th/9509034 [nucl-th].

Haftel, Michael I., and Frank Tabakin (1970), "NUCLEAR SATURATION AND THE SMOOTHNESS OF NUCLEON-NUCLEON POTENTIALS," *Nucl. Phys. A* **158**, 1–42.

Hagen, G, *et al.* (2015), "Neutron and weak-charge distributions of the ^{48}Ca nucleus," *Nature Phys.* **12** (2), 186–190, arXiv:1509.07169 [nucl-th].

Halzen, F, and Alan D. Martin (1984), *QUARKS AND LEPTONS: AN INTRODUCTORY COURSE IN MODERN PARTICLE PHYSICS* (Wiley, New York).

Haxel, Otto, J. Hans D. Jensen, and Hans E. Suess (1949), "On the "magic numbers" in nuclear structure," *Phys. Rev.* **75**, 1766–1766.

Haxton, W C, B. F. Gibson, and E. M. Henley (1980), "PARTY NONCONSERVATION IN F-18, F-19, AND NE-21," *Phys. Rev. Lett.* **45**, 1677–1681.

Hen, O, A. Accardi, W. Melnitchouk, and E. Piasetzky (2011a), "Constraints on the large- x d/u ratio from electron-nucleus scattering at $x > 1$," *Phys. Rev. D* **84**, 117501.

Hen, O, E. Piasetzky, and L. B. Weinstein (2012), "New data strengthen the connection between short range correlations and the emc effect," *Phys. Rev. C* **85**, 047301.

Hen, O, A. W. Steiner, E. Piasetzky, and L. B. Weinstein (2016), "Analysis of Neutron Stars Observations Using a Correlated Fermi Gas Model," arXiv:1608.00487 [nucl-ex].

Hen, O, L. B. Weinstein, E. Piasetzky, G. A. Miller, M. M. Sargsian, and Y. Sagi (2015a), "Correlated fermions in nuclei and ultracold atomic gases," *Phys. Rev. C* **92**, 045205.

Hen, O, L. B. Weinstein, E. Piasetzky, G. A. Miller, M. M. Sargsian, and Y. Sagi (2015b), "Correlated fermions in nuclei and ultracold atomic gases," *Phys. Rev. C* **92** (4), 045205, arXiv:1407.8175 [nucl-ex].

Hen, O, L.B. Weinstein, E.I. Piasetzky, and H. Hakobyan (2014a), "In Medium Proton Structure Functions, SRC, and the EMC effect, Jefferson Lab experiment E12-11-003A.",

Hen, O, L.B. Weinstein, S.A. Wood, and S. Gilad (2011b), "In Medium Nucleon Structure Functions, SRC, and the EMC effect, Jefferson Lab experiment E12-11-107.",

Hen, O, *et al.* (2013a), *Int. J. Mod. Phys. E* **22**, 133017.

Hen, O, *et al.* (CLAS Collaboration) (2014b), *Science* **346**, 614.

Hen, O, *et al.* (2014c), "Momentum sharing in imbalanced Fermi systems," *Science* **346**, 614–617, arXiv:1412.0138 [nucl-ex].

Hen, Or, D. W. Higinbotham, Gerald A. Miller, Eli Piasetzky, and Lawrence B. Weinstein (2013b), "The EMC Effect and High Momentum Nucleons in Nuclei," *Int. J. Mod. Phys. E* **22**, 1330017, arXiv:1304.2813 [nucl-th].

Hen, Or, Bao-An Li, Wen-Jun Guo, L. B. Weinstein, and Eli Piasetzky (2015c), "Symmetry energy of nucleonic matter with tensor correlations," *Phys. Rev. C* **91**, 025803.

Hobbs, T J, Mary Alberg, and Gerald A. Miller (2016), "A Euclidean bridge to the relativistic constituent quark model," arXiv:1608.07319 [nucl-th].

Holt, Jeremy W, Norbert Kaiser, and Wolfram Weise (2013), "Nuclear chiral dynamics and thermodynamics," *Prog. Part. Nucl. Phys.* **73**, 35–83, arXiv:1304.6350 [nucl-th].

Holt, Roy J (2013), "Large x physics: recent results and future plans," in *Proceedings, 43rd International Symposium on Multiparticle Dynamics (ISMD 13)*, arXiv:1311.1527 [nucl-ex].

Holt, Roy J, and Craig D. Roberts (2010), "Nucleon and pion distribution functions in the valence region," *Rev. Mod. Phys.* **82**, 2991–3044.

Horikawa, T, and W. Bentz (2005), "Medium modifications of nucleon electromagnetic form-factors," *Nucl. Phys. A* **762**, 102–128, arXiv:nucl-th/0506021 [nucl-th].

Horowitz, C J (1985), "Relativistic Love-Franey model: Covariant representation of the NN interaction for N-nucleus scattering," *Phys. Rev. C* **31**, 1340–1348.

Hugenholtz, N M, and L. van Hove (1958), "A theorem on the single particle energy in a Fermi gas with interaction," *Physica* **24**, 363–376.

Ioffe, B L (1969), "Space-time picture of photon and neutrino scattering and electroproduction cross-section asymptotics," *Phys. Lett. B* **30**, 123–125.

Jaffe, R L (1983), "Quark Distributions in Nuclei," *Phys. Rev. Lett.* **50**, 228.

Ji, Xiangdong (2013), "Parton Physics on a Euclidean Lattice," *Phys. Rev. Lett.* **110**, 262002, arXiv:1305.1539 [hep-ph].

Jones, M K, *et al.* (Jefferson Lab Hall A) (2000), "G(E(p)) / G(M(p)) ratio by polarization transfer in polarized e p \rightarrow e polarized p," *Phys. Rev. Lett.* **84**, 1398–1402, arXiv:nucl-ex/9910005 [nucl-ex].

Jourdan, J (1995), "Longitudinal response functions: The Coulomb sum revisited," *Phys. Lett. B* **353**, 189–195.

Jourdan, J (1996), "Quasielastic response functions: The Coulomb sum revisited," *Nucl. Phys. A* **603**, 117–160.

Jung, H, and G. A. Miller (1988), "NUCLEONIC CONTRIBUTION TO LEPTON NUCLEUS DEEP INELASTIC SCATTERING," *Phys. Lett. B* **200**, 351–356.

Jung, H, and G. A. Miller (1990), "Pionic contributions to deep inelastic nuclear structure functions," *Phys. Rev. C* **41**, 659–664.

Kelly, JJ (1996), "Nucleon knockout by intermediate energy electrons," *Adv. Nucl. Phys.* **23**, 75.

Kim, K S, B. G. Yu, and M. K. Cheoun (2006), "Coulomb sum rule in quasielastic region," *Phys. Rev. C* **74**, 067601, arXiv:nucl-th/0611067 [nucl-th].

Klimenko, A V, *et al.* (CLAS Collaboration) (2006), "Electron scattering from high-momentum neutrons in deuterium," *Phys. Rev. C* **73** (3), 035212.

Koch, V, and G. A. Miller (1985), "SIX QUARK CLUSTER EFFECTS AND BINDING ENERGY DIFFERENCES BETWEEN MIRROR NUCLEI," *Phys. Rev. C* **31**, 602–612, [Erratum: *Phys. Rev. C* 32, 1106 (1985)].

Korover, I, N. Muangma, O. Hen, *et al.* (2014), "Probing the Repulsive Core of the Nucleon-Nucleon Interaction via the $4\text{He}(e,e'pN)$ Triple-Coincidence Reaction," *Phys. Rev. Lett.* **113**, 022501, arXiv:1401.6138 [nucl-ex].

Kramer, GJ, H.P. Blok, and L. Lapikas (2001), "A consistent analysis of (e,ep) and (d,3he) experiments," *Nuclear*

Physics A **679** (3), 267 – 286.

Kuhn, S.E., and W.K. Brooks (2014), “Jefferson lab experiment e12-14-001: The emc effect in spin structure functions,”.

Kulagin, S.A., and R. Petti (2010), “Structure functions for light nuclei,” Phys. Rev. C **82**, 054614.

Kulagin, S.A., and R. Petti (2014), “Nuclear parton distributions and the Drell-Yan process,” Phys. Rev. C **90** (4), 045204, arXiv:1405.2529 [hep-ph].

Kulagin, S.A., and R. Petti (2006), “Global study of nuclear structure functions,” Nuclear Physics A **765** (1), 126 – 187.

Lacombe, M., B. Loiseau, R. Vinh Mau, J. Ct, P. Pirs, and R. de Tourreil (1981), “Parametrization of the deuteron wave function of the paris nn potential,” Physics Letters B **101** (3), 139 – 140.

Lapikas, L (1993), “Quasi-elastic electron scattering off nuclei,” Nuclear Physics A **553**, 297 – 308.

Lin, Huey-Wen, Jiunn-Wei Chen, Saul D. Cohen, and Xiang-dong Ji (2015), “Flavor Structure of the Nucleon Sea from Lattice QCD,” Phys. Rev. D **91**, 054510, arXiv:1402.1462 [hep-ph].

Liyanage, N., et al. (The Jefferson Lab Hall A Collaboration) (2001), “Dynamics of the $^{16}o(e, e' p)$ reaction at high missing energies,” Phys. Rev. Lett. **86**, 5670–5674.

Llewellyn Smith, C.H. (1983), “A Possible Explanation of the Difference Between the Structure Functions of Iron and Deuterium,” Phys. Lett. B **128**, 107–111.

Lovato, A., S. Gandolfi, Ralph Butler, J. Carlson, Ewing Lusk, Steven C. Pieper, and R. Schiavilla (2013), “Charge Form Factor and Sum Rules of Electromagnetic Response Functions in ^{12}C ,” Phys. Rev. Lett. **111** (9), 092501, arXiv:1305.6959 [nucl-th].

Lovato, A., S. Gandolfi, J. Carlson, Steven C. Pieper, and R. Schiavilla (2016), “Electromagnetic response of ^{12}C : a first-principles calculation,” arXiv:1605.00248 [nucl-th].

Lu, Ding-Hui, Kazuo Tsuchimura, Anthony William Thomas, Anthony Gordon Williams, and K. Saito (1999), “Electromagnetic form-factors of the bound nucleon,” Phys. Rev. C **60**, 068201, arXiv:nucl-th/9807074 [nucl-th].

Macfarlane, M.H., and J.B. French (1960), “Stripping reactions and the structure of light and intermediate nuclei,” Rev. Mod. Phys. **32**, 567–691.

Machleidt, R. (1989), “The Meson theory of nuclear forces and nuclear structure,” Adv. Nucl. Phys. **19**, 189–376.

Machleidt, R., and D.R. Entem (2011), “Chiral effective field theory and nuclear forces,” Physics Reports **503** (1), 1 – 75.

Machleidt, R., K. Holinde, and C. Elster (1987), “The Bonn Meson Exchange Model for the Nucleon Nucleon Interaction,” Phys. Rept. **149**, 1–89.

Malace, S.P., et al. (2011), “A precise extraction of the induced polarization in the $4He(e, e' p)3H$ reaction,” Phys. Rev. Lett. **106**, 052501, arXiv:1011.4483 [nucl-ex].

Malace, Simona, David Gaskell, Douglas W. Higinbotham, and Ian C. Clot (2014), “The challenge of the emc effect: Existing data and future directions,” International Journal of Modern Physics E **23** (08), 1430013.

Marco, E., E. Oset, and P. Fernandez de Cordoba (1996), “Mesonic and binding contributions to the EMC effect in a relativistic many body approach,” Nucl. Phys. A **611**, 484–513, arXiv:nucl-th/9510060 [nucl-th].

Mayer, Maria Goeppert (1950), “Nuclear configurations in the spin-orbit coupling model. i. empirical evidence,” Phys. Rev. **78**, 16–21.

McVoy, K.W., and L. Van Hove (1962), “Inelastic Electron-Nucleus Scattering and Nucleon-Nucleon Correlations,” Phys. Rev. **125**, 1034–1043.

Melnitchouk, W., and A.W. Thomas (1996a), Phys. Lett. B **377**, 11.

Melnitchouk, W., and A.W. Thomas (1996b), “Neutron proton structure function ratio at large x,” Physics Letters B **377** (1), 11 – 17.

Meziani, Z.E., et al. (1984), “Coulomb Sum Rule for Ca-40, Ca-48, and Fe-56 for $-\vec{q}$ (Vector) $\parallel \vec{p}$ = 550-MeV/c,” Phys. Rev. Lett. **52**, 2130–2133.

Mihaila, Bogdan, and Jochen Heisenberg (2000), “Microscopic calculation of the inclusive electron scattering structure function in O-16,” Phys. Rev. Lett. **84**, 1403–1406, arXiv:nucl-th/9910007 [nucl-th].

Miller, G.A. (1984a), “SIX QUARK CLUSTER COMPONENTS OF NUCLEAR WAVE FUNCTIONS AND THE PION NUCLEUS DOUBLE CHARGE EXCHANGE REACTION,” Phys. Rev. Lett. **53**, 2008–2011.

Miller, G.A., and R. Machleidt (1999a), “Infinite nuclear matter on the light front: Nucleon-nucleon correlations,” Phys. Rev. C **60**, 035202, arXiv:nucl-th/9903080 [nucl-th].

Miller, G.A., and R. Machleidt (1999b), “Light front theory of nuclear matter,” Phys. Lett. B **455**, 19–24, arXiv:nucl-th/9811050 [nucl-th].

Miller, Gerald A (1984b), “Building the Nucleus From Quarks: The Cloudy Bag Model and the Quark Description of the Nucleon-nucleon Wave Function,” Int. Rev. Nucl. Phys. **1**, 189–323.

Miller, Gerald A (1988), “NUCLEAR WAVE FUNCTIONS IN DEEP INELASTIC SCATTERING AND DRELL-YAN PROCESSES,” in *Workshop on Nuclear and Particle Physics on the Light Cone Los Alamos, New Mexico, July 18–22, 1988*, pp. 0042–64.

Miller, Gerald A (2000), “Light front quantization: A Technique for relativistic and realistic nuclear physics,” Prog. Part. Nucl. Phys. **45**, 83–155, arXiv:nucl-th/0002059 [nucl-th].

Miller, Gerald A (2014), “Pionic and Hidden-Color, Six-Quark Contributions to the Deuteron b1 Structure Function,” Phys. Rev. C **89** (4), 045203, arXiv:1311.4561 [nucl-th].

Miller, Gerald A., and Leonard S. Kisslinger (1983), “Quark Contributions to the $pp \leftrightarrow d\pi^+$ Reaction,” Phys. Rev. C **27**, 1669.

Miller, Gerald A., and Jason Robert Smith (2002), “Return of the EMC effect,” Phys. Rev. C **65**, 015211, [Erratum: Phys. Rev. C66,049903(2002)], arXiv:nucl-th/0107026 [nucl-th].

Miller, Gerald A., and James E. Spencer (1976), “A Survey of Pion Charge-Exchange Reactions with Nuclei,” Annals Phys. **100**, 562.

Mineo, H., Wolfgang Bentz, N. Ishii, Anthony William Thomas, and K. Yazaki (2004), “Quark distributions in nuclear matter and the EMC effect,” Nucl. Phys. A **735**, 482–514, arXiv:nucl-th/0312097 [nucl-th].

Morgenstern, J., and Z. E. Meziani (2001), “Is the Coulomb sum rule violated in nuclei?” Phys. Lett. B **515**, 269–275, arXiv:nucl-ex/0105016 [nucl-ex].

Mulders, P.J. (1990), “Modifications of Nucleons in Nuclei and Other Consequences of the Quark Substructure,” Phys. Rept. **185**, 83–169.

Murdock, D.P., and C.J. Horowitz (1987), “Microscopic Relativistic Description of Proton - Nucleus Scattering,” Phys.

Rev. **C35**, 1442–1462.

Neff, Thomas, Hans Feldmeier, and Wataru Horiuchi (2015), “Short-range correlations in nuclei with similarity renormalization group transformations,” Phys. Rev. **C92** (2), 024003, arXiv:1506.02237 [nucl-th].

Negele, John W (1999), “Instantons, the QCD vacuum, and hadronic physics,” *Lattice Field Theory. Proceedings: 16th International Symposium, Lattice '98, Boulder, USA, Jul 13-18, 1998*, Nucl. Phys. Proc. Suppl. **73**, 92–104, arXiv:hep-lat/9810053 [hep-lat].

Noble, J V (1981), “Modification of the nucleon’s properties in nuclear matter,” Phys. Rev. Lett. **46**, 412–415.

Norton, P R (2003), Rep. Prog. Phys. **66**, 1253.

Olive, K A, *et al.* (Particle Data Group) (2014), “Review of Particle Physics,” Chin. Phys. **C38**, 090001.

Owens, J F, A. Accardi, and W. Melnitchouk (2013), “Global parton distributions with nuclear and finite- Q^2 corrections,” Phys. Rev. D **87**, 094012.

Palli, V, C. Ciofi degli Atti, L. P. Kaptari, C. B. Mezzetti, and M. Alvioli (2009), “Slow Proton Production in Semi-Inclusive Deep Inelastic Scattering off Deuteron and Complex Nuclei: Hadronization and Final State Interaction Effects,” Phys. Rev. **C80**, 054610, arXiv:0911.1377 [nucl-th].

Paolone, M, *et al.* (2010), “Polarization Transfer in the ${}^4\text{He}(\text{e},\text{e}'\text{p}){}^3\text{H}$ Reaction at $Q^2 = 0.8$ and 1.3 (GeV/c) 2 ,” Phys. Rev. Lett. **105**, 072001, arXiv:1002.2188 [nucl-ex].

Perdrisat, C F, V. Punjabi, and M. Vanderhaeghen (2007), “Nucleon Electromagnetic Form Factors,” Prog. Part. Nucl. Phys. **59**, 694–764, arXiv:hep-ph/0612014 [hep-ph].

Petratos, GG, J. Gomez, R.J. Holt, and R.D. Ransome (2010), “MeAsurement of the F2n/F2p, d/u RAtios and A=3 EMC Effect in Deep Inelastic Electron Scattering Off the Tritium and Helium MirrOr Nuclei, Jefferson Lab Experiment E12-10-103,”.

Piasetzky, E, M. Sargsian, L. Frankfurt, M. Strikman, and J. W. Watson (2006), “Evidence for the strong dominance of proton-neutron correlations in nuclei,” Phys. Rev. Lett. **97**, 162504, arXiv:nucl-th/0604012 [nucl-th].

Piller, Gunther, and Wolfram Weise (2000), “Nuclear deep inelastic lepton scattering and coherence phenomena,” Phys. Rept. **330**, 1–94, arXiv:hep-ph/9908230 [hep-ph].

Pirner, Hans J, and James P. Vary (1981), “Deep Inelastic electron Scattering and the Quark Structure of He-3,” Phys. Rev. Lett. **46**, 1376–1379.

Polls, A, A. Ramos, J. Ventura, S. Amari, and W. H. Dickhoff (1994), “Energy weighted sum rules for spectral functions in nuclear matter,” Phys. Rev. **C49**, 3050–3054.

Punjabi, V, *et al.* (2005), “Proton elastic form-factor ratios to $Q^{**2} = 3.5\text{-GeV}^{**2}$ by polarization transfer,” Phys. Rev. **C71**, 055202, [Erratum: Phys. Rev.C71,069902(2005)], arXiv:nucl-ex/0501018 [nucl-ex].

Riordan, S, R. Beminiwatha, and A. Arrington (2016), “the emc pvdis experiment, a constraint on isovector-dependent nuclear modification effects using parity-violating deep inelastic scattering, proposal pr12-16-006”,.

Rios, A, A. Polls, and W. H. Dickhoff (2014), “Density and isospin asymmetry dependence of high-momentum components,” Phys. Rev. **C89** (4), 044303, arXiv:1312.7307 [nucl-th].

Roberts, Craig D, Roy J. Holt, and Sebastian M. Schmidt (2013), “Nucleon spin structure at very high-x,” Phys. Lett. **B727**, 249–254, arXiv:1308.1236 [nucl-th].

Roberts, R G (1994), *The Structure of the proton: Deep inelastic scattering* (Cambridge University Press).

Ryckebusch, J, D. Debruyne, P. Lava, S. Janssen, B. Van Overmeire, and T. Van Cauteren (2003), “Relativistic formulation of Glauber theory for $\text{A}(\text{e}, \text{e}'\text{p})$ reactions,” Nucl. Phys. **A728**, 226–250, arXiv:nucl-th/0305066 [nucl-th].

Ryckebusch, Jan, Maarten Vanhalst, and Wim Cosyn (2015), “Stylized features of single-nucleon momentum distributions,” Journal of Physics G: Nuclear and Particle Physics **42** (5), 055104.

Saito, K, Kazuo Tsuchimura, and Anthony William Thomas (1999), “Effect of nucleon structure variation on the longitudinal response function,” Phys. Lett. **B465**, 27–35, arXiv:nucl-th/9904055 [nucl-th].

Sargsian, M M, T. V. Abrahamyan, M. I. Strikman, and L. L. Frankfurt (2005a), “Exclusive electro-disintegration of He-3 at high Q^2 . II. Decay function formalism,” Phys. Rev. **C71**, 044615, arXiv:nucl-th/0501018 [nucl-th].

Sargsian, M M, T. V. Abrahamyan, M. I. Strikman, and L. L. Frankfurt (2005b), “Exclusive electrodisintegration of he3 at high q^2 . ii. decay function formalism,” Phys. Rev. C **71** (4), 044615.

Sargsian, Misak M (2014a), “New properties of the high-momentum distribution of nucleons in asymmetric nuclei,” Phys. Rev. C **89**, 034305.

Sargsian, Misak M (2014b), “New properties of the high-momentum distribution of nucleons in asymmetric nuclei,” Phys. Rev. **C89** (3), 034305, arXiv:1210.3280 [nucl-th].

Sargsian, Misak M (2014c), “Protons in High Density Neutron Matter,” *Proceedings, 2nd International Symposium on the Modern Physics of Compact Stars and Relativistic Gravity: Yerevan, Armenia, September 18-21, 2013*, J. Phys. Conf. Ser. **496**, 012007, arXiv:1312.2263 [nucl-th].

Schiavilla, R, O. Benhar, A. Kievsky, L. E. Marcucci, and M. Viviani (2005), “Polarization transfer in He-4(polarized-e, e-prime polarized-p) H-3: Is the ratio G(Ep) / G(Mp) modified in medium?” Phys. Rev. Lett. **94**, 072303, arXiv:nucl-th/0412020 [nucl-th].

Schiavilla, R, R. B. Wiringa, Steven C. Pieper, and J. Carlson (2007), “Tensor forces and the ground-state structure of nuclei,” Physical Review Letters **98** (13), 132501.

Schlumpf, Felix (1992), *Relativistic constituent quark model for baryons*, Ph.D. thesis (Zurich U.), arXiv:hep-ph/9211255 [hep-ph].

Schlumpf, Felix (1993), “Relativistic constituent quark model of electroweak properties of baryons,” Phys. Rev. **D47**, 4114, [Erratum: Phys. Rev.D49,6246(1994)], arXiv:hep-ph/9212250 [hep-ph].

Seely, J, *et al.* (2009a), “New measurements of the european muon collaboration effect in very light nuclei,” Phys. Rev. Lett. **103**, 202301.

Seely, J, *et al.* (2009b), “New measurements of the european muon collaboration effect in very light nuclei,” Phys. Rev. Lett. **103**, 202301.

Shneor, R, *et al.* (2007), “Investigation of proton-proton short-range correlations via the ${}^{12}\text{C}(\text{e}, \text{e}'\text{pp})$ reaction,” Phys. Rev. Lett. **99** (7), 072501.

Sloan, T, R. Voss, and G. Smadja (1988), “The Quark Structure of the Nucleon from the CERN Muon Experiments,” Phys. Rept. **162**, 45–167.

Smith, Jason Robert, and Gerald A. Miller (2002), “Return of the EMC effect: Finite nuclei,” Phys. Rev. **C65**, 055206, arXiv:nucl-th/0202016 [nucl-th].

Smith, Jason Robert, and Gerald A. Miller (2003), “Chiral solitons in nuclei: Saturation, EMC effect and Drell-

Yan experiments,” Phys. Rev. Lett. **91**, 212301, [Erratum: Phys. Rev. Lett. 98, 099902(2007)], arXiv:nucl-th/0308048 [nucl-th].

Smith, Jason Robert, and Gerald A. Miller (2004), “Chiral solitons in nuclei: Electromagnetic form-factors,” Phys. Rev. **C70**, 065205, arXiv:nucl-th/0407093 [nucl-th].

Smith, Jason Robert, and Gerald A. Miller (2005), “Polarized quark distributions in nuclear matter,” Phys. Rev. **C72**, 022203, arXiv:nucl-th/0505048 [nucl-th].

Solvignon-Sliker, P, and J. Arrington (2011), “Precision measurement of the isospin dependence in the 2N and 3N short range correlation region, Jefferson Lab Experiment E12-11-112,”.

Souder, P A (2016), “Parity Violation in Deep Inelastic Scattering with the SoLID Spectrometer at JLab,” *Proceedings, 21st International Symposium on Spin Physics (SPIN 2014): Beijing, China, October 20-24, 2014*, Int. J. Mod. Phys. Conf. Ser. **40**, 1660077.

Stoks, V G J, R. A. M. Klomp, C. P. F. Terheggen, and J. J. de Swart (1994a), “Construction of high quality N N potential models,” Phys. Rev. **C49**, 2950–2962, arXiv:nucl-th/9406039 [nucl-th].

Stoks, V G J, R. A. M. Klomp, C. P. F. Terheggen, and J. J. de Swart (1994b), “Construction of high-quality nn potential models,” Phys. Rev. C **49**, 2950–2962.

Stone, J R, P. A. M. Guichon, P. G. Reinhard, and A. W. Thomas (2016), “Finite Nuclei in the Quark-Meson Coupling Model,” Phys. Rev. Lett. **116** (9), 092501, arXiv:1601.08131 [nucl-th].

Strauch, S, et al. (Jefferson Lab E93-049) (2003), “Polarization transfer in the He-4 (polarized-e, e-prime polarized-p) H-3 reaction up to Q**2 = 2.6-(GeV/c)**2,” Phys. Rev. Lett. **91**, 052301, arXiv:nucl-ex/0211022 [nucl-ex].

Strauch, Steffen (2012), “Hadron medium modifications,” *Proceedings, Resonance Workshop at UT Austin on Hadronic resonance production in heavy ion and elementary collisions*, EPJ Web Conf. **36**, 00016.

Subedi, R, et al. (2008), “Probing Cold Dense Nuclear Matter,” Science **320**, 1476–1478, arXiv:0908.1514 [nucl-ex].

Tang, A, et al. (2003), “n-p short-range correlations from (p,2p+n) measurements,” Phys. Rev. Lett. **90**, 042301.

Thomas, Anthony William, and Wolfram Weise (2001), *The Structure of the Nucleon*.

Tkachenko, S, et al. (CLAS Collaboration) (2014), “Measurement of the structure function of the nearly free neutron using spectator tagging in inelastic $^2\text{H}(e,e' p_s)x$ scattering with clas,” Phys. Rev. C **89**, 045206.

Udias, J M, J. A. Caballero, E. Moya de Guerra, Jose Enrique Amaro, and T. W. Donnelly (1999), “Quasielastic scattering from relativistic bound nucleons: Transverse longitudinal response,” Phys. Rev. Lett. **83**, 5451–5454, arXiv:nucl-th/9905030 [nucl-th].

Udias, J M, and Javier R. Vignote (2000), “Relativistic nuclear structure effects in (e,e-prime polarized-p),” Phys. Rev. **C62**, 034302, arXiv:nucl-th/0007047 [nucl-th].

Vanhalst, Maarten, Wim Cosyn, and Jan Ryckebusch (2011), “Counting the amount of correlated pairs in a nucleus,” Phys. Rev. **C84**, 031302, arXiv:1105.1038 [nucl-th].

Vanhalst, Maarten, Jan Ryckebusch, and Wim Cosyn (2012), “Quantifying short-range correlations in nuclei,” Phys. Rev. C **86**, 044619.

Vary, J P, P. U. Sauer, and C. W. Wong (1973), “Convergence Rate of Intermediate-State Summations in the Effective Shell-Model Interaction,” Phys. Rev. **C7**, 1776–1785.

Walecka, J D (2005), *Electron scattering for nuclear and nucleon structure* (Cambridge University Press).

Wallace, S J, and J. A. Tjon (2008), “Coulomb corrections in quasi-elastic scattering: Tests of the effective-momentum approximation,” Phys. Rev. **C78**, 044604, arXiv:0808.2029 [nucl-th].

Weinstein, L B, O. Hen, and E. Piasetzky (2016), “Hammer events, neutrino energies, and nucleon-nucleon correlations,” Phys. Rev. **C94** (4), 045501, arXiv:1604.02482 [hep-ex].

Weinstein, L B, E. Piasetzky, D. W. Higinbotham, J. Gomez, O. Hen, and R. Shneor (2011), “Short range correlations and the emc effect,” Phys. Rev. Lett. **106** (5), 052301.

Weiss, Ronen, Betzalel Bazak, and Nir Barnea (2015), “Generalized nuclear contacts and momentum distributions,” Phys. Rev. **C92** (5), 054311, arXiv:1503.07047 [nucl-th].

Wiringa, R B, R. Schiavilla, Steven C. Pieper, and J. Carlson (2014a), “Nucleon and nucleon-pair momentum distributions in $A \leq 12$ nuclei,” Phys. Rev. **C89** (2), 024305, arXiv:1309.3794 [nucl-th].

Wiringa, R B, R. Schiavilla, Steven C. Pieper, and J. Carlson (2014b), “Nucleon and nucleon-pair momentum distributions in $a \leq 12$,” Phys. Rev. C **89**, 024305.

Wiringa, R B, V. G. J. Stoks, and R. Schiavilla (1995a), “Accurate nucleon-nucleon potential with charge-independence breaking,” Phys. Rev. C **51**, 38–51.

Wiringa, Robert B, V. G. J. Stoks, and R. Schiavilla (1995b), “An Accurate nucleon-nucleon potential with charge independence breaking,” Phys. Rev. C **51**, 38–51, arXiv:nucl-th/9408016 [nucl-th].

Wong, S S M (1998), *Introductory nuclear physics*.

Yaron, I, et al. (A1) (2016), “Polarization-transfer measurement to a large-virtuality bound proton in the deuteron,” arXiv:1602.06104 [nucl-ex].

Zeller, G P, et al. (2002), “Precise determination of electroweak parameters in neutrino-nucleon scattering,” Phys. Rev. Lett. **88**, 091802.

Zeller, G P, et al. (2003), “Erratum: Precise determination of electroweak parameters in neutrino-nucleon scattering [phys. rev. lett. **88**, 091802 (2002)],” Phys. Rev. Lett. **90**, 239902.